BioMed Research International

Pathogenesis and Clinical Treatment Strategies of Oral Cancer

Lead Guest Editor: Wei Han
Guest Editors: Zhien Feng, Jing Zhang, Jinjun Shao, and Yu Xiong Su

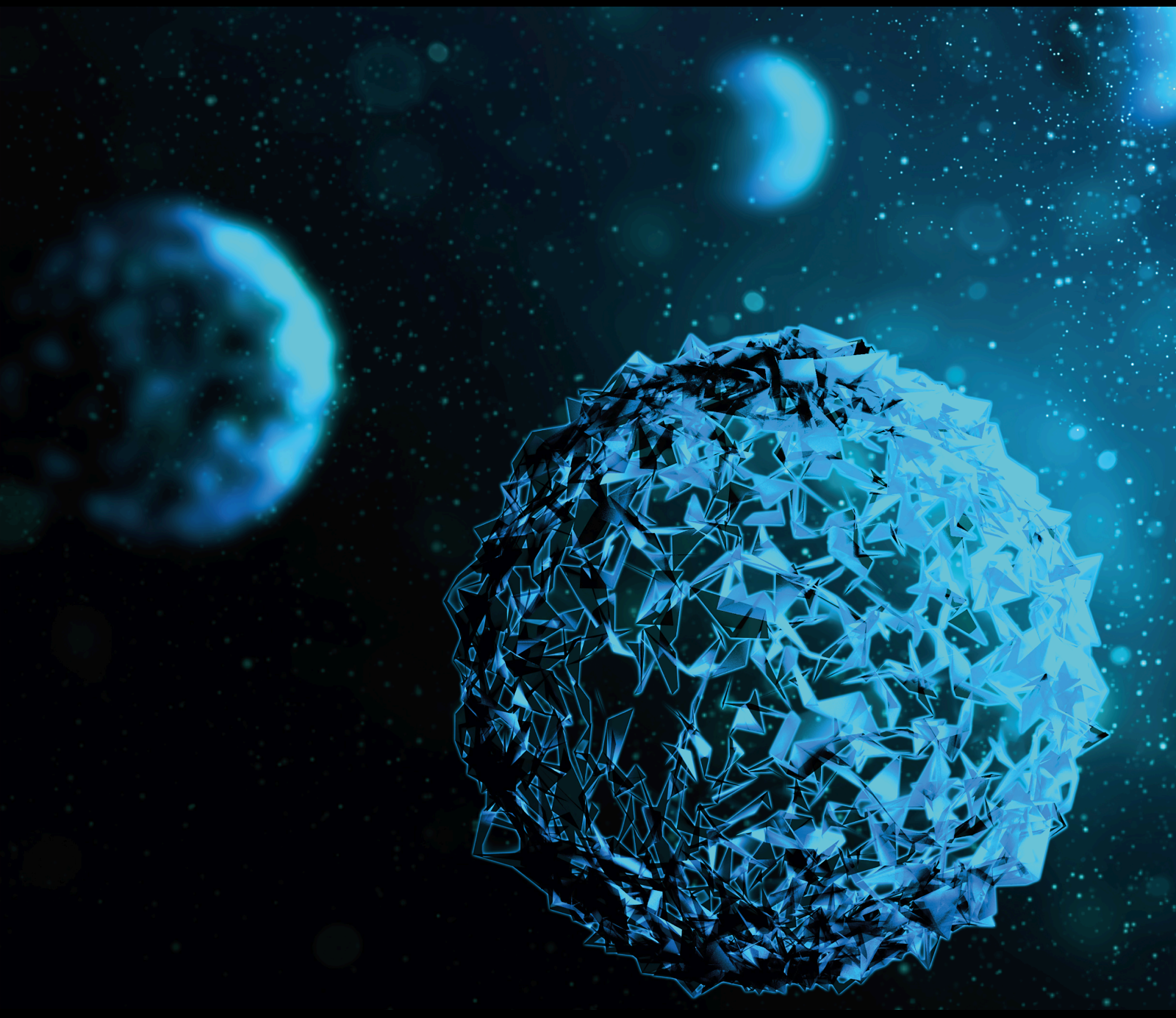

Pathogenesis and Clinical Treatment Strategies of Oral Cancer

BioMed Research International

Pathogenesis and Clinical Treatment Strategies of Oral Cancer

Lead Guest Editor: Wei Han
Guest Editors: Zhien Feng, Jing Zhang, Jinjun Shao, and Yu Xiong Su

Section Editors

Penny A. Asbell, USA
David Bernardo, Spain
Gerald Brandacher, USA
Kim Bridle, Australia
Laura Chronopoulou, Italy
Gerald A. Colvin, USA
Aaron S. Dumont, USA
Pierfrancesco Franco, Italy
Raj P. Kandpal, USA
Fabrizio Montecucco, Italy
Mangesh S. Pednekar, India
Letterio S. Politi, USA
Jinsong Ren, China
William B. Rodgers, USA
Harry W. Schroeder, USA
Andrea Scribante, Italy
Germán Vicente-Rodriguez, Spain
Momiao Xiong, USA
Hui Zhang, China

Academic Editors

Oncology

Fawzy A.S., Australia
Gitana Maria Aceto, Italy
Amedeo Amedei, Italy
Aziz ur Rehman Aziz, China
Riadh Badraoui, Tunisia
Stergios Boussios, Greece
Alberto Briganti, Italy
Franco M. Buonaguro, Italy
Xianbin Cai, Japan
Melchiorre Cervello, Italy
Winson Cheung, Canada
Somchai Chutipongtanate, Thailand
Kate Cooper, USA
Enoc Mariano Cortes-Malagon, Mexico
Alessandro De Vita, Italy
Hassan, El-Abid, Morocco
Yujiang Fang, USA
Zhien Feng, China
Stefano Gambardella, Italy
Dian Gao, China
Piotr Gas, Poland
Nebu Abraham George, India
Xin-yuan Guan, Hong Kong
Hirotaka Iwase, Japan
Arumugam R. Jayakumar, USA
Mitomu Kioi, Japan
Krzysztof Ksiazek, Poland
Yuan Li, China
Anna Licata, Italy
Wey-Ran Lin, Taiwan
César López-Camarillo, Mexico
João F Mota, Brazil
Rakesh Sathish Nair, USA
Peter J. Oefner, Germany
Mana Oloomi, Iran
Vera Panzarella, Italy
Pierpaolo Pastina, Italy
Georgios G. Pissas, Greece
Kyoung-Ho Pyo, Republic of Korea
Giandomenico Roviello, Italy
Daniele Santini, Italy
Wen Shi, USA
Krzysztof Siemianowicz, Poland
Henrique César Santejo Silveira, Brazil
Himangshu Sonowal, USA
Maurizio Soresi, Italy
Kenichi Suda, Japan
Farzad Taghizadeh-Hesary, Iran
Seyithan Taysi, Turkey
Fernando Toshio Ogata, Sweden
Abhishek Tyagi, USA
Marco A. Velasco-Velázquez, Mexico
Thirunavukkarasu Velusamy, India
Navin Viswakarma, USA
Ya-Wen Wang, China
Hushan Yang, USA
Zongguo Yang, China
Hui Yu, USA
Baotong Zhang, USA
Yi Zhang, China

Eugenio Zoni, Switzerland

Contents

Hindawi
BioMed Research International
Volume 2023, Article ID 4444869, 14 pages
https://doi.org/10.1155/2023/4444869

Research Article

Development and Validation of a Prognostic Signature Based on the Lysine Crotonylation Regulators in Head and Neck Squamous Cell Carcinoma

Linlin Jiang,[1] Xiteng Yin,[2,3] Hongbo Zhang,[2,3] Xinyu Zhang,[2,3] Zichen Cao,[2,3] Meng Zhou ,[4] and Wenguang Xu [2,3]

[1]*Department of Medical Oncology, The Second Hospital of Nanjing, Nanjing University of Chinese Medicine, Nanjing, China*
[2]*Department of Oral and Maxillofacial Surgery, Nanjing Stomatological Hospital, Medical School of Nanjing University, Nanjing, China*
[3]*Central Laboratory of Stomatology, Nanjing Stomatological Hospital, Medical School of Nanjing University, Nanjing, China*
[4]*Department of Oral and Maxillofacial Surgery, The Affiliated Stomatological Hospital of Xuzhou Medical University, Xuzhou, China*

Correspondence should be addressed to Meng Zhou; drzhoumeng87@126.com and Wenguang Xu; wenguang.xu@foxmail.com

Received 30 March 2022; Revised 4 January 2023; Accepted 10 January 2023; Published 13 February 2023

Academic Editor: Andrey Cherstvy

Background. Lysine crotonylation (Kcr) is a newly identified posttranslational modification type regulated by various enzymes and coenzymes, including lysine crotonyltransferase, lysine decrotonylase, and binding proteins. However, the role of Kcr regulators in head and neck squamous cell carcinoma (HNSCC) remains unknown. The aim of this study was to establish and validate a Kcr-related prognostic signature of HNSCC and to assess the clinical predictive value of this signature. *Methods*. The mRNA expression profiles and clinicopathological data from The Cancer Genome Atlas (TCGA) database were downloaded to explore the clinical significance and prognostic value of these regulators in HNSCC. The least absolute shrinkage and selection operator (LASSO) Cox regression model was used to generate the Kcr-related prognostic signature for HNSCC. Subsequently, the GSE65858 dataset from the Gene Expression Omnibus (GEO) database was used to validate the signature. The prognostic value of the signature was evaluated using the Kaplan-Meier survival, receiver operating characteristic (ROC) curve, and univariate and multivariate Cox regression analyses. *Results*. We established a nine-gene risk signature associated with the prognosis of HNSCC based on Kcr regulators. High-risk patients demonstrated significantly poorer overall survival (OS) than low-risk patients in the training (TCGA) and validation (GEO) datasets. Then, the time-dependent receiver operating characteristic (ROC) curve analysis showed that the nine-gene risk signature was more accurate for predicting the 5-year OS than other clinical parameters, including age, gender, T stage, N stage, and histologic grade in the TCGA and GEO datasets. Moreover, the Cox regression analysis showed that the constructed risk signature was an independent risk factor for HNSCC. *Conclusion*. Our study identified and validated a nine-gene signature for HNSCC based on Kcr regulators. These results might contribute to prognosis stratification and treatment escalation for HNSCC patients.

1. Introduction

Head and neck cancer ranks as the seventh most common cancer worldwide in 2018, accounting for 3% of all malignancies [1]. Head and neck squamous cell carcinomas (HNSCC) are the most common malignancies in the head and neck region, developing from the mucosal epithelium in the oral cavity, pharynx, and larynx [2]. Despite considerable therapeutic advances in managing HNSCC, the overall survival (OS) rate of HNSCC patients remained dismal in recent decades [3, 4]. Currently, the TNM (tumor, node, and metastasis) staging system established by the American

Joint Committee on Cancer (AJCC) is used to classify HNSCC and determine treatment modalities [5]. However, the TNM stage performance is not ideal, as HNSCC patients with the same TNM stage still differ in clinical outcomes. Numerous efforts have been made to develop an optimal tool for HNSCC risk stratification and prognosis prediction, but no consensus has been achieved. With the rapid development of next-generation sequencing technologies, integrating prognostic gene signatures and traditional clinicopathologic factors has shown an excellent advantage for HNSCC prognosis prediction [2]. Therefore, developing accurate and robust prognostic signatures is critical to help oncologists optimize therapeutic strategies for HNSCC.

Posttranslational modification of proteins occurs in all living organisms and has been increasingly recognized to play a vital role in various biological processes, including gene expression regulation, cell growth, embryo development, and metabolism [6, 7]. As an amphipathic residue with a hydrophobic side chain, lysine acylation neutralizes the positive charge of the amino group, changing protein conformation. Lysine acylations include acetylation, succinylation, malonylation, glutarylation, crotonylation, and β-hydroxybutyrylation [8]. Lysine crotonylation (Kcr) is a newly discovered posttranslational modification identified on histones and nonhistones [9].

Lysine crotonylation is a dynamic reversible process composed of crotonyltransferase complex (writers), decrotonylases (erasers), and binding proteins (readers). Crotonyltransferases, colloquially termed writers, promote the covalent modification of Kcr proteins, including CBP/p300, MOF, Gcn5, Esa1, and PCAF [10–14]. In contrast, decrotonylases, colloquially termed erasers, remove the covalent modification of Kcr proteins, including SIRT1, SIRT2, SIRT3, HDAC1, HDAC2, HDAC3, and HDAC8 [15–17]. Readers are responsible for "reading" Kcr information and participating in the recruitment of downstream readers, such as TAF1, AF9, YEATS2, Taf14, MOZ, and DPF2 [18–21]. Previously, a quantitative proteomics study revealed that p300-targeted Kcr substrates were potentially linked to cancer and might act as carcinogenic factors to promote tumor progress [22]. Additionally, p300 upregulates HNRNPA1 expression by lysine crotonylation to promote the proliferation, invasion, and migration of HeLa cells *in vitro* [23]. In hepatocellular carcinoma, lysine crotonylation expression is associated with TNM stages. However, no correlation was found between lysine crotonylation expression and the prognosis of patients [24]. Currently, the underlying processes and molecular alterations of lysine crotonylation in HNSCC remain unknown, especially regarding its prognostic potential.

In the present study, we systematically analyzed the expression patterns of 18 widely reported Kcr regulators in 491 HNSCC patients with RNA sequencing (RNA-seq) data from The Cancer Genome Atlas (TCGA) database. We explored their potential roles in HNSCC oncogenesis and progression. Finally, a nine-gene risk signature was built to stratify HNSCC prognoses based on TCGA cohort. This robust prognostic signature was successfully validated in an independent external cohort from the Gene Expression Omnibus (GEO) database.

2. Materials and Methods

2.1. Data Acquisition. The RNA-seq transcriptome data normalized by the Expectation-Maximization (RSEM) approach of HNSCC and normal control samples and the corresponding clinical data of HNSCC patients were retrieved from TCGA (https://portal.gdc.cancer.gov/). The RNA expression profiles of HNSCC samples and corresponding clinical data in the GSE65858 dataset were acquired from the GEO database. The clinicopathological information for TCGA and GEO datasets is summarized in Supplementary Tables S1 and S2.

2.2. Selection of Kcr Regulators. First, we manually collected a list of Kcr regulators from the literature [25–27]. The selection criteria for inclusion of Kcr regulators were (1) corresponding regulatory mechanisms validated *in vivo* or *in vitro*, (2) regulators implicated in various physiological and pathological processes, and (3) available RNA expression data in TCGA and GEO datasets. Finally, we collected 18 Kcr regulators. The expression matrix of these genes and the clinicopathological data of samples were extracted and used for subsequent bioinformatics analysis. These genes and corresponding aliases are listed in Supplementary Table S3.

2.3. Differential Expression Analysis of Kcr Regulators. The "limma" R package was used to screen differentially expressed Kcr regulators in 502 tumor and 44 normal control samples. An adjusted $p < 0.05$ and $|\log 2\,\mathrm{fFold\,cChange}\,(\mathrm{FC})| > 1$ were set as the cutoff threshold. Heatmap and violin plots were used to visualize the differential expression of the 18 genes in 502 tumor and 44 normal samples.

Next, the differential expressions of the 18 genes in tumor samples with different clinicopathological parameters were determined using the "limma" R package and visualized in heatmaps using the "pheatmap" package. Differentially expressed genes significantly correlated with clinicopathological parameters were further visualized in bar plots.

2.4. Protein-Protein Interaction (PPI) Network Construction and Correlation Analysis. The STRING database was used to analyze the PPI network among Kcr regulators [28]. The Pearson correlation analysis was used to explore the associations among different Kcr regulators.

2.5. Prognostic Signature Construction and Validation. The univariate Cox regression analysis was performed to identify Kcr regulators harboring prognostic value in TCGA database. Genes with hazard ratio $(\mathrm{HR}) < 1$ have better OS, while genes with $\mathrm{HR} > 1$ have worse OS. Considering the limited number of prognostic genes, all genes were included in the subsequent analysis to develop a risk signature with the least absolute shrinkage and selection operator (LASSO) Cox regression algorithm. The prognostic gene signature is represented by the following: risk score = (coefficient of mRNA1 × expression of mRNA1) + (coefficient of mRNA2 × expression of mRNA2) + ⋯ + (coefficient of mRNAn × expression mRNAn). This formula was used to calculate a risk score for each patient in the training (TCGA)

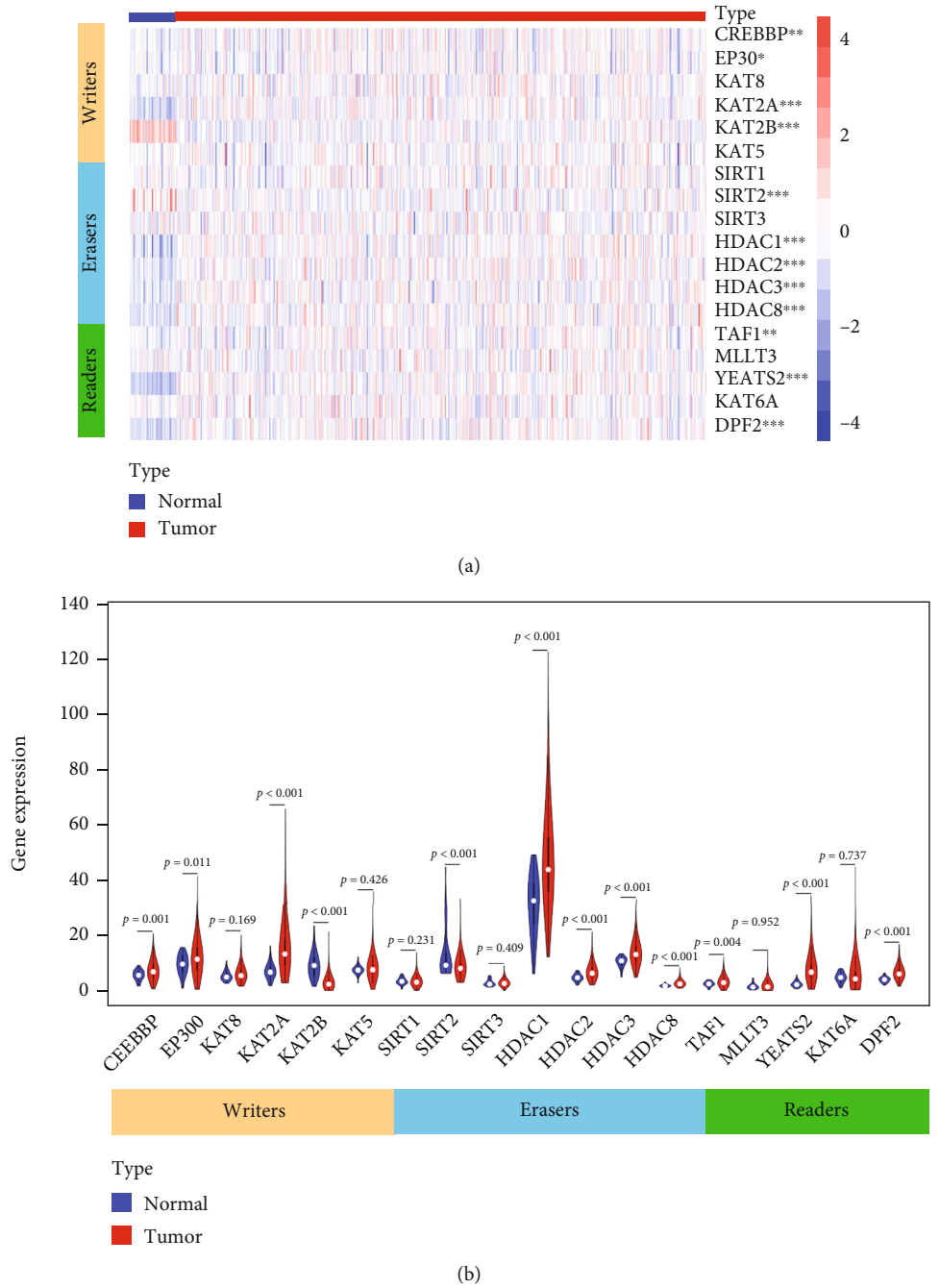

Figure 1: Expression levels of lysine crotonylation regulators between cancerous and adjacent normal samples in TCGA HNSCC cohort. (a) Heatmap with expression levels of lysine crotonylation regulators in each clinical sample. (b) Violin plot of significantly differentially expressed lysine crotonylation regulators between cancerous and adjacent normal samples.

and validation (GEO) cohorts. The cohort was stratified into high- and low-risk groups based on the median value of the risk scores.

Before validation, the "sva" R package was used to conduct batch normalization of the expression data between TCGA and GEO datasets. The "survminer" package was used to draw the Kaplan-Meier survival curve. The "survivalROC" package was used to investigate the time-dependent prognostic value of the gene signature and clinicopathological variables.

2.6. Gene Set Enrichment Analysis (GSEA). The GSEA was performed to identify enriched Gene Ontology (GO) terms and reveal potential underlying Kyoto Encyclopedia of Genes and Genomes (KEGG) pathways of the gene signature. A $p < 0.05$ and a false discovery rate $q < 0.25$ were considered statistically significant.

2.7. Statistical Analysis. All statistical analyses were conducted using R software (v. 3.5.2). The Wilcoxon test was used to compare the expression of genes among different

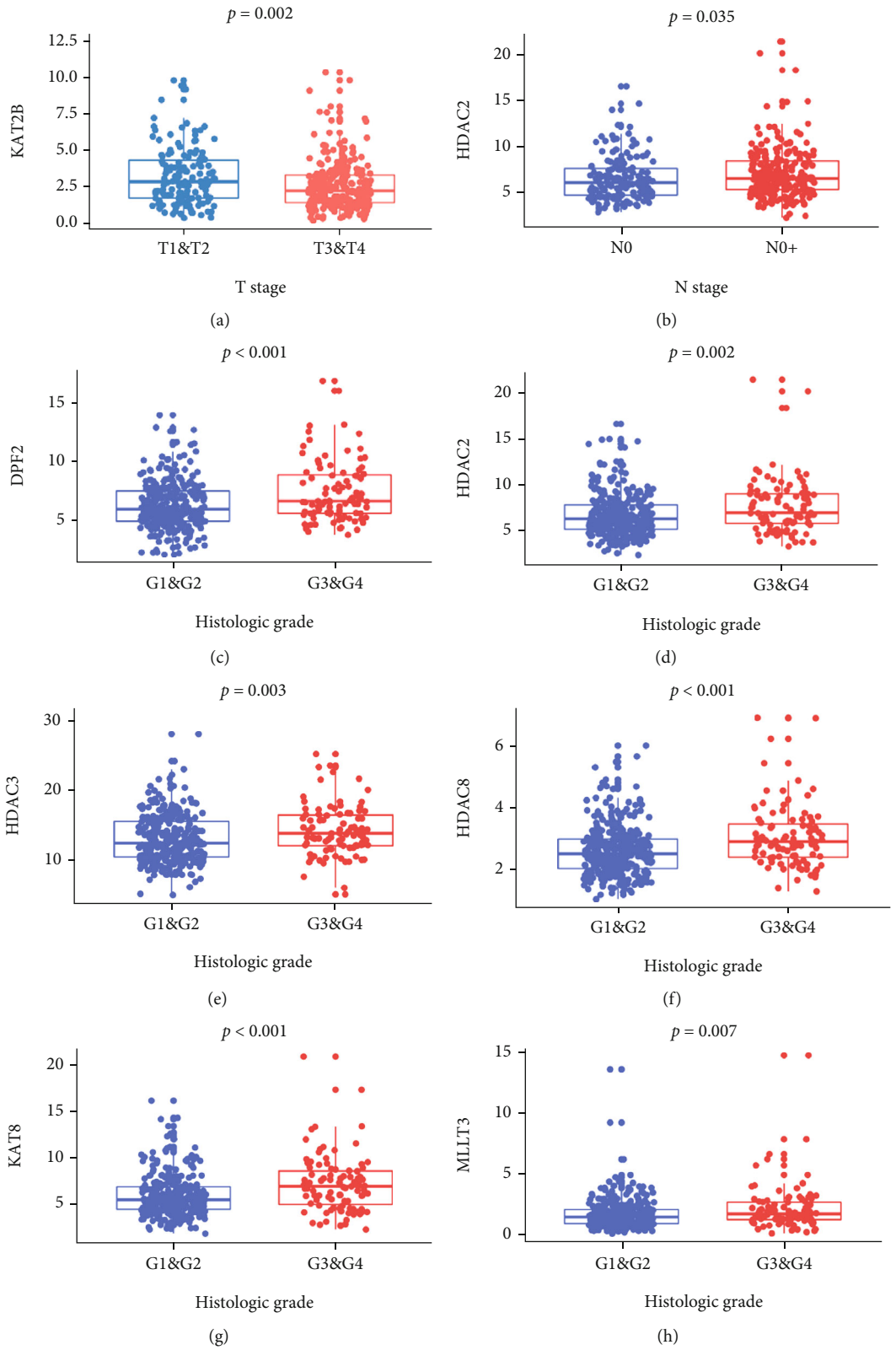

Figure 2: Continued.

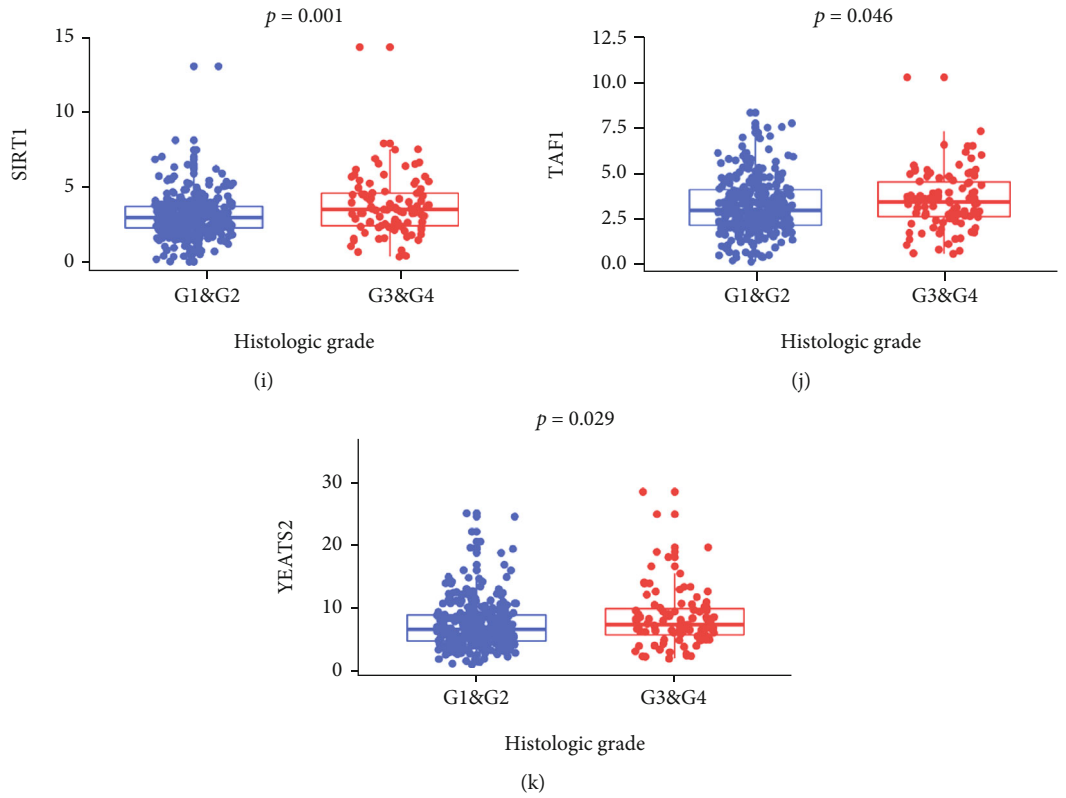

Figure 2: Significantly differentially expressed lysine crotonylation regulators in HNSCC with different clinicopathological features. (a) KAT2B expression in HNSCC patients with early T stage (T1 and T2) and advanced T stage (T3 and T4). (b) HDAC2 expression in HNSCC patients with and without lymph node metastasis. (c–k) Expression levels of DPF2, HDAC2, HDAC3, HDAC8, KAT8, MLLT3, SIRT1, TAF1, and YEATS2 in HNSCC patients with different histologic grades, respectively.

groups. The χ^2 test was conducted to compare the distribution of clinicopathological variables between high- and low-risk groups. The Kaplan-Meier analysis was conducted to compare the OS between high- and low-risk groups using the log-rank test. Univariate and multivariate Cox regression analyses were used to determine independent prognostic factors for the training and validation cohorts. The ROC curve was used to evaluate the accuracy of the constructed gene signature. All statistical tests were performed using a two-sided $p < 0.05$ as the significant threshold.

3. Results

3.1. The Expression of Kcr Regulators Is Correlated with HNSCC Tumorigenesis and Progression. First, we visualized the expression pattern of Kcr regulators between HNSCC and normal controls using a heatmap and violin plot (Figure 1). We found that CREBBP ($p = 0.001$), EP300 ($p = 0.011$), KAT2A ($p < 0.001$), HDAC1 ($p < 0.001$), HDAC2 ($p < 0.001$), HDAC3 ($p < 0.001$), HDAC8 ($p < 0.001$), TAF1 ($p = 0.004$), and YEATS2 ($p < 0.001$) were significantly upregulated in HNSCC samples compared to normal samples, while KAT2B ($p < 0.001$) and SIRT2 ($p < 0.001$) were remarkably downregulated in HNSCC samples (Figure 1(b)). Next, we systematically investigated the relationships between each Kcr regulator and the clinicopathologic features of HNSCC patients, including tumor stage, presence of lymph node metastasis, and histologic grade. The expressions of each Kcr regulator stratified by tumor stage, presence of lymph node metastasis, and histologic grade are presented as heatmaps (Supplementary Figure 1). Specifically, KAT2B was downregulated in the advanced T stage compared to the early T stage ($p = 0.0016$). Meanwhile, HDAC2 was upregulated in HNSCC patients with lymph node metastasis compared to those without lymph node metastasis ($p = 0.035$). Additionally, most Kcr regulators, including DPF2, HDAC2, HDAC3, HDAC8, KAT8, MLLT3, SIRT1, TAF1, and YEATS2, were significantly upregulated in HNSCC patients with higher histologic grade (Figure 2).

3.2. Interaction and Correlation among Kcr Regulators. The PPIs among the 18 Kcr regulators are presented in Figure 3(a). According to the degree of connectivity of each gene in the interaction network, the "writers" CREBBP, KAT2A, and KAT2B were hub genes (Figure 3(b)). The correlation analysis revealed that CREBBP was most relevant with EP300 ($r^2 = 0.75$) among all interactions of crotonylation regulators. Interestingly, several independent interaction groups were detected for "writers," "readers," and "erasers," indicating the diverse functional pathways of different regulators. More specifically, the expressions of

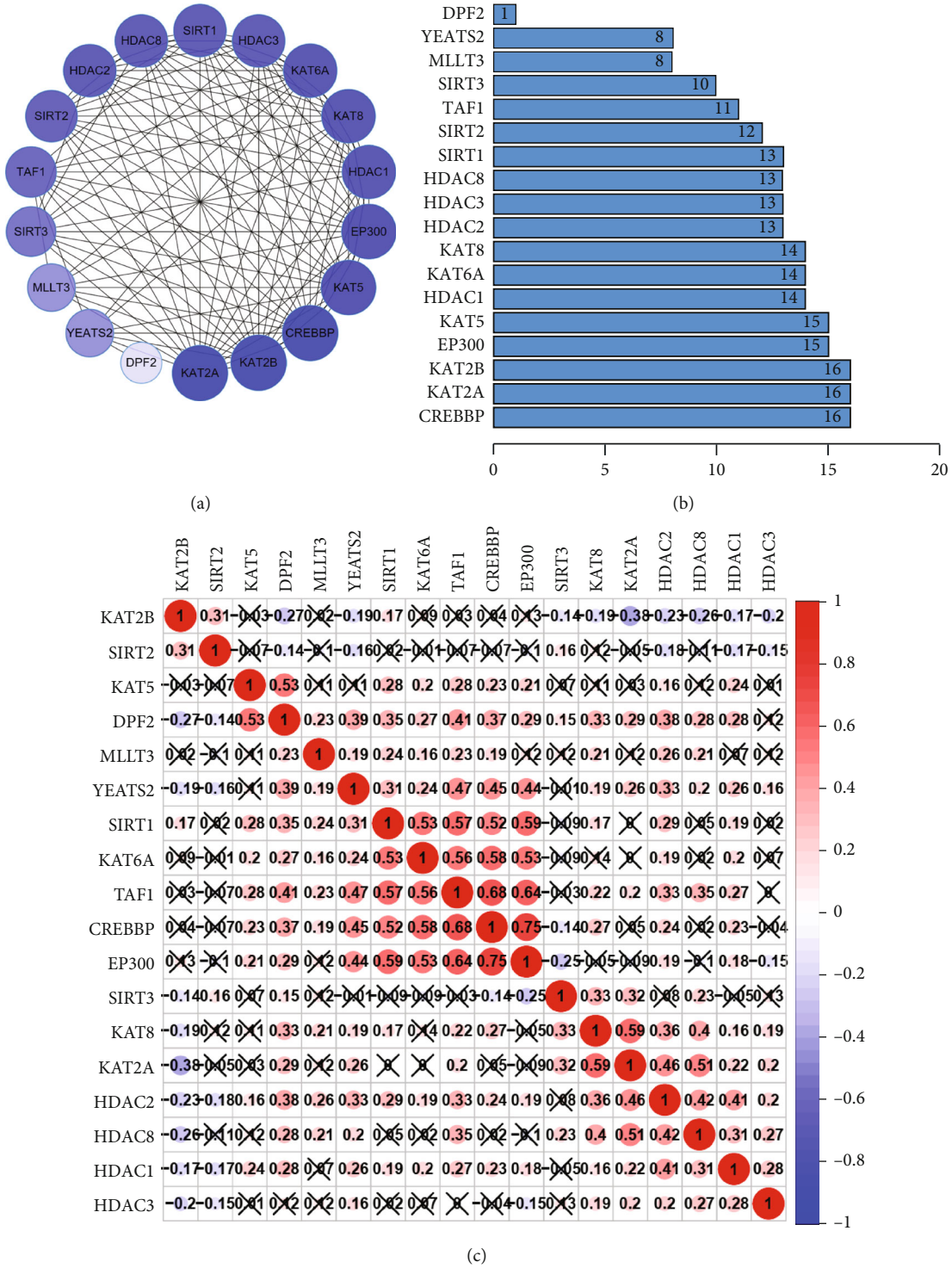

Figure 3: Continued.

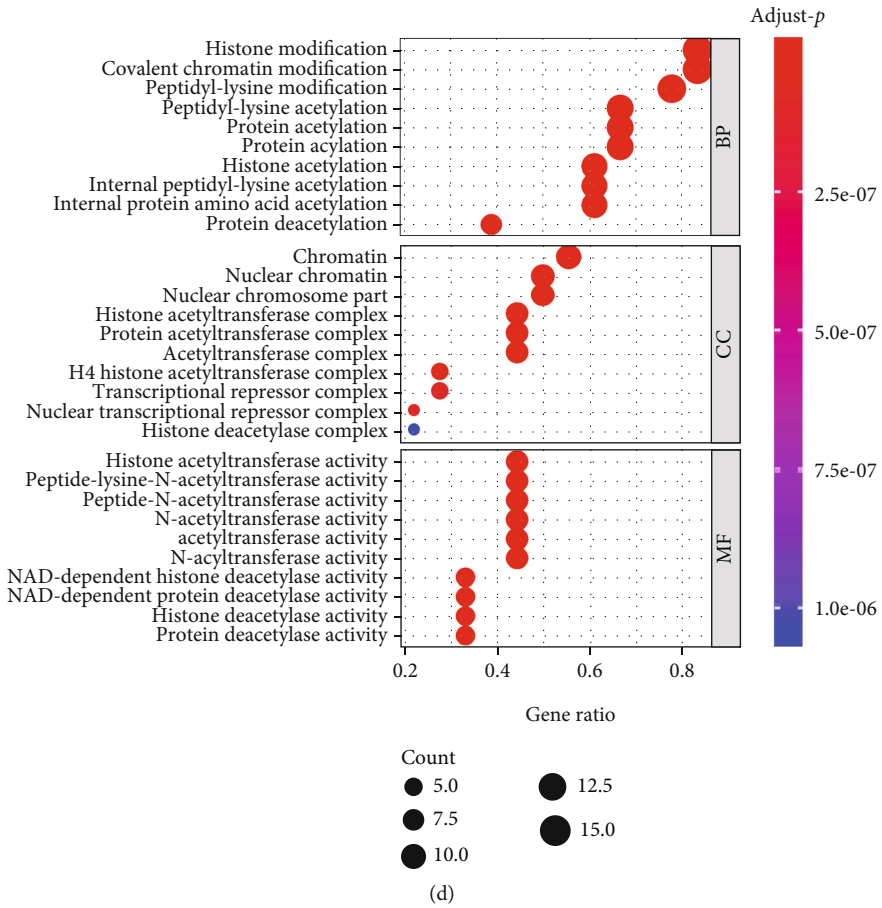

Figure 3: Interaction among lysine crotonylation regulators and functional annotation. (a) Protein-protein interactions between the 18 lysine crotonylation regulators. The color intensity in each node is proportional to the degree of connectivity in the network. (b) Degree of connectivity of each gene in the network. (c) Spearman correlation analysis of the 18 lysine crotonylation regulators in HNSCC. (d) Functional annotation of lysine crotonylation regulators by GO analysis.

CREBBP, EP300, TAF1, KAT6A, YEATS2, and SIRT1 and KAT2A, KAT8, HDAC1, HDAC2, HDAC3, and HDAC8 were significantly correlated with each other in HNSCC (Figure 3(c)). To explore the potential functions of Kcr regulators, we conducted a GO analysis. These regulators were mainly involved in some biological processes, including histone modification, covalent chromatin modification, and peptidyl-lysine modification, and some molecular functions, including histone acetyltransferase, peptide-lysine-N-acetyltransferase, and peptide N-acetyltransferase activities (Figure 3(d)).

3.3. Development and Validation of a Prognostic Signature Based on Kcr Regulators. To investigate the prognostic value of Kcr regulators, we first performed a univariate Cox regression on the expression levels in TCGA dataset. The results revealed that CREBBP, KAT2B, and KAT6A were significantly correlated with OS ($p < 0.05$) and were protective genes (HR < 1) (Supplementary Figure 2A). Then, we applied the LASSO Cox regression algorithm to better predict the clinical outcomes of HNSCC patients using Kcr regulators. Finally, nine genes were screened out to construct the risk signature based on the minimum criteria, and the coefficients from the LASSO algorithm were used to establish the risk signature for both the training (TCGA) and validation (GEO) datasets (Supplementary Figures 2B and C): Risk score = (0.001876 × expression value of EP300) + (−0.049122 × expression value of KAT8) + (−0.001630 × expression value of KAT2A) + (−0.047159 × expression value of KAT2B) + (0.029484 × expression value of HDAC2) + (0.024618 × expression value of HDAC3) + (0.061997 × expression value of MLLT3 + (0.008895 × expression value of YEATS2) + (−0.051189 × expression value of KAT6A).

Based on the nine-gene risk signature, all 491 HNSCC patients in the training dataset were divided into high- and low-risk groups according to the median risk score. Significant differences were observed between the two groups ($p < 0.0001$) (Figure 4(a)). To test the robustness and clinical practice of the nine-gene risk signature, 267 HNSCC patients from another independent external dataset (GEO) were also divided into high- and low-risk groups according to the same risk score cutoff point obtained from the training dataset. The nine-gene risk signature could also effectively stratify patients into low- and high-risk groups with significantly different OS in the GEO-HNSCC dataset

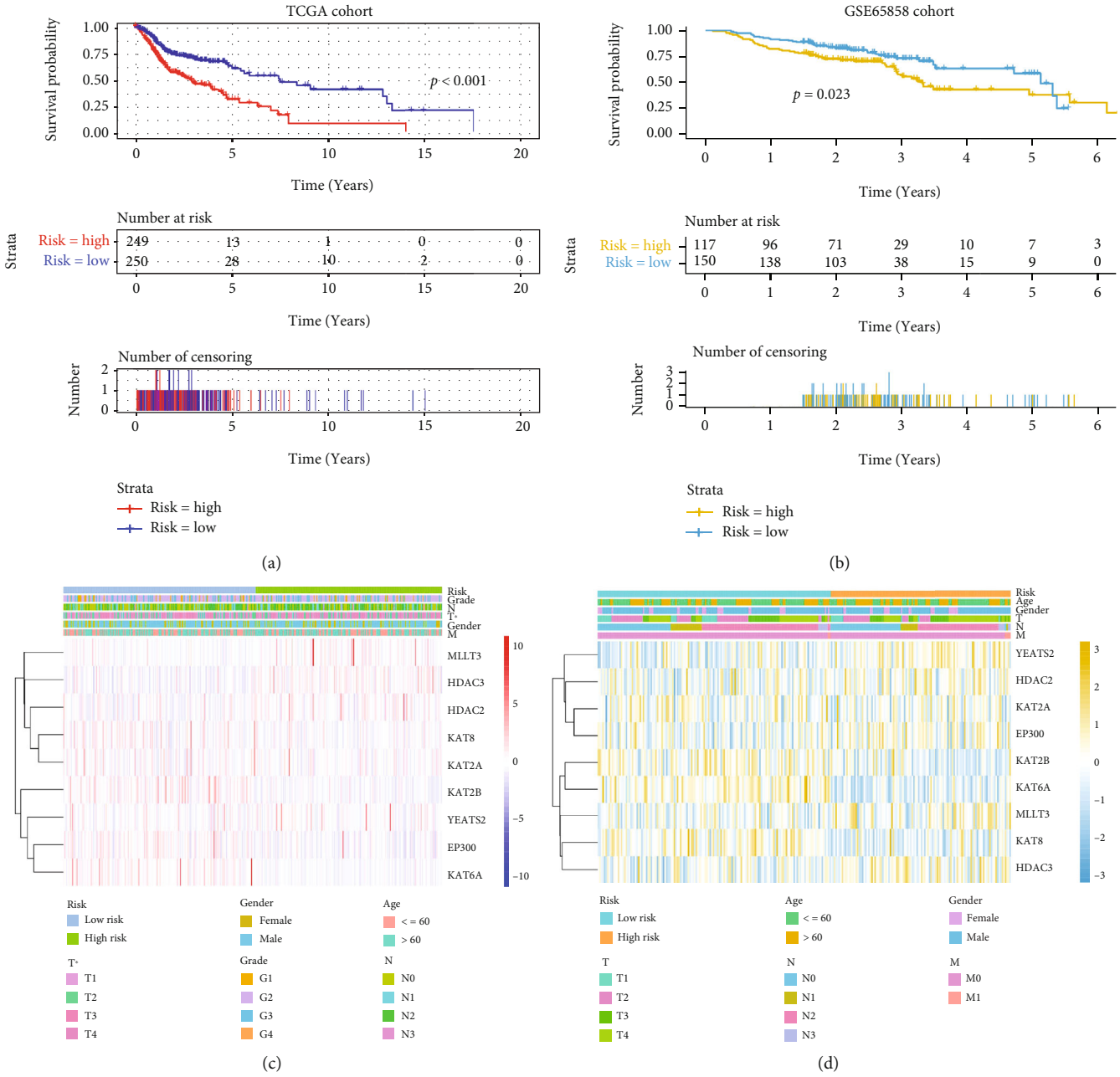

Figure 4: Continued.

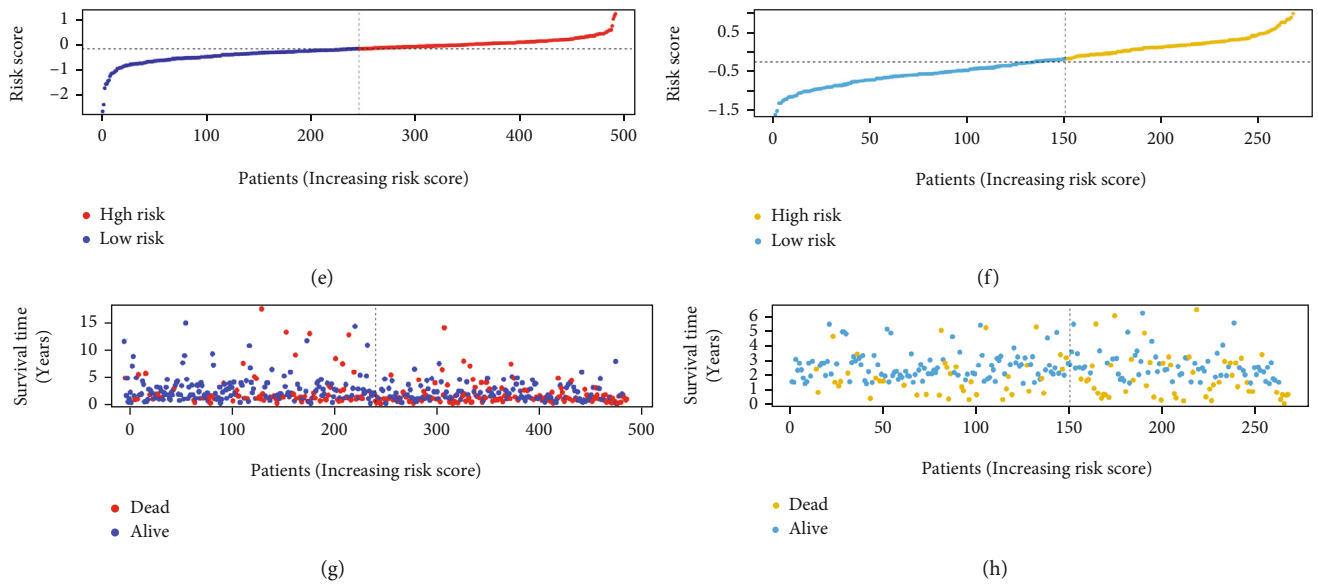

FIGURE 4: Risk signature with nine lysine crotonylation regulators in the training and validation cohorts. (a, b) Kaplan-Meier curves for the OS of patients stratified by the nine-gene prognostic signature into high- and low-risk groups in the training and validation cohorts. (c, d) Heatmap of the nine prognostic genes that were differentially expressed between the high- and low-risk groups in the training and validation cohorts. (e, f) Risk scores plotted in ascending order and marked as low or high risk for all patients in the training and validation cohorts. (g, h) Survival status distribution of HNSCC patients in the training and validation cohorts.

($p < 0.05$) (Figure 4(b)). Additionally, the expressions of the nine prognostic genes in high- and low-risk groups in TCGA and GEO datasets are presented in Figures 4(c) and 4(d).Notably, we found a significant difference between high- and low-risk groups for T stages ($p < 0.05$) in TCGA dataset. Moreover, all patients in the training and validation cohorts were ranked from left to right according to the risk score (Figures 4(e) and 4(f)). Accordingly, the distribution of the survival status of each patient in the training and validation cohorts is presented in Figures 4(g) and 4(h).

3.4. Performance Comparison by Time-Dependent ROC Curve Analysis. We performed the time-dependent ROC curve analysis to compare the prediction performance of the nine-gene risk signature with other clinicopathologic variables, including age, gender, T stage, N stage, and histologic grade in TCGA and GSE65858 cohorts. In TCGA cohort, the risk signature could predict well the 1-, 3-, and 5-year OS rates of HNSCC patients (Figures 5(a)–5(c)). Particularly, the predictive efficiency of the risk signature at 5 years was better than the T stage, N stage, histologic grade, age, and gender (Figure 5(c)). The validation in the GSE65858 cohort further demonstrated a moderate sensitivity and specificity of the risk signature at 1, 3, and 5 years (Figures 5(d)–5(f)).

3.5. Independent Prognostic Role of the Gene Signature. To determine whether the risk signature was an independent prognostic indicator for HNSCC, univariate and multivariate Cox regression analyses were performed in TCGA and GSE65858 cohorts. In the training cohort, the univariate analysis revealed that the T stage ($p = 0.003$, HR = 1.301, 95% confidence interval (CI) = 1.095 – 1.545), N stage ($p < 0.001$, HR = 1.549, 95%CI = 1.290 – 1.860), and risk signature ($p < 0.001$, HR = 4.175, 95%CI = 2.573 – 6.776) were significantly correlated with OS (Figure 6(a)). The multivariate analysis further identified N stage ($p < 0.001$, HR = 1.487, 95%CI = 1.223 – 1.808) and risk signature ($p < 0.001$, HR = 3.500, 95%CI = 2.178 – 5.625) as independent prognostic factors (Figure 6(b)). Next, we performed univariate and multivariate Cox regression analyses for HNSCC patients in the GSE65858 cohort to validate the prognostic value of the risk signature. The risk score ($p = 0.002$, HR = 2.200, 95%CI = 1.351 – 3.583), T stage ($p < 0.001$, HR = 1.544, 95%CI = 1.241 – 1.921), N stage ($p = 0.002$, HR = 1.427, 95%CI = 1.134 – 1.797), and M stage ($p = 0.009$, HR = 3.221, 95%CI = 1.335 – 7.771) were significantly associated with the OS in the univariate analysis (Figure 6(c)). In the multivariate analysis, the risk score ($p = 0.007$, HR = 1.985, 95%CI = 1.208 – 3.262), T stage ($p = 0.011$, HR = 1.348, 95%CI = 1.071 – 1.698), and N stage ($p = 0.046$, HR = 1.287, 95%CI = 1.005 – 1.647) remained independent prognostic factors for HNSCC patients (Figure 6(d)). Altogether, these results indicated that the risk signature derived from the Kcr regulators was an independent prognostic indicator for HNSCC.

3.6. Identification of the Involved Biological Processes and KEGG Pathways by GSEA. Further, we performed GSEA to determine the biological processes and KEGG pathways enriched in high- and low-risk HNSCC patients. Five representative biological processes—mitochondrial gene expression, mitochondrial translation, negative regulation of IκB kinase NF-κB signaling, phosphatidylinositol metabolic process, and phospholipid metabolic process—were enriched in high-risk patients. In contrast, positive

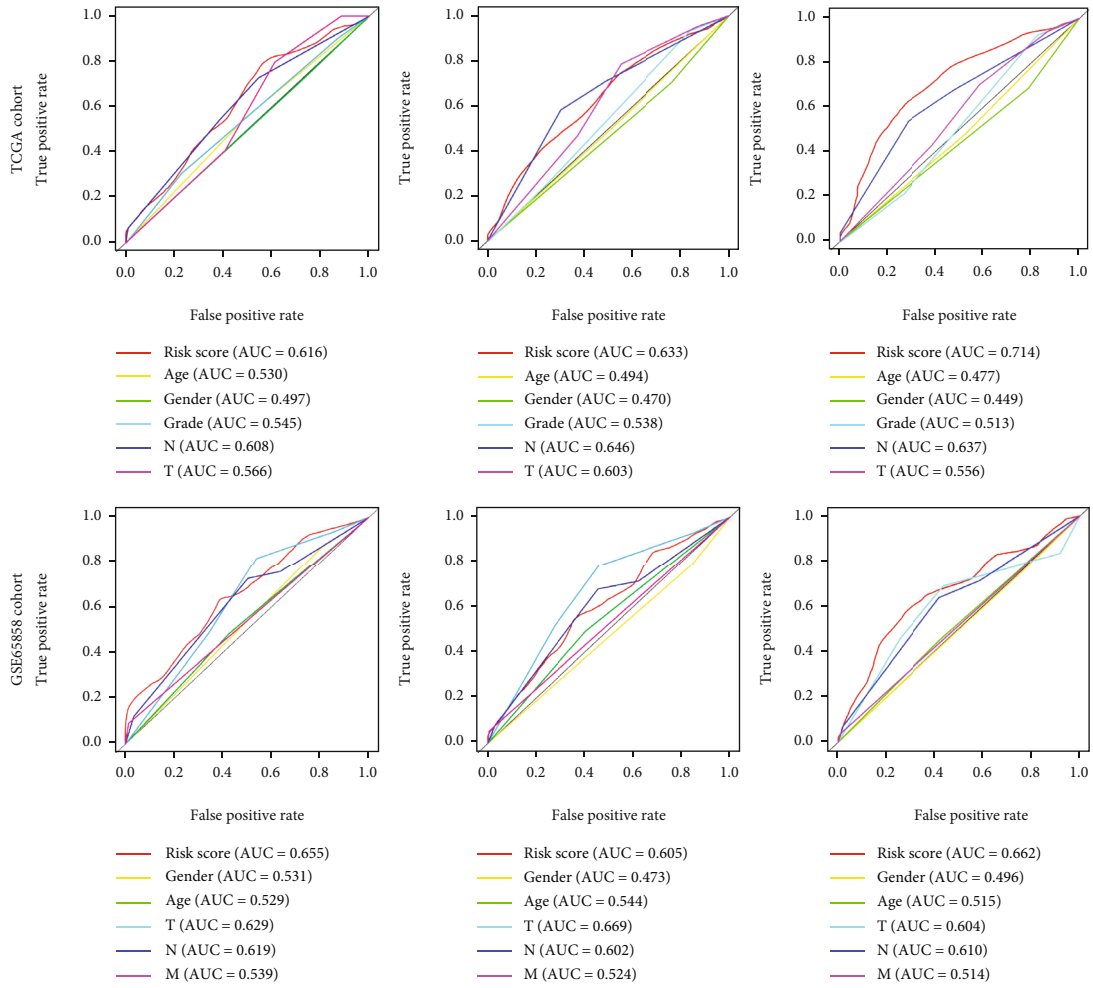

Figure 5: Time-dependent ROC analysis of the sensitivity and specificity for survival prediction at 1, 3, and 5 years in the training and validation cohorts. (a–c) Time-dependent ROC curves for survival prediction of the nine-gene prognostic signature compared to clinicopathologic variables at 1, 3, and 5 years in the training cohort. (d–f) Time-dependent ROC curves for survival prediction of the nine-gene prognostic signature compared to clinicopathologic variables at 1, 3, and 5 years in the validation cohort.

regulation of sodium ion transport, protein targeting to membrane, regulation of cellular amino acid metabolic processes, translation termination, and water homeostasis were enriched in low-risk patients (Figure 7(a)). Regarding KEGG pathways, the B cell receptor signaling pathway, chemokine signaling pathway, FC epsilon RI signaling pathway, oxidative phosphorylation, and proteasome were enriched in high-risk patients. On the other hand, protein export, pyrimidine metabolism, RNA polymerase, T cell receptor signaling pathway, and VEGF signaling pathway were enriched in low-risk patients (Figure 7(b)).

4. Discussion

In our study, we identified a robust nine-gene risk signature for HNSCC patients in TCGA database using LASSO and univariate Cox regression analyses. With further validation in the GSE65858 dataset, the risk signature was shown to be an independent prognostic indicator for HNSCC patients. Risk scores derived from this signature could effectively stratify HNSCC patients into low- and high-risk groups. Importantly, the time-dependent ROC curve analysis revealed that the nine-gene risk signature was more accurate for predicting the 5-year OS than other clinical parameters, including age, gender, T stage, N stage, and histologic grade. Therefore, compared to the traditional staging system, the constructed risk signature showed an advantage in predicting the prognosis of HNSCC patients, which might contribute to prognosis stratification and treatment escalation for HNSCC patients.

As a newly identified posttranslational modification, Kcr is specifically enriched on active gene promoters or potential enhancers in mammalian cell genomes [29]. Since it was reported in 2011, emerging evidence has demonstrated that Kcr is involved in multiple physiological and pathological processes, including spermatogenesis, neuropsychiatric disease, tissue injury, inflammation, and tumorigenesis [25]. Previously, few studies have focused on the relationship between Kcr and cancer. Wan et al. found that the global expression of Kcr was downregulated in liver, gastric, and renal carcinomas, while it was upregulated in thyroid,

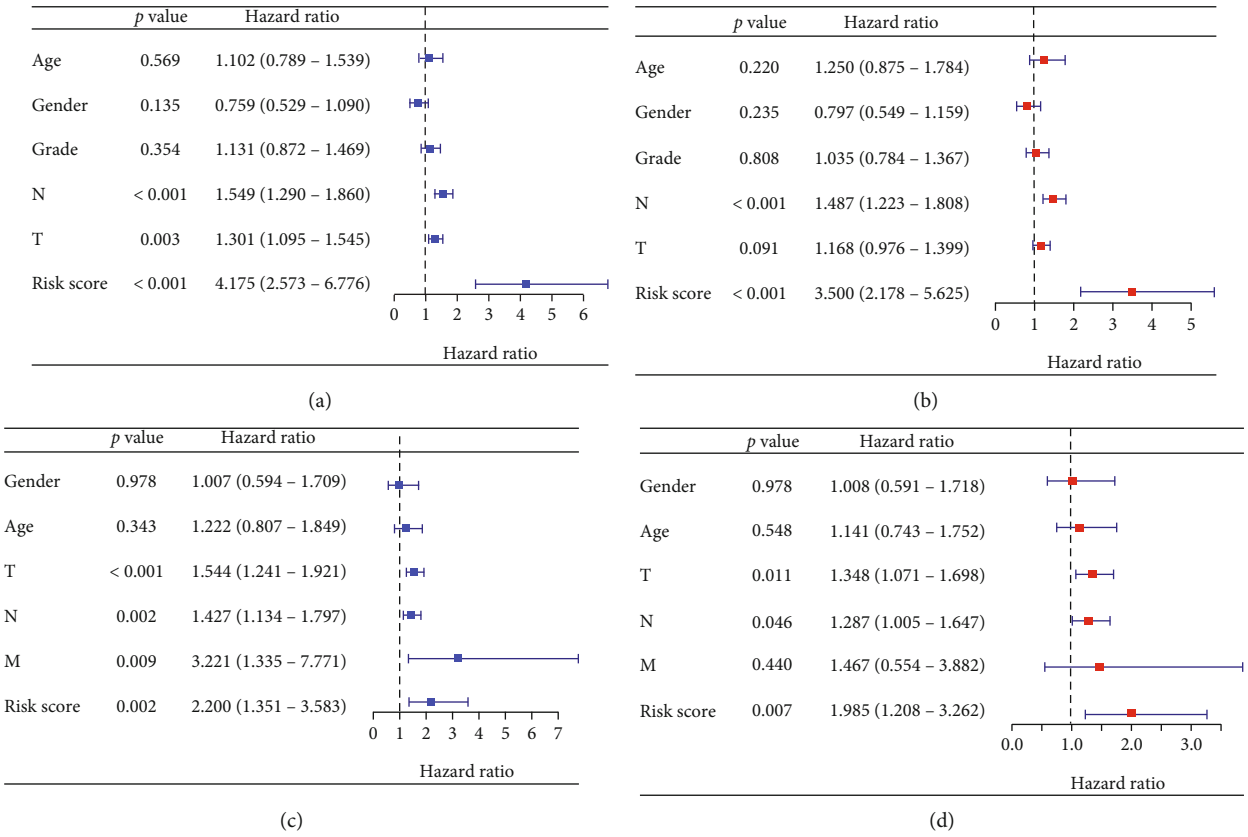

FIGURE 6: Forrest plot for the univariate and multivariate Cox regression analyses in HNSCC patients in the training and validation cohorts. (a, b) Forrest plots of the univariate and multivariate Cox regression analyses in HNSCC patients in TCGA cohort. (c, d) Forrest plots of the univariate and multivariate Cox regression analyses in HNSCC patients in the GSE65858 cohort.

esophagus, colon, pancreas, and lung malignancies by immunohistochemical staining [24]. Particularly, Kcr expression was associated with the TNM stage in hepatocellular carcinoma. However, no prognostic significance of lysine crotonylation was found in hepatocellular carcinoma.

In this study, the clinical significance of Kcr in HNSCC was initially investigated. The differential analysis revealed that most Kcr regulators were aberrantly expressed in HNSCC. Specifically, CREBBP, EP300, KAT2A, HDAC1, HDAC2, HDAC3, HDAC8, TAF1, and YEATS2 were significantly upregulated, while KAT2B and SIRT2 were downregulated in HNSCC samples. Besides, various Kcr regulators, including KAT2B, DPF2, HDAC2, HDAC3, HDAC8, KAT8, MLLT3, SIRT1, TAF1, and YEATS2, were correlated with T stage, lymph node metastasis, and histologic grade. These results indicated that Kcr regulators might contribute to cancer progression in HNSCC.

Based on the interactions between Kcr regulators, CREBBP seemed to be the most relevant regulator with EP300, consistent with previous studies [30, 31]. CREBBP and EP300 are widely recognized histone acetyltransferases and transcriptional coactivators that share approximately 60% homology and play vital roles in various cellular activities such as cell growth, differentiation, DNA repair, and apoptosis [32–34]. Notably, CREBBP was previously reported as a novel tumor suppressor, and CREBBP dysfunction was correlated with carcinogenesis and progression in several human malignancies [35, 36]. Similarly, our findings also revealed that high CREBBP expression was associated with a favorable HNSCC prognosis, indicating that CREBBP might play a tumor-suppressive role in HNSCC. However, Hu et al. demonstrated that CREBBP acted as an oncogene and predicted a poor prognosis in ovarian cancer [37]. These differences might be due to tumor heterogeneity among different malignancies.

Furthermore, KAT2B was also identified as a hub gene in the PPI network. Previous studies have revealed the relationship between KAT2B and tumor occurrence and development. Bharathy et al. found that KAT2B was overexpressed in primary alveolar rhabdomyosarcoma, and its acetylation activated the PAX3-FOXO1 pathway and promoted carcinogenesis [38]. Malatesta et al. demonstrated that KAT2B was an important factor in the Hedgehog signaling pathway, and its downregulation in medulloblastoma and glioblastoma cells contributed to decreased proliferation and increased apoptosis [39]. Conversely, KAT2B plays an oncogenic role in multiple types of cancer, such as gastric, liver, and cervical cancers. Moreover, KAT2B suppressed the tumorigenicity of gastric cancer *in vitro* and *in vivo* and was correlated with aggressive clinical features [40]. KAT2B was downregulated in hepatocellular carcinoma tissues and significantly associated with a favorable prognosis for patients [41]. Similarly, KAT2B was significantly downregulated in cervical cancer

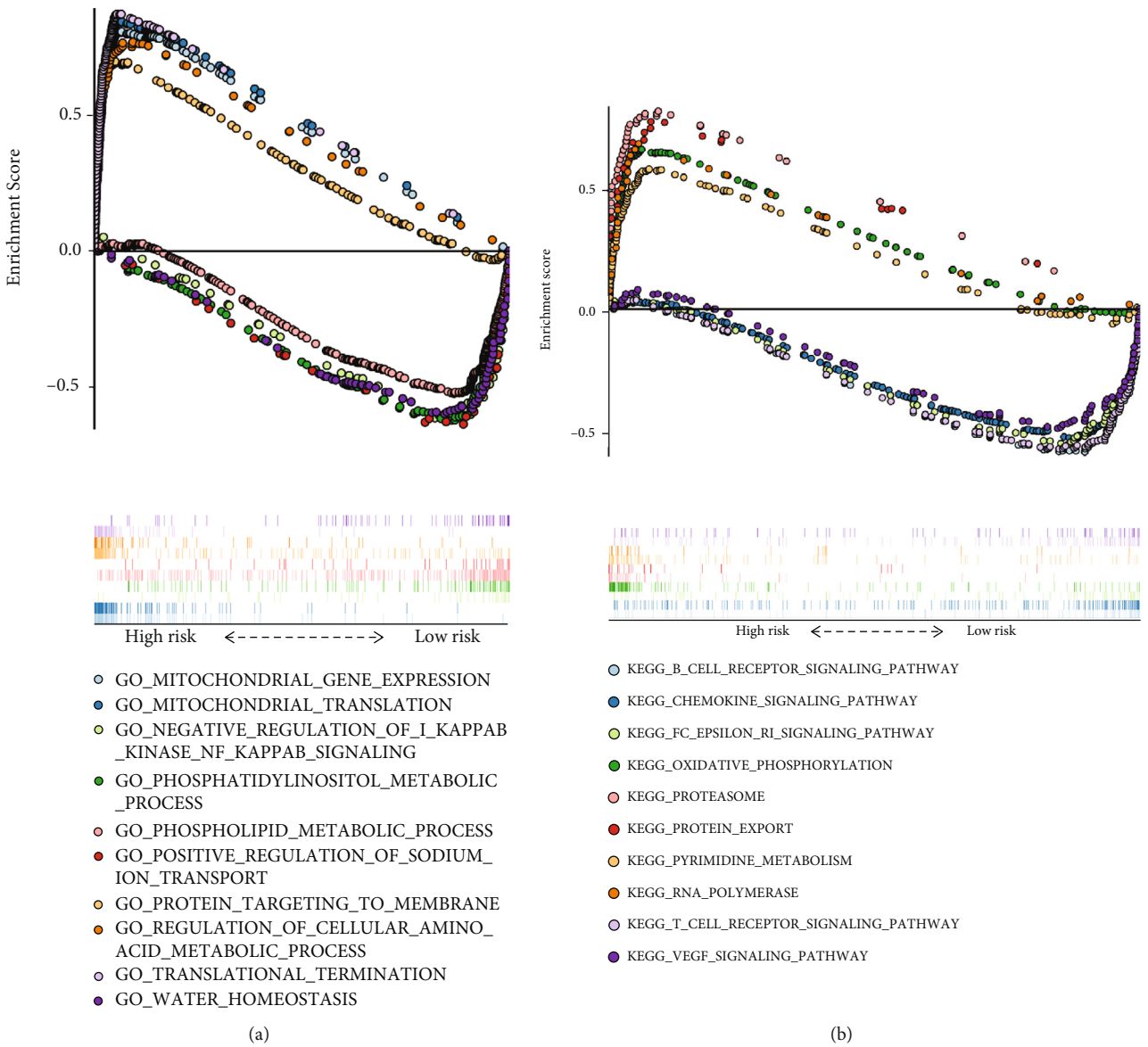

Figure 7: Biological processes and KEGG pathways enriched by GSEA. (a) Representative biological processes enriched and (b) KEGG pathways in high- and low-risk HNSCC patients.

tissues, and its low expression was closely associated with a poor prognosis [41]. Here, KAT2B was downregulated in HNSCC samples and was negatively correlated with the T stage. The survival analysis also validated KAT2B as a favorable prognostic biomarker for HNSCC.

In our study, we identified a robust nine-gene risk signature for HNSCC patients in TCGA database using LASSO and univariate Cox regression analyses. With further validation in the GSE65858 dataset, the risk signature was shown to be an independent prognostic indicator for HNSCC patients. Risk scores derived from this signature could effectively stratify HNSCC patients into low- and high-risk groups. Importantly, the time-dependent ROC curve analysis revealed that the nine-gene risk signature was more accurate for predicting the 5-year OS than other clinical parameters, including age, gender, T stage, N stage, and histologic grade. Therefore, compared to the traditional staging system, the constructed risk signature showed an advantage in predicting the prognosis of HNSCC patients, which might contribute to prognosis stratification and treatment escalation for HNSCC patients.

However, our current study also has some limitations. Given the retrospective nature of this study, further validation in prospective and multicenter clinical trials is essential to validate the accuracy and efficiency of the constructed signature. Moreover, further experimental studies are needed to verify the role of Kcr and elucidate the underlying mechanisms of the signature in HNSCC. Additionally, due to the few studies investigating the role of Kcr in tumors, the information on Kcr regulators was manually extracted from the literature. Thus, some latent and unidentified Kcr regulators might be omitted in the gene sets.

5. Conclusion

In summary, we systematically demonstrated the expression profiles and clinical significance of Kcr regulators in HNSCC patients. We established a nine-gene prognostic signature based on the Kcr regulators and validated it in an external HNSCC cohort. The constructed risk signature was an independent prognostic factor for HNSCC patients, which could effectively predict the survival of HNSCC patients and facilitate clinical decision-making for oncologists. Multicenter and prospective studies with large sample sizes are needed to further validate the clinical practicality and accuracy of the risk signature.

Data Availability

The data that support the findings of this study are available in TCGA database at https://www.cancer.gov/ and GEO database at https://www.ncbi.nlm.nih.gov/geo/ (reference number: GSE65858).

Conflicts of Interest

The authors declare no potential conflicts of interest.

Authors' Contributions

Wenguang Xu, Linlin Jiang, and Meng Zhou were involved in the study conception and design. Hongbo Zhang, Xinyu Zhang, and Zichen Cao helped analyze and interpret the data. Wenguang Xu and Linlin Jiang were involved in the drafting and composition of the manuscript.

Acknowledgments

This study was supported by the Natural Science Foundation of Jiangsu Province (BK20210080), Key Research and Development Projects of Jiangsu Province (BE2022671), and Nanjing Cancer Clinical Medical Center.

Supplementary Materials

Supplementary Table S1: clinicopathologic characteristics of HNSCC patients in TCGA cohort. Supplementary Table S2: clinicopathologic characteristics of HNSCC patients in the GEO cohort. Supplementary Table S3: gene symbols of lysine crotonylation regulators. Supplementary Figure 1: expression of lysine crotonylation regulators in HNSCC with different clinicopathological features. Expression levels of 18 lysine crotonylation regulators in HNSCC with (A) different T stage groups, (B) with or without lymph node metastasis, and (C) different histologic grades. $^{*}p < 0.05$, $^{**}p < 0.01$, and $^{***}p < 0.001$. Supplementary Figure 2: construction of prognostic signatures based on the crotonylation regulators in TCGA-HNSCC. (A) Univariate Cox regression of lysine crotonylation regulators on the prognosis of HNSCC patients in TCGA dataset. (B) The coefficient profile was plotted against the log (lambda) sequence. Selection of the optimal parameter (lambda) in the LASSO model for HNSCC. (C) LASSO coefficient profiles of the 18 crotonylation regulators in HNSCC. *(Supplementary Materials)*

References

[1] F. Bray, J. Ferlay, I. Soerjomataram, R. L. Siegel, L. A. Torre, and A. Jemal, "Global cancer statistics 2018: GLOBOCAN estimates of incidence and mortality worldwide for 36 cancers in 185 countries," *CA: a Cancer Journal for Clinicians*, vol. 68, no. 6, pp. 394–424, 2018.

[2] D. E. Johnson, B. Burtness, C. R. Leemans, V. W. Y. Lui, J. E. Bauman, and J. R. Grandis, "Head and neck squamous cell carcinoma," *Nature Reviews Disease Primers*, vol. 6, no. 1, p. 92, 2020.

[3] B. Patel and N. F. Saba, "Current aspects and future considerations of EGFR inhibition in locally advanced and recurrent metastatic squamous cell carcinoma of the head and neck," *Cancers*, vol. 13, no. 14, p. 3545, 2021.

[4] Z. S. Buchwald and N. C. Schmitt, "Immunotherapeutic strategies for head and neck cancer," *Otolaryngologic Clinics of North America*, vol. 54, no. 4, pp. 729–742, 2021.

[5] M. B. Amin, F. L. Greene, S. B. Edge et al., "The Eighth Edition AJCC Cancer Staging Manual: continuing to build a bridge from a population-based to a more "personalized" approach to cancer staging," *CA: A Cancer Journal for Clinicians*, vol. 67, no. 2, pp. 93–99, 2017.

[6] B. R. Sabari, D. Zhang, C. D. Allis, and Y. Zhao, "Metabolic regulation of gene expression through histone acylations," *Nature Reviews: Molecular Cell Biology*, vol. 18, no. 2, pp. 90–101, 2017.

[7] G. Figlia, P. Willnow, and A. A. Teleman, "Metabolites regulate cell signaling and growth via covalent modification of proteins," *Developmental Cell*, vol. 54, no. 2, pp. 156–170, 2020.

[8] A. T. Blasl, S. Schulze, C. Qin, L. G. Graf, R. Vogt, and M. Lammers, "Post-translational lysine ac(et)ylation in health, ageing and disease," *Biological Chemistry*, vol. 403, 2021.

[9] J. Y. Hou, L. Zhou, J. L. Li, D. P. Wang, and J. M. Cao, "Emerging roles of non-histone protein crotonylation in biomedicine," *Cell & Bioscience*, vol. 11, no. 1, p. 101, 2021.

[10] W. Xu, J. Wan, J. Zhan et al., "Global profiling of crotonylation on non-histone proteins," *Cell Research*, vol. 27, no. 7, pp. 946–949, 2017.

[11] B. R. Sabari, Z. Tang, H. Huang et al., "Intracellular crotonyl-CoA stimulates transcription through p300-catalyzed histone crotonylation," *Molecular Cell*, vol. 69, no. 3, p. 533, 2018.

[12] X. Liu, W. Wei, Y. Liu et al., "MOF as an evolutionarily conserved histone crotonyltransferase and transcriptional activation by histone acetyltransferase-deficient and crotonyltransferase-competent CBP/p300," *Cell Discovery*, vol. 3, no. 1, p. 17016, 2017.

[13] L. Kollenstart, A. J. L. de Groot, G. M. C. Janssen et al., "Gcn5 and Esa1 function as histone crotonyltransferases to regulate crotonylation-dependent transcription," *Journal of Biological Chemistry*, vol. 294, no. 52, pp. 20122–20134, 2019.

[14] E. Koutelou, A. T. Farria, and S. Y. R. Dent, "Complex functions of Gcn5 and Pcaf in development and disease," *Biochimica et Biophysica Acta (BBA) - Gene Regulatory Mechanisms*, vol. 1864, no. 2, article 194609, 2021.

[15] W. Wei, X. Liu, J. Chen et al., "Class I histone deacetylases are major histone decrotonylases: evidence for critical and broad function of histone crotonylation in transcription," *Cell Research*, vol. 27, no. 7, pp. 898–915, 2017.

[16] J. L. Feldman, J. Baeza, and J. M. Denu, "Activation of the protein deacetylase SIRT6 by long-chain fatty acids and

widespread deacylation by mammalian sirtuins," *Journal of Biological Chemistry*, vol. 288, no. 43, pp. 31350–31356, 2013.

[17] X. Bao, Y. Wang, X. Li et al., "Identification of 'erasers' for lysine crotonylated histone marks using a chemical proteomics approach," *eLife*, vol. 3, 2014.

[18] Y. Li, B. R. Sabari, T. Panchenko et al., "Molecular coupling of histone crotonylation and active transcription by AF9 YEATS domain," *Molecular Cell*, vol. 62, no. 2, pp. 181–193, 2016.

[19] D. Zhao, H. Guan, S. Zhao et al., "YEATS2 is a selective histone crotonylation reader," *Cell Research*, vol. 26, no. 5, pp. 629–632, 2016.

[20] F. H. Andrews, S. A. Shinsky, E. K. Shanle et al., "The Taf14 YEATS domain is a reader of histone crotonylation," *Nature Chemical Biology*, vol. 12, no. 6, pp. 396–398, 2016.

[21] X. Xiong, T. Panchenko, S. Yang et al., "Selective recognition of histone crotonylation by double PHD fingers of MOZ and DPF2," *Nature Chemical Biology*, vol. 12, no. 12, pp. 1111–1118, 2016.

[22] H. Huang, D. L. Wang, and Y. Zhao, "Quantitative crotonylome analysis expands the roles of p300 in the regulation of lysine crotonylation pathway," *Proteomics*, vol. 18, no. 15, article e1700230, 2018.

[23] X. Han, X. Xiang, H. Yang et al., "p300-catalyzed lysine crotonylation promotes the proliferation, invasion, and migration of HeLa cells via heterogeneous nuclear ribonucleoprotein A1," *Analytical Cellular Pathology (Amsterdam)*, vol. 2020, article 5632342, 6 pages, 2020.

[24] J. Wan, H. Liu, and L. Ming, "Lysine crotonylation is involved in hepatocellular carcinoma progression," *Biomedicine and Pharmacotherapy*, vol. 111, pp. 976–982, 2019.

[25] K. Li and Z. Wang, "Histone crotonylation-centric gene regulation," *Epigenetics & Chromatin*, vol. 14, no. 1, p. 10, 2021.

[26] G. Jiang, C. Li, M. Lu, K. Lu, and H. Li, "Protein lysine crotonylation: past, present, perspective," *Cell Death & Disease*, vol. 12, no. 7, p. 703, 2021.

[27] A. Ntorla and J. R. Burgoyne, "The regulation and function of histone crotonylation," *Frontiers in Cell and Developmental Biology*, vol. 9, article 624914, 2021.

[28] D. Szklarczyk, A. L. Gable, D. Lyon et al., "STRING v11: protein-protein association networks with increased coverage, supporting functional discovery in genome-wide experimental datasets," *Nucleic Acids Research*, vol. 47, no. D1, pp. D607–D613, 2019.

[29] M. Tan, H. Luo, S. Lee et al., "Identification of 67 histone marks and histone lysine crotonylation as a new type of histone modification," *Cell*, vol. 146, no. 6, pp. 1016–1028, 2011.

[30] Z. Arany, W. R. Sellers, D. M. Livingston, and R. Eckner, "E1A-associated p300 and CREB-associated CBP belong to a conserved family of coactivators," *Cell*, vol. 77, no. 6, pp. 799-800, 1994.

[31] I. Dutto, C. Scalera, and E. Prosperi, "CREBBP and p300 lysine acetyl transferases in the DNA damage response," *Cellular and Molecular Life Sciences*, vol. 75, no. 8, pp. 1325–1338, 2018.

[32] E. Kalkhoven, "CBP and p300: HATs for different occasions," *Biochemical Pharmacology*, vol. 68, no. 6, pp. 1145–1155, 2004.

[33] N. Vo and R. H. Goodman, "CREB-binding protein and p300 in transcriptional regulation," *Journal of Biological Chemistry*, vol. 276, no. 17, pp. 13505–13508, 2001.

[34] R. H. Goodman and S. Smolik, "CBP/p300 in cell growth, transformation, and development," *Genes and Development*, vol. 14, no. 13, pp. 1553–1577, 2000.

[35] M. Muraoka, M. Konishi, R. Kikuchi-Yanoshita et al., "p300 gene alterations in colorectal and gastric carcinomas," *Oncogene*, vol. 12, no. 7, pp. 1565–1569, 1996.

[36] F. Ruhlmann, I. M. Windhof-Jaidhauser, C. Menze et al., "The prognostic capacities of CBP and p300 in locally advanced rectal cancer," *World Journal of Surgical Oncology*, vol. 17, no. 1, p. 224, 2019.

[37] H. Hu, S. Yin, R. Ma et al., "CREBBP knockdown suppressed proliferation and promoted chemo-sensitivity via PERK-mediated unfolded protein response in ovarian cancer," *Journal of Cancer*, vol. 12, no. 15, pp. 4595–4603, 2021.

[38] N. Bharathy, S. Suriyamurthy, V. K. Rao et al., "P/CAF mediates PAX3–FOXO1-dependent oncogenesis in alveolar rhabdomyosarcoma," *Journal of Pathology*, vol. 240, no. 3, pp. 269–281, 2016.

[39] M. Malatesta, C. Steinhauer, F. Mohammad, D. P. Pandey, M. Squatrito, and K. Helin, "Histone acetyltransferase PCAF is required for Hedgehog-Gli-dependent transcription and cancer cell proliferation," *Cancer Research*, vol. 73, no. 20, pp. 6323–6333, 2013.

[40] M. Z. Ying, J. J. Wang, D. W. Li et al., "The p300/CBP associated factor is frequently downregulated in intestinal-type gastric carcinoma and constitutes a biomarker for clinical outcome," *Cancer Biology & Therapy*, vol. 9, no. 4, pp. 312–320, 2010.

[41] X. Gai, K. Tu, C. Li, Z. Lu, L. R. Roberts, and X. Zheng, "Histone acetyltransferase PCAF accelerates apoptosis by repressing a GLI1/BCL2/BAX axis in hepatocellular carcinoma," *Cell Death & Disease*, vol. 6, no. 4, article e1712, 2015.

Hindawi
BioMed Research International
Volume 2022, Article ID 3191474, 22 pages
https://doi.org/10.1155/2022/3191474

Research Article

Predicting the Immune Microenvironment and Prognosis with a NETosis-Related lncRNA Signature in Head and Neck Squamous Cell Carcinoma

Xiaohua He,[1,2] Yinglu Xiao,[1] Shan Liu,[1,2] Ruyan Deng,[1,2] Zhiming Li,[1,2] and Xianying Zhu[1,3]

[1]*State Key Laboratory of Oncology in South China, Collaborative Innovation Center for Cancer Medicine, Sun Yat-sen University Cancer Center, Guangzhou, China*
[2]*Department of Medical Oncology, Sun Yat-sen University Cancer Center, Sun Yat-sen University, Guangzhou, China*
[3]*Department of Intensive Care Unit, Sun Yat-sen University Cancer Center, Sun Yat-sen University, Guangzhou, China*

Correspondence should be addressed to Zhiming Li; lizhm@sysucc.org.cn and Xianying Zhu; zhuxy@sysucc.org.cn

Xiaohua He, Yinglu Xiao, and Shan Liu contributed equally to this work.

Received 20 April 2022; Revised 16 July 2022; Accepted 9 August 2022; Published 12 September 2022

Academic Editor: Jing Zhang

Background. The mechanistic aspects of the involvement of long noncoding RNAs (lncRNAs) in NETosis, the process of neutrophil extracellular trap (NET) formation in head and neck squamous cell carcinoma (HNSCC), lack comprehensive elucidation. The involvement of these molecules in the immune microenvironment and plausible HNSCC prognosis remain to see the light of the day. The plausible functioning of NETosis-related lncRNAs with their plausible prognostic impact in HNSCC was probed in this work. *Methods*. The scrutiny of lncRNAs linked to NETosis entailed the probing of twenty-four genes associated with the process employing Pearson's correlation analysis on HNSCC patients' RNA sequencing data from The Cancer Genome Atlas (TCGA) database. The application of univariate, least absolute shrinkage and selection operator (LASSO), and multivariate Cox regression analyses yielded a NETosis-related lncRNA signature that was subjected to probing for its suitability in prognosis employing survival and nomogram analyses. *Results*. The NETosis-related lncRNA signature inclusive of five lncRNAs facilitated patients to be segregated as high-risk and low-risk groups with the former documenting a poor prognosis. Regression unearthed that the risk score was an independent factor for prognosis. The receiver operating characteristic (ROC) or receiver operating characteristic curve analysis documented a one-year area under time-dependent ROC curve (AUC) value of 0.711 that is corroborative of the accuracy of this signature. Additional probing documented an evident enriching of immune-linked pathways in the low-risk patients, while the high-risk patients documented an immunologically "cold" profile as per the infiltration of immune cells. We verified lncRNA expression from our NETosis-related lncRNA signature in vitro, which reflects the reliability of our model to a certain extent. Moreover, we also verified the function of the lncRNA. We found that LINC00426 contributes to the innate immune cGAS-STING signaling pathway, which explain to some extent the role of our prognostic model in predicting "hot" and "cold" tumors. *Conclusions*. The plausible prognostic relevance of the NETosis-related lncRNA signature (with five lncRNAs) emerges that is suggestive of its promise in targeting HNSCC.

1. Introduction

HNSCCs arise from the mucosal epithelium in the oral cavity, pharynx, and larynx and occupy the sixth position in global cancer incidence [1]. The most ubiquitously implicated risk factors for HNSCC encompass oncogenic human papillomavirus (HPV) infection, tobacco smoke, and excessive alcohol consumption [2]. HNSCC is remarkably heterogeneous for the anatomical location of cell origination, various etiologies, and carcinogenic mechanisms [3]. Most

patients receive a late-stage HNSCC diagnosis without a clinical history of premalignancy [1]. Notwithstanding expanding surgical and nonsurgical approaches (inclusive of the radiotherapy, chemotherapy, and immunotherapy), the clinical prognosis of HNSCC still remains a roadblock, with the 5-year survival rate below 50% [4, 5]. Therefore, the probing of several plausible prognostic markers that accurately predict the outcome of HNSCC emerges as vital to assist the delineation of individualized treatment plans.

Neutrophil extracellular traps (NETs) are web-like DNA structures coated with histones, proteases, and granular and cytosolic proteins [6] and are released by neutrophils to trap microorganisms, and the process of their formation is referred to as NETosis [7]. The possible involvement of NETs in noninfectious diseases, such as autoimmunity, coagulation, acute injuries, and cancer, has been documented [6]. Its involvement in increased primary tumor growth, metastasis, and complications like venous thromboembolism in malignancies has also been probed [8]. It has been corroborated that NET extrusion induced by tumor-secreted CXCR1 and CXCR2 ligands exerts a protective effect on the malignancies from the cytotoxicity of natural killer (NK) cells and T cells [9]. The augmentation of the cell cycle to boost metastasis within the bloodstream by NETs to expand the metastatic potential of circulating tumor cells is also known [10]. Yang et al. demonstrated that the DNA component of NETs (NET-DNA) promotes cancer metastasis via the transmembrane protein CCDC25 [11]. However, studies probing the role of NETosis in HNSCC are few. Li et al. found that a hypercoagulable state is driven in oral squamous cell carcinoma via systemic inflammation to stimulate neutrophils to prime and release NETs [12]. While a recent study documented the scrutiny of a NET-related gene signature for predicting non-small-cell lung cancer prognosis [13], the role and functioning of NETosis warrants more research. Therefore, it is meaningful to discern novel NETosis-linked biomarkers to recognize the molecular mechanistic aspects of NETosis for prognosis prediction in HNSCC patients.

lncRNAs are RNAs exceeding 200 nucleotides in length and do not participate in protein coding but are involved in controlling gene expression [14]. In lung cancer, the involvement of lncRNAs to regulate NETs is known [13]. However, the probing of NETosis-associated lncRNAs in HNSCC is yet to see the light of the day making the prognostic value of NETosis-associated lncRNAs unclear.

Immunotherapy has revolutionized cancer treatment over the past two decades, mostly employing immune checkpoint blockade (ICB) approaches. As of 2019, ICB (pembrolizumab, an IgG4 humanized antibody to PD-1) was approved as first-line or subsequent therapy of recurrent or metastatic squamous cell carcinoma of the head and neck [15]. The tumor microenvironment is vitally linked to the response to ICB. ICB efficacy is poor in "cold" tumors documenting lower PD-L1 levels in tumor cells, macrophages, and immune cells [4]. The conversion of these "cold" tumors into "hot" ones for ICB therapy in HNSCC can augment the response [16]. Although the sensitization of tumors to immunotherapy (PD-1 + CTLA-4 dual checkpoint blockade) by NETosis inhibition has been documented recently [9], such studies are still limited. The probing of the relationship between NETosis and the tumor immune microenvironment to further comprehend "cold" HNSCC is warranted to facilitate optimal treatment systems for "cold" HNSCC.

This work was aimed at scrutinizing NETosis-related lncRNAs in HNSCC to comprehend the molecular and signaling pathways of this phenomenon in this malignancy and predict the prognosis in these patients. In addition, the links between NETosis and tumor immune microenvironment were further probed to provide a speculative basis in "cold" HNSCC therapy.

2. Materials and Methods

2.1. Patient Details. The RNA sequencing data and patient characteristics of HNSCC patients (502 malignant and 44 normal samples) were sourced from the TCGA database (https://portal.gdc.cancer.gov/repository). The clinicopathological attributes were inclusive of age, gender, smoking status, HPV status, tumor grade, tumor stage, survival time, and survival status. Following the exclusion of the normal samples ($n = 44$) and a patient with the overall survival (OS) missing, 499 patients documenting complete survival and sequencing data were enrolled in this work. Figure S1 is illustrative of the workflow employed.

2.2. Identifying NETosis-Related lncRNAs. Firstly, 24 NETosis-associated genes were identified by searching literature (Table S1) [9, 17–25]. lncRNA and protein-coding gene annotations in the Ensembl human genome browser GRCh38.p13 (http://asia.ensembl.org/index.html) then ensued [26]. The correlation between the lncRNAs and the expression of NETosis-associated genes was probed employing Pearson's correlation coefficients. NETosis-related lncRNAs were determined at $P < 0.001$ and $|R| > 0.4$.

2.3. Establishment and Validation of the NETosis-Related lncRNAs Prognostic Signature. This entailed the random assignment (2 : 1) of 499 patients into a training cohort and a validation cohort. NETosis-related lncRNAs for prognosis were first scored employing univariate Cox regression analysis of the patients' survival data in the training cohort ($P < 0.05$). LASSO Cox regression ensued of these prognostic NETosis-related lncRNAs to diminish the chance of overfitting as much as possible. Subsequent application of multivariate analyses facilitated the indication of the candidate lncRNAs significantly involved in OS prognosis prediction. Five relevant NETosis-related lncRNAs were identified for the prognostic model as per the lowest Akaike information criterion (AIC) value. The risk scores of the HNSCC patients were obtained by the normalized lncRNA expression levels and the corresponding regression coefficients. This entailed the following formula for its computation ($\text{risk score} = \beta\text{gene}(1) \times \text{EXPgene}(1) + \beta\text{gene}(2) \times \text{EXPgene}(2) + \cdots + \beta\text{gene}(n) \times \text{EXPgene}(n)$) with the discerned lncRNA expression level as EXPgene and its multivariate Cox regression analysis coefficient as β.

The median value of the risk score was employed to categorize patients in the training cohort into high-risk (≥ median number) and low-risk (<median number) groups. The following tests ensued to corroborate the signature: intergroup OS was scored by Kaplan-Meier analysis with the "survival" and "survminer" R package. The prediction accuracy was probed by the "survival ROC" R package employing time-dependent receiver operating characteristic (ROC) curve analysis. The scrutiny of the utility of this signature as an independent prognostic factor as opposed to other clinical attributes entailed multivariate Cox regression analysis. Subsequent corroboration of this signature in the validation cohort entailed the use of the aforementioned formula to quantitate the risk score in individual patients. The cutoff value employed in the training cohort was applied in validation cohort with the categorization of patients as high-risk and low-risk groups. Corroboration entailed both the Kaplan-Meier and the time-dependent ROC analyses.

2.4. The Predictive Nomogram. We further depicted nomograms built on the "rms" R package with the aforementioned lncRNA signature and other prognostic contributors for OS prediction in HNSCC patients (1 year, 3 years, and 5 years). We also computed the calibration curve to probe its accuracy.

2.5. Functional Enrichment Analysis. This entailed scrutiny of the Kyoto Encyclopedia of Genes and Genomes (KEGG) pathway analysis with Gene set enrichment analysis (GSEA) (versionv4.1.0, http://www.gsea-msigdb.org/gsea/downloads) in the risk groups employing our NETosis-related lncRNA signature.

2.6. All-Inclusive Probing of Immune Cell Profile and ICB Therapy in Both Risk Groups. The measure of tumor-infiltrating immune cells in HNSCC samples was probed employing CIBERSORT [27], CIBERSORT–ABS [27], QUANTISEQ [28], XCELL [29], MCPcounter [30], EPIC [31], and TIMER [32] algorithms. Both risk groups were scrutinized for NETosis and immune functioning by ssGSEA or single-sample GSEA employing the "GSVA" package, while literature was scored for plausible genes of immune checkpoint molecules. In order to gauge the impact of the signature in patient prognosis post-ICB therapy, ssGSEA was done with the gene set of NETosis employing that the "GSVA" package of R in two cohorts in which ICB therapy (anti-PD-L1/PD-1) was administered [33, 34] to get individual NETosis scores. These scores (median values) were utilized to group patients into high and low scores. The relevance of the signature to predict ICB therapy response entailed relevant survival analyses.

2.7. Chemotherapy Response with Our NETosis-Related lncRNA Signature. The response to chemotherapy in the patients was scored employing the R package "pRRophetic" [35].

2.8. Cell Culture. This work entailed the use of normal human immortalized nasopharyngeal epithelial cell line (NP69) and human nasopharyngeal carcinoma cell lines (CNE1, HNE1, TW03, and SUNE1). All cells were cultivated in RPMI-1640 medium (GIBCO) supplemented with 7% fetal bovine serum (ExCell Bio) in 5% CO_2 at 37°C.

2.9. Quantitative Real-Time PCR. Total RNA of NP69, CNE1, HNE1, or TW03 cells was collected employing the RNA-Quick Purification kit (ESscience) adhering to the requisite and prescribed protocols. cDNA was synthesized employing the RNA reverse transcription kit (ESscience) as per the prescribed instructions. Real-time PCR amplification ensued with SYBR Green (Vazyme) and the following sets of primers: AC079336.5 (5′-CACAATCCCACGCTGTACCT-3′ and 5′-CAGGTGTCCTCAGAAAGCGT-3′), AL645933.2 (5′-GCTTGCTGACTCTGTGGACT-3′ and 5′-AGTTCA GGTCACCAGTCCCT-3′), LINC00426 (5′-TGCAGGCTT TGTAGACCCTC-3′ and 5′-TTGCGGGTGATTTACT GGGG-3′), LINC00623 (5′-AGCTTCTCTGCAGGTCACA C-3′ and 5′-TGGGCCACCCTTGAACATTT-3′), and GADPH (5′-CTGGGCTACACTGAGCACC-3′ and 5′-AAGTGGTCGTTGAGGGCAATG-3′). All samples were subjected to scrutiny in triplicate, and each target gene was normalized by GADPH. qPCR and analyses were performed using the LightCycler 480 Instrument (ROCHE) and software.

2.10. Colony Formation Assay. CNE1 or SUNE1 cells were placed in triplicate with 500 cells per well in 12-well plates (BIOFIL) and cultured in RPMI-1640 medium (GIBCO) supplemented with 7% fetal bovine serum (ExCell Bio) for 10 days. Then, the plates were washed twice with PBS and fixed with 75% alcohol for 1 hour. After washing twice with PBS, the cells were stained with crystal violet for 2 hours. Then, the crystal violet was washed off, and the number of colonies was counted.

2.11. Cell Proliferation Assay. MTT assay was used to assess the relative viability of the cells. Briefly, cells were seeded at 1000 cells per well in 96-well plates and cultured overnight in RPMI-1640 medium containing 7% FBS at 24 hours post-transfection, respectively. Add 10 μL of MTT labeling reagent and continue incubation for 4-6 h. Read the spectrophotometry of the samples at 570 nm. Data were analyzed using GraphPad Prism 8 (GraphPad Software, La Jolla, CA, USA).

2.12. Wound Healing Assay. Cells were seeded into 6-well tissue culture plates at an appropriate density of 50-60% and cultured in RPMI-1640 medium (GIBCO) supplemented with 7% fetal bovine serum (ExCell Bio) for 24 hours before becoming a monolayer. A linear wound was scraped on the cell monolayer with a 20 μL pipette tip. After scraping, the cells were washed off by gently rinsing the medium twice and then cultured in RPMI-1640 medium without fetal bovine serum. Wounds were imaged under a microscope at 0, 24, 48, and 72 hours. Three areas were randomly photographed.

2.13. Plasmids and Transfection. LINC00426 plasmids and control plasmids were purchased from Shanghai Genechem

Table 1: Clinical characteristics of patients in the training cohort and validation cohort.

	Training cohort $N = 333$		Validation cohort $N = 166$		P value
	No.	%	No.	%	
Age					
≤60	164	49.2	80	48.2	0.824
>60	169	50.8	86	51.8	
Gender					
Female	87	26.4	46	27.7	0.706
Male	246	73.9	120	72.3	
Smoking					
Former and current smoker	204	61.3	110	66.3	0.276
Nonsmoker	129	38.7	56	33.7	
HPV status					
Negative	53	15.9	26	15.7	
Positive	23	6.9	10	6.0	0.926
Unknown	257	77.2	130	78.3	
Grade					
G1-2	236	70.9	123	74.1	
G3-4	84	25.2	37	22.3	0.749
Unknown	13	3.9	6	3.6	
Stage					
I	17	5.1	8	4.8	
II	45	13.5	24	14.5	
III	56	16.8	22	13.3	0.888
IV	170	51.1	89	53.6	
Unknown	45	13.5	23	13.9	

Co. Ltd. Plasmid transient transfection was performed using Lipofectamine 3,000 (Invitrogen) according to the manufacturer's instructions. And then, cells were collected for subsequent experiments after 24 hours of transfection.

2.14. Western Blotting. Whole-cell extracts were generated by direct lysis with 1× Cell Lysis Buffer (Cell Signaling Technology, #9873) with 1 mM phenylmethylsulphonyl fluoride (PMSF) added immediately before use. Samples with 6× SDS sample buffer added were heated at 100°C for 10 min and resolved by SDS-PAGE and then transferred to a PVDF membrane. The membranes were then examined with primary antibodies, followed by the corresponding HRP-conjugated anti-mouse or anti-rabbit (Proteintech) secondary antibodies. The following antibodies were used: α-tubulin (1 : 1000, Proteintech), cGAS (1 : 1000, Abcepta), TBK1 (1 : 1000, Proteintech), phospho-TBK1 (1 : 1000, CST), STING (1 : 1000, Proteintech), phospho-STING (1 : 1000,CST), IRF3 (1 : 1000, Proteintech), and phospho-IRF3 (1 : 1000, CST).

2.15. Statistical Analyses. The Wilcox test was employed to probe the relative amounts of immune checkpoint molecules and immune cells infiltrating the malignancy in both the risk groups. The lncRNA signature and its link with clinicopathological factors were probed by the chi-squared test. As elucidated above, the identification of the independent factors in OS prognosis entailed multivariate Cox regression analyses. The accuracy of prognosis prediction was gauged by ROC analyses. R software (Version 4.1.0) and SPSS (Version 23.0) were employed for all these computations.

3. Results

3.1. Patient Characteristics in Both Cohorts. Random assignment of HNSCC patients who met eligibility criteria ($n = 499$) was done into training ($N = 333$) and validation ($N = 166$) cohorts in a 2 : 1 ratio. The clinical characteristics and pathological records have been detailed in Table 1. The training cohort included 246 (73.9%) male and 87 (26.4%) female patients with 50.8% patients over 60 years old, while the validation cohort included 120 (72.3%) male and 46 (27.7%) female patients with 51.8% patients over 60 years old. A total of 204 (61.3%) patients and 110 (66.3%) patients had smoking history in the training cohort and validation cohort, respectively. Most of the patients had absence of HPV evaluation in both groups. There were 23 patients (6.9%) confirmed with positive HPV status and 53 patients (15.9%) confirmed with negative HPV status in the training cohort. Similarly, there were 10 patients (6.0%) confirmed with positive HPV status and 26 patients (15.7%) confirmed with negative HPV status in the validation cohort. For the

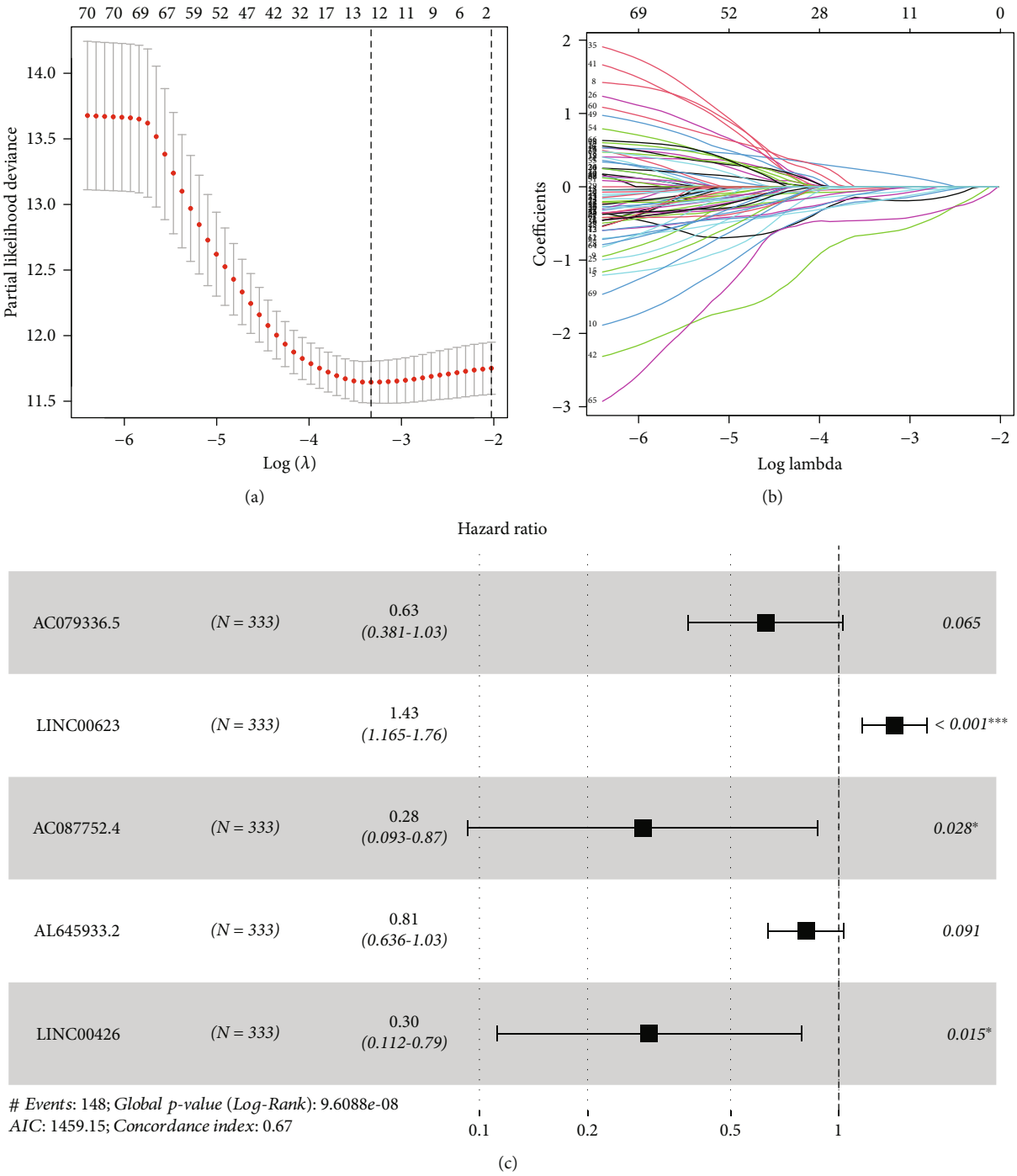

Figure 1: The construction of a prognostic model in head and neck squamous cell carcinoma (HNSCC) patients. (a) 12 NETosis-related lncRNAs were selected by the least absolute shrinkage and selection operator (LASSO) regression model according to minimum criteria. (b) The coefficient of NETosis-related lncRNAs was calculated by LASSO regression. (c) Forest plots showing the results of the multivariate Cox regression analysis between the 5 NETosis-related lncRNAs and overall survival (OS) of HNSCC.

training cohort, pathological evaluation showed that 236 (70.9%) patients were classified as moderate to poor differentiation grade (grade 1-2), and 84 (25.2%) patients were classified as well differentiation grade (grade 3-4). Besides, 17 (5.1%) patients, 45 (13.5%) patients, and 56 (16.8%) patients, and 170 (51.1%) were classified as TNM stages I, II, III, and IV HNSCC, respectively. For the validation cohort, pathological evaluation showed that 123 (74.1%) patients were classified as moderate to poor differentiation grade (grade 1-2), and 37 (22.3%) patients were classified as well differentiation grade (grade 3-4). Besides, 8 (4.8%) patients, 24 (14.5%) patients, and 22 (13.3%) patients and

Table 2: Signature was identified based on the lowest Akaike information criterion (AIC).

Model	Prognostic signature combination	AIC
1	AC093278.2 + AC114730.3 + AC015911.3 + AC079336.5 + AC087392.5 + LINC00623 + RAB11B-AS1+ AL359881.1 + AC087752.4 + AL359921.1 + AL645933.2 + LINC00426	1468.15
2	AC093278.2 + AC015911.3 + AC079336.5 + AC087392.5 + LINC00623 + RAB11B-AS1 + AL359881.1 + AC087752.4 + AL359921.1 + AL645933.2 + LINC00426	1466.15
3	AC093278.2 + AC079336.5 + AC087392.5 + LINC00623 + RAB11B-AS1 + AL359881.1 + AC087752.4 + AL359921.1 + AL645933.2 + LINC00426	1464.52
4	AC093278.2 + AC079336.5 + AC087392.5 + LINC00623 + RAB11B-AS1 + AC087752.4 + AL359921.1 + AL645933.2 + LINC00426	1463.14
5	AC079336.5 + AC087392.5 + LINC00623 + RAB11B-AS1 + AC087752.4 + AL359921.1 + AL645933.2 + LINC00426	1461.83
6	AC079336.5 + LINC00623 + RAB11B-AS1 + AC087752.4 + AL359921.1 + AL645933.2 + LINC00426	1460.50
7	AC079336.5 + LINC00623 + AC087752.4 + AL359921.1 + AL645933.2 + LINC00426	1459.89
8	AC079336.5 + LINC00623 + AC087752.4 + AL645933.2 + LINC00426	1459.15

Table 3: Association between signature and clinicopathological manifestations.

	Training cohort ($N = 333$)		P	Validation cohort ($N = 166$)		P
	High risk $n = 166$	Low risk $n = 167$		High risk $n = 81$	Low risk $n = 85$	
Age (%)						
≤60	76 (45.8)	88 (52.7)	0.207	35 (43.2)	45 (52.9)	0.210
>60	90 (54.2)	79 (47.3)		46 (56.8)	40 (47.1)	
Gender (%)						
Female	46 (27.7)	41 (24.6)	0.512	26 (32.1)	20 (23.5)	0.218
Male	120 (72.3)	126 (75.4)		55 (67.9)	65 (76.5)	
Smoking (%)						
Former and current smoker	96 (57.8)	108 (64.7)	0.200	55 (67.9)	55 (64.7)	0.663
Nonsmoker	70 (42.2)	59 (35.3)		26 (32.1)	30 (35.3)	
HPV status (%)						
Negative	24 (14.5)	29 (17.4)		12 (14.8)	14 (16.5)	
Positive	1 (0.6)	22 (13.2)	<0.001	1 (1.2)	14 (16.5)	0.034
Unknown	141 (84.9)	116 (69.5)		68 (84.0)	62 (72.9)	
Grade (%)						
G1-2	129 (77.7)	107 (64.1)		64 (70.9)	59 (69.4)	
G3-4	33 (19.9)	51 (30.5)	0.020	16 (19.8)	21 (24.7)	0.178
Unknown	4 (2.4)	9 (5.4)		1 (1.2)	5 (5.9)	
Stage (%)						
I	5 (3.0)	12 (7.2)		7 (8.6)	1 (1.2)	
II	20 (12.0)	25 (15.0)		10 (12.3)	14 (16.5)	
III	33 (19.9)	23 (13.8)	0.261	13 (16.0)	9 (10.6)	<0.001
IV	86 (51.8)	84 (50.3)		48 (59.3)	41 (48.2)	
Unknown	22 (13.3)	23 (13.8)		3 (3.7)	20 (23.5)	

89 (53.6%) were classified as TNM stage I, II, III, and IV HNSCC, respectively. Overall, no significant differences were detected in age, gender, smoking history, HPV status, tumor grade, and tumor stage between training and validation cohorts.

3.2. Data Collection and Identification of NETosis-Related lncRNAs. Firstly, we included the data of RNA-seq and clinical data of 528 HNSCC patients from TCGA; then, 44 normal samples and 1 sample lacked survival data were excluded (final patient number = 499). Then, 24 NETosis-linked genes were delineated in HNSCC patients as outlined above. The correlation between 564 NETosis-related lncRNAs and 24 NETosis-linked genes was evaluated by Pearson's correlation analysis, and the NETosis-related lncRNAs were identified according to the standard that the

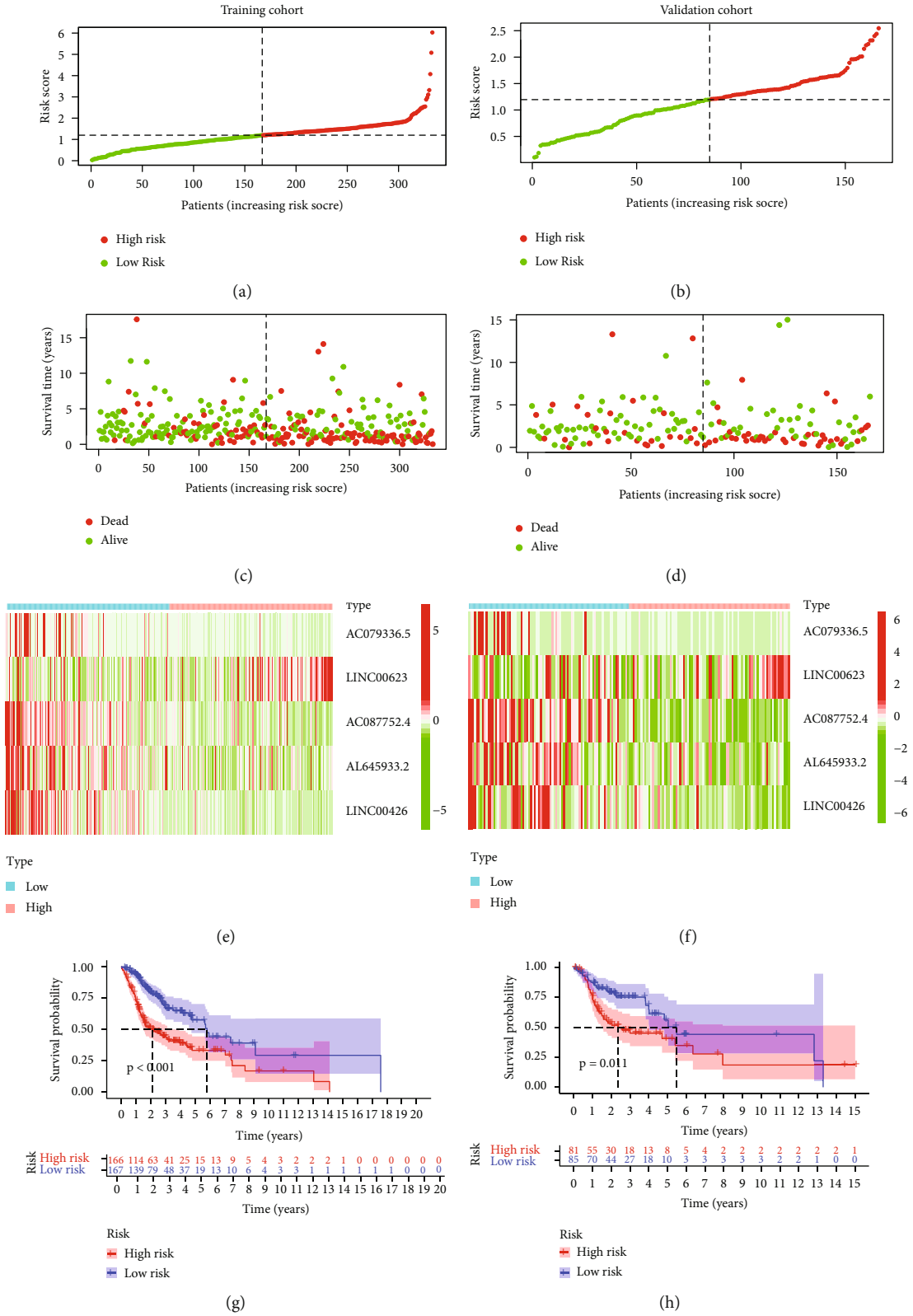

Figure 2: Continued.

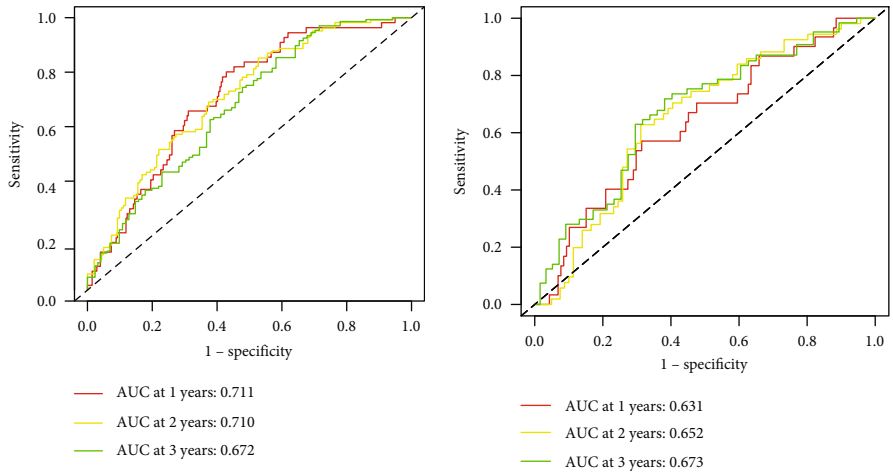

Figure 2: The prognostic performance of the NETosis-related lncRNA signature in the training cohort and validation cohort. (a)The distribution of the risk scores in the training cohort. (b) The distribution of the risk scores in the validation cohort. (c)The scatter plots showing whether the samples were alive or not in the training cohort. (d) The scatter plots showing whether the samples were alive or not in the validation cohort. (e) Heat map of the expression of 5 NETosis-related lncRNAs in the training cohort. (f) Heat map of the expression of 5 NETosis-related lncRNAs in the validation cohort. (g) Kaplan-Meier curves for the overall survival of patients in the high- and low-risk groups in the training cohort. (h) Kaplan-Meier curves for the overall survival of patients in the high- and low-risk groups in the validation cohort. (i) Area under time-dependent ROC curve (AUC) of time-dependent receiver operating characteristic (ROC) curves verified the prognostic accuracy of the risk score in the training cohort. (j) AUC of time-dependent ROC curves verified the prognostic accuracy of the risk score in the validation cohort.

P value was less than 0.001 ($P < 0.001$), and the absolute value of Pearson's correlation coefficient was more than 0.4 ($|R| > 0.4$).

3.3. Building a Prognostic NETosis-Related lncRNA Signature in HNSCC Patients. A total of 499 HNSCC patients were randomly assigned to either training set or validation set. The initial univariate Cox regression analysis unveiled the prognostic lncRNAs in HNSCC patients based on training set. The overlapping prognostic lncRNAs and NETosis-related lncRNAs were identified as the candidate lncRNAs for the NETosis-related lncRNA signature, which resulted in 113 lncRNAs. In other words, these 113 lncRNAs were significantly associated not only with NETosis but also with prognosis of HNSCC patients. Subsequent LASSO Cox regression to reduce the multicollinearity unearthed 12 lncRNAs (Figures 1(a) and 1(b)). Ensuing multivariate Cox regression analysis ultimately highlighted five NETosis-related lncRNAs as optimal prognostic factors in HNSCC patients (Figure 1(c)). The lncRNA signature (AC079336.5, LINC00623, AC087752.4, AL645933.2, and LINC00426) was unveiled employing the least AIC score (Table 2). The computation of the risk score based on the signature was as per the following formula: risk score = $-0.468 \times$ AC 079336.5 + $0.360 \times$ LINC00623 – $1.257 \times$ AC087752.4 – $0.209 \times$ AL645933.2 – $1.215 \times$ LINC00426. Then, each patient in the training set got a risk score based on the formula. The grading of patients in training set was done as high-risk ($n = 166$) and low-risk ($n = 167$) groups with the median risk score value. No evident differences between both risk groups emerged for age, gender, smoking status, and tumor stage, while HPV positive and grade 3-4 were more common in the low-risk group ($P < 0.001$ and $P = 0.020$, respectively) (Table 3). The survival outcome, risk status, and expression profile of lncRNAs of each patient are documented in Figures 2(a), 2(c), and 2(e), respectively, with the high-risk patients documenting a lower probability of survival vs. the low-risk patients. Further, the OS was shortened in the high-risk patients as evidenced by the Kaplan-Meier method (Figure 2(g), $P < 0.001$). The signature documented significant predictive roles regarding the 1-year OS, 2-year OS, and 3-years OS with the AUC of the ROC analyses at 0.711, 0.710, and 0.672, respectively (Figure 2(i)).

3.4. Corroboration of the lncRNA Signature in the Validation Cohort. To verify the accuracy of the NETosis-related lncRNA signature, the computation of the risk score of validation cohort entailed the one employed in the training cohort. On the same lines, the categorization of the validation group patients ensued as high-risk ($N = 81$) and low-risk ($N = 85$) groups (Table 3) employing the aforementioned cutoff value. As shown in Table 3, both groups documented no conspicuous differences for age, gender, smoking status, and tumor grade, while HPV positive and stage I were more common in the low-risk patients ($P = 0.034$ and $P < 0.001$, respectively). The survival outcome, risk status, and lncRNA profile are illustrated in Figures 2(b), 2(d), and 2(f), respectively. On similar lines, the low-risk patient group was demonstrative of an elevated survival vs. the high-risk patients with the latter group demonstrative of a diminished

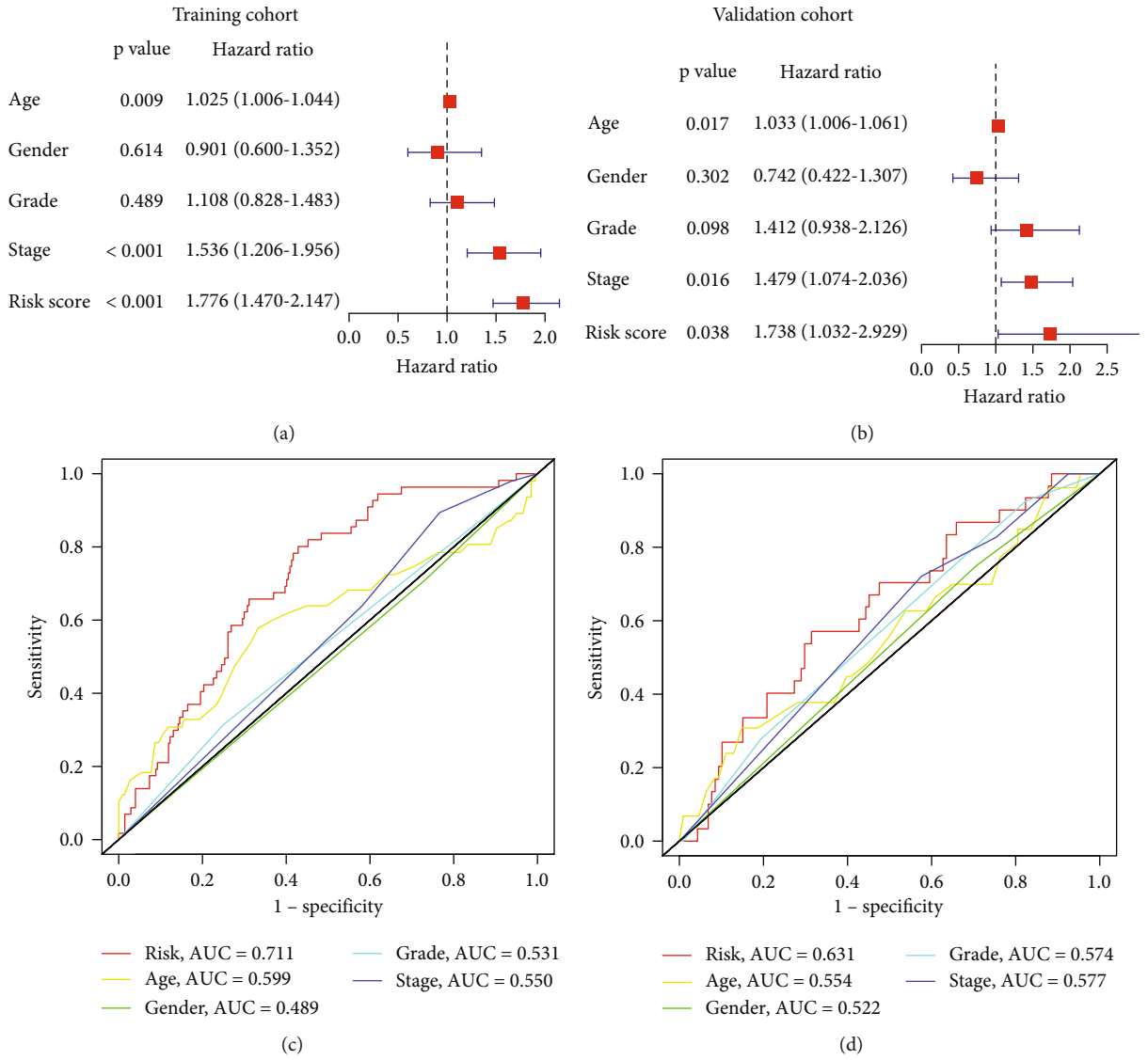

Figure 3: Independent prognostic value of the NETosis-related lncRNA signature in the training cohort and validation cohort. (a) Results of the multivariate Cox regression analysis regarding OS in the training cohort. (b) Results of the multivariate Cox regression analysis regarding OS in the validation cohort. (c) Area under time-dependent ROC curve (AUC) of receiver operating characteristic (ROC) curves compared to the prognostic accuracy of the risk score and other clinicopathological in the training cohort. (d) AUC of ROC curves compared to the prognostic accuracy of the risk score and other clinicopathological in the validation cohort.

OS as evidenced by the Kaplan-Meier method (Figure 2(h), $P = 0.011$). The signature documented significant predictive roles in the 1-year OS, 2-years OS, and 3-years OS with the AUC at 0.631, 0.652, and 0.673, respectively (Figure 2(j)).

3.5. The Independent Functioning of the lncRNA Signature for HNSCC Prognosis. Multivariate Cox regression facilitated the ascertaining of our lncRNA signature as an independent factor in HNSCC prognosis (training cohort: HR = 1.776, 95%CI = 1.470 – 2.147, $P < 0.001$; validation cohort: HR = 1.738, 95%CI = 1.032 – 2.929, $P = 0.038$, respectively) (Figures 3(a) and 3(b)). The ROC curve analysis probing its specificity and sensitivity documented the strength of the signature with an AUC of 0.711 and 0.631 for the training and validation cohorts, respectively, exceeding that of the remaining factors probed (Figures 3(c) and 3(d)). Thus, our NETosis-related lncRNA signature could function as an independent tool for prognosis prediction of HNSCC patients.

3.6. The Predictive Nomogram: Development and Corroboration. To provide a useful prediction model for survival probability of HNSCC patients, a nomogram including clinical features and risk score was constructed. As the multivariate Cox regression analysis indicated the clinical feature including stage, age, and risk score as independent factors, the nomogram was constructed employing the stage, age, and signature (Figure 4(a)).The prediction of the OS (1 year, 3 years, and 5 years) entailed the construction of a prognostic

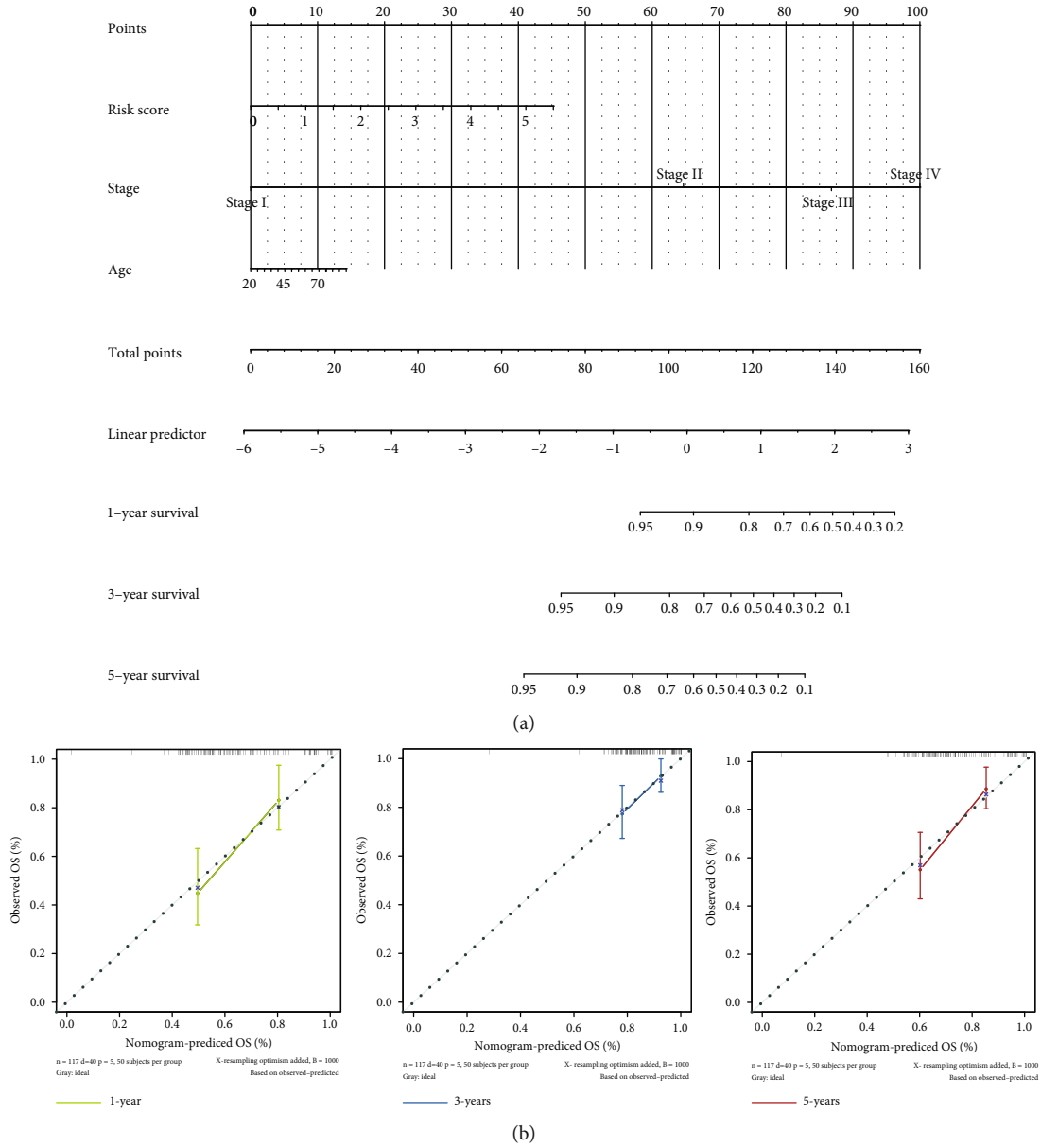

Figure 4: Building and validation of the nomogram to predict the overall survival of patients. (a) Nomogram plot was built based on risk score, age, and stage in the whole cohort. (b) Calibration curve of the nomogram.

nomogram encompassing all the independent factors discerned to depict a risk gauging system comprehensively and visually. The gauging of the OS employing this nonogram via calibration curves was illustrated in Figure 4(b). A conspicuous agreement emerged for the OS predicted by the nonogram and the authentic values across various follow-up periods. The stability and accuracy of our nomogram encompassing our lncRNA signature with clinical features can predict the outcome of individual patients, thus bringing benefits to clinicians and patients.

3.7. GSEA for Vital Pathway Scoring. To explore the potential signal pathways or functions of NETosis-related lncRNAs in HNSCC, we applied gene set enrichment analysis (GSEA) to two cohorts. As elucidated above, this entailed scoring both groups for pathways documenting variations by KEGG analysis employing GSEA. An upregulation emerged for genes in focal adhesion, ECM receptor interaction, and actin cytoskeleton regulation in the high-risk patient set (Figure 5(a)). The low-risk dataset documented a conspicuous upregulation for anticancer immune pathways inclusive of B cell receptor, T cell receptor and FcεRI signaling, natural killer cell-mediated cytotoxicity, and primary immunodeficiency along with the chemokine signaling pathway (Figure 5(b)).The results of the KEGG of NETosis-related lncRNAs suggested that high-risk patient set was more possibly to exhibit tumor metastasis and worse prognosis, while the upregulation of anticancer immune pathways in low-risk

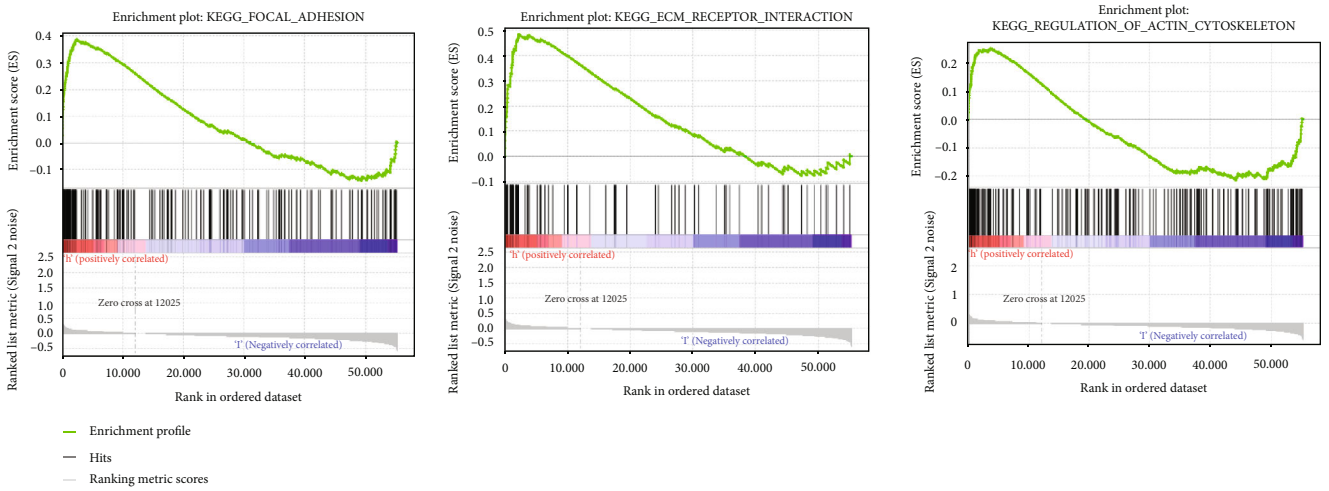

(a)

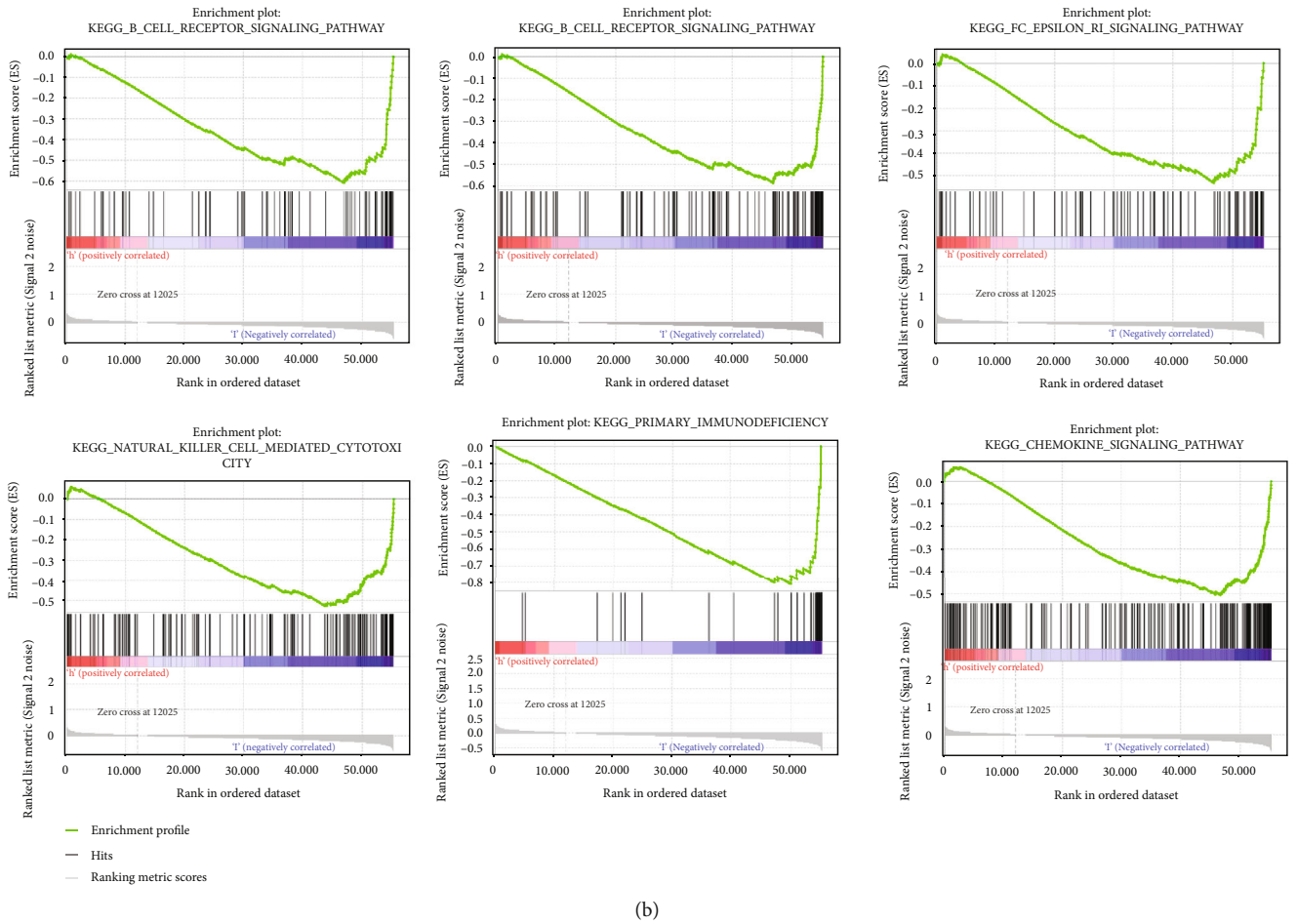

(b)

Figure 5: Gene set enrichment analysis (GSEA) of the two groups based on the NETosis-related lncRNA prognostic signature. (a) GSEA results show significant enrichment of glucose and protein metabolism pathways in the high-risk head and neck squamous cell carcinoma (HNSCC) patients. (b) GSEA results show significant enrichment of immunoregulatory pathways against cancer in the low-risk HNSCC patients.

patient set indicated an immune status unfavorable to tumor growth and better prognosis.

3.8. ICB Therapy Outcome Determined by the Immune and NETosis Status across Both Risk Groups. To investigate the relationship between NETosis-related lncRNAs and immune status, the various algorithms outlined mentioned in the materials section were employed to probe the immune cells and pathways in both the risk groups, which showed significant difference for proportions of different tumor-infiltrating

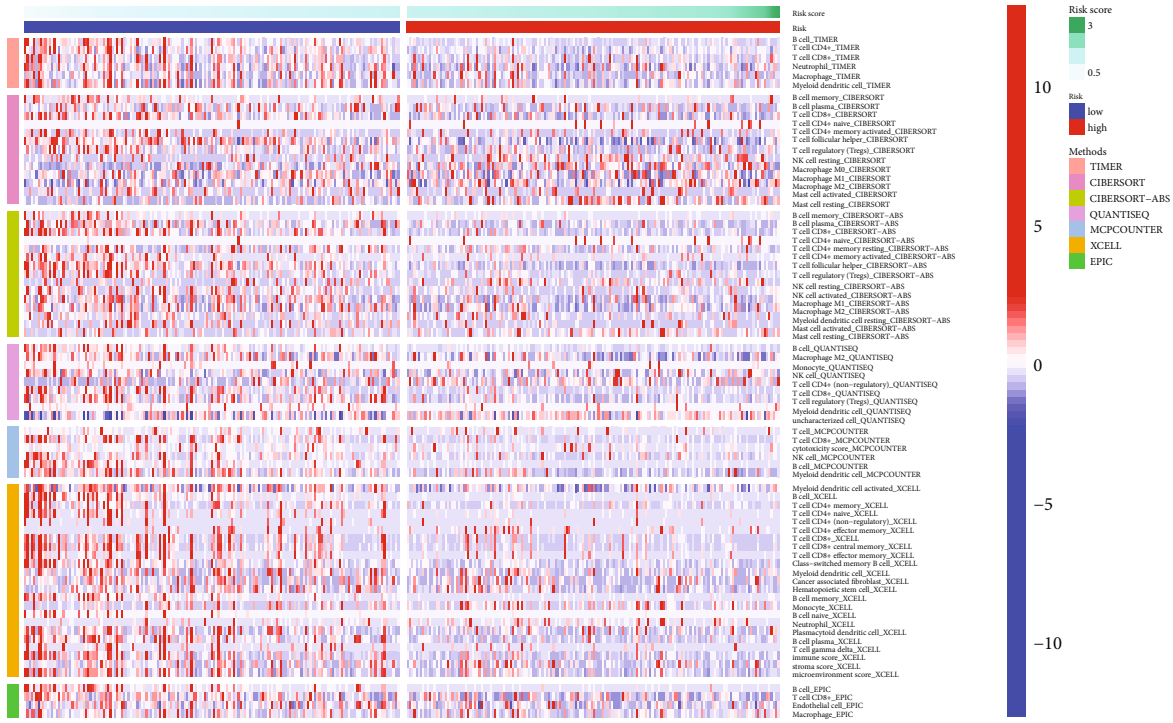

(a)

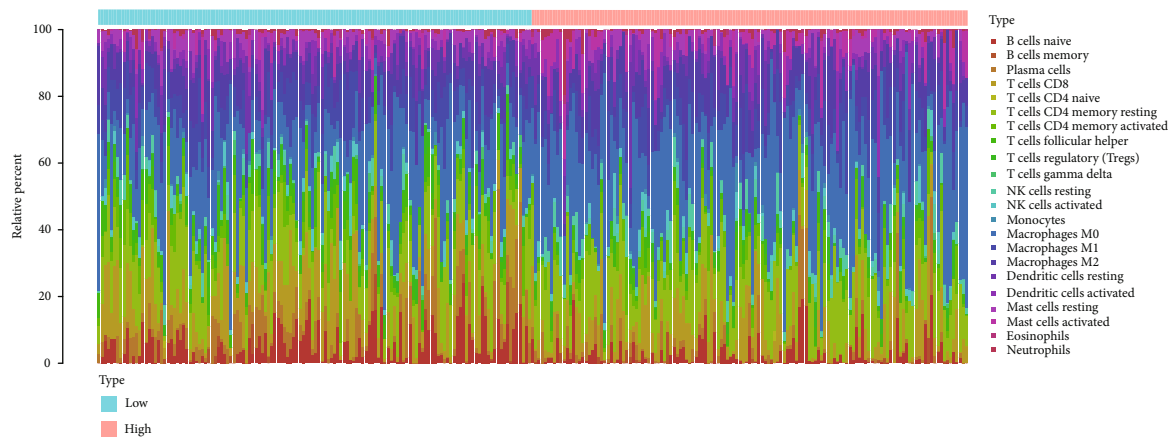

(b)

Figure 6: Continued.

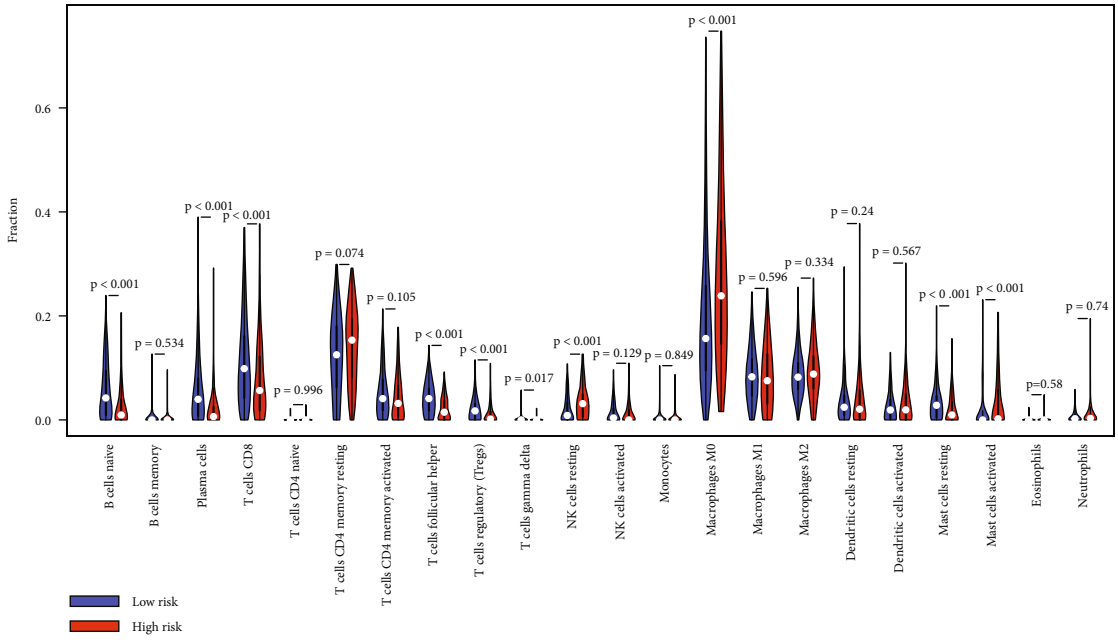

(c)

Figure 6: The immune cell infiltration landscape in head and neck squamous cell carcinoma (HNSCC). (a) Heat map for immune cell infiltration landscape based on the CIBERSORT, CIBERSORT−ABS, QUANTISEQ, XCELL, MCPcounter, EPIC, and TIMER algorithms among high- and low-risk groups. Only items with significant differences will be displayed; P value < 0.05 was controlled. (b) Barplot of the tumor-infiltrating cell proportions based on CIBERSORT algorithm. (c) Violin plot showed the different proportions of tumor-infiltrating cells between different groups based on CIBERSORT algorithm.

immune cells between the low-risk and high-risk groups (Figure 6(a)). Further, CIBERSORT facilitated the immune cell infiltration to be gauged. As shown in Figures 6(b) and 6(c), the high-risk group documented an evident diminishing of naive B cell, plasma cells, CD8+ T cell, follicular helper T cells, regulatory T cells, gamma and delta T cells, and resting and activated mast cells vs. that in the low-risk patient set; however, the proportion of resting NK cells and M0 macrophages was significantly higher in high-risk group.

Then, the difference in immune functions between the two groups was compared. Both groups were demonstrative of evident variations in the ssGSEA for T cell functions like checkpoint (inhibition), cytolytic activity, HLA, inflammation status, T cell coinhibition, and T cell costimulation, which is indicative of the low-risk group documenting an elevated T cell functions (Figure 7(a)). Based on the above considerations, the low-risk cohort can be assigned plausibly as a "hot tumor" demonstrative of elevated immune checkpoint (inhibition) as per the augmented immune cell infiltration and immune responses. Our prognostic signature is demonstrative of an augmented effects in the low-risk group by ICB therapy. The immune checkpoint molecule profiles were then scored in both groups. We found that the low-risk group documented an elevated level of PDL1 (CD274), CTLA4, IDO1, and LAG3 documented vs. the high-risk patient group (Figure 7(b)).

To further explore the prognostic value of NETosis score in patients with immunotherapy, firstly, we confirmed that patients in the high-risk group of HNSCC have higher NETosis score by using the "GSVA" package, which revealed activation of NETosis in the high-risk group vs. the low-risk group (Figure 8(a)). Then, we performed ssGSEA by using the NETosis gene panel in two cohorts administered with immunotherapy employing the "GSVA" package as documented in Materials and Methods to compute the NETosis score of individual samples. Following the categorization of samples as high and low scores employing the median score value, the patients documented a better survival profile when the NETosis score was lowered (Figures 8(b) and 8(c)). This suggests that the low-risk group based on our NETosis-related lncRNA signature has a lower NETosis score and better survival after receiving ICB therapy. These documented outcomes are also corroborative of the plausible impact of our NETosis-related lncRNA signature to predict how fitting ICB would be in these patients.

To summarize, a link between the immune cell status and NETosis score with this lncRNA signature emerged with the high-risk group possibly documenting a diminishing of immune cell infiltration and activity with downregulation of immune checkpoint molecules with lowered survival post-ICB therapy as opposed to the lower-risk cohort. NETosis-related lncRNAs-NETosis-antitumor immunity may be a signaling cascade, which may pave the way for a future novel therapeutic approach to target the malignancy in HNSCC patients.

3.9. Scoring the Chemotherapy Response with the NETosis-Related lncRNA Signature. To further probe the value of our lncRNA signature in patients undergoing varying chemotherapy regimens, the "pRRophetic" approach was

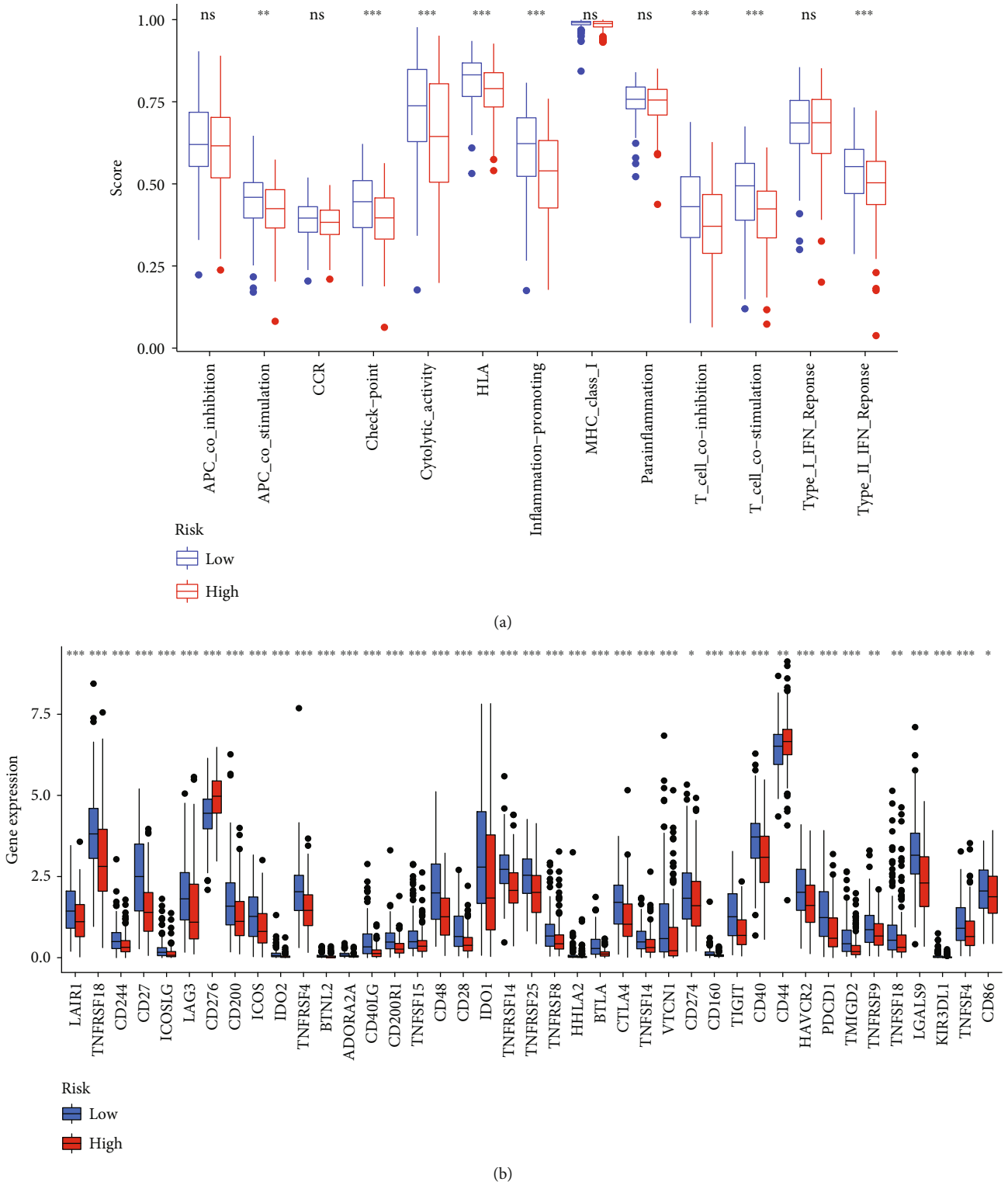

FIGURE 7: Barplot shows that the low-risk group and high-risk groups exhibit different immune statuses. (a) Single-sample gene set enrichment analysis (ssGSEA) for the immune functions between high and low head and neck squamous cell carcinoma (HNSCC) risk groups. (b) The expression levels of immune checkpoints between high and low HNSCC risk groups ($^{*}P < 0.05$, $^{**}P < 0.01$, and $^{***}P < 0.001$).

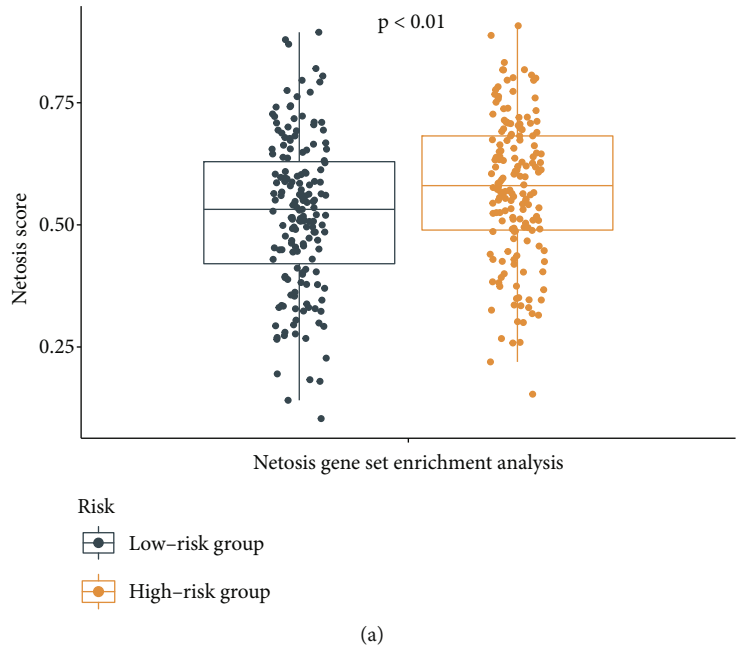

(a)

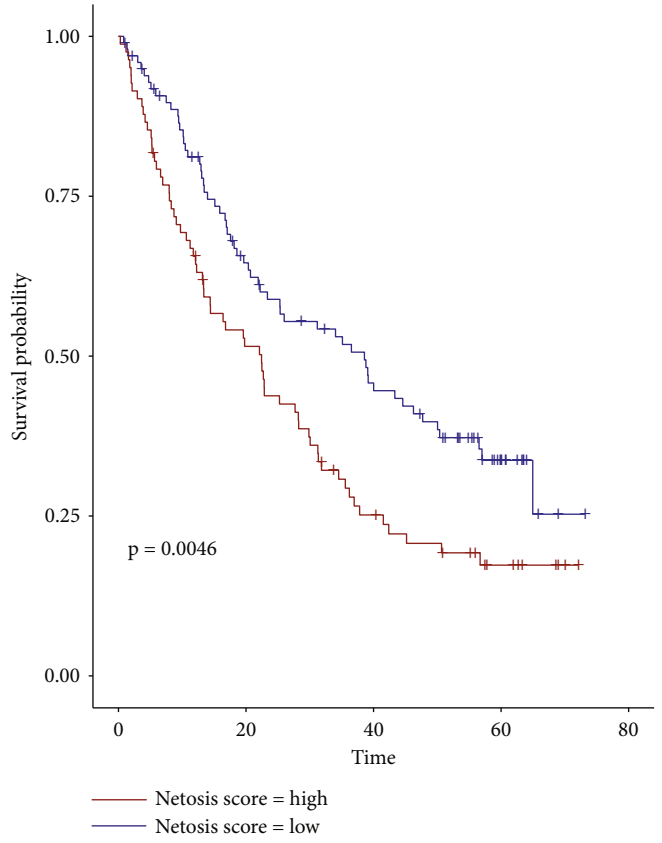

(b)

Figure 8: Continued.

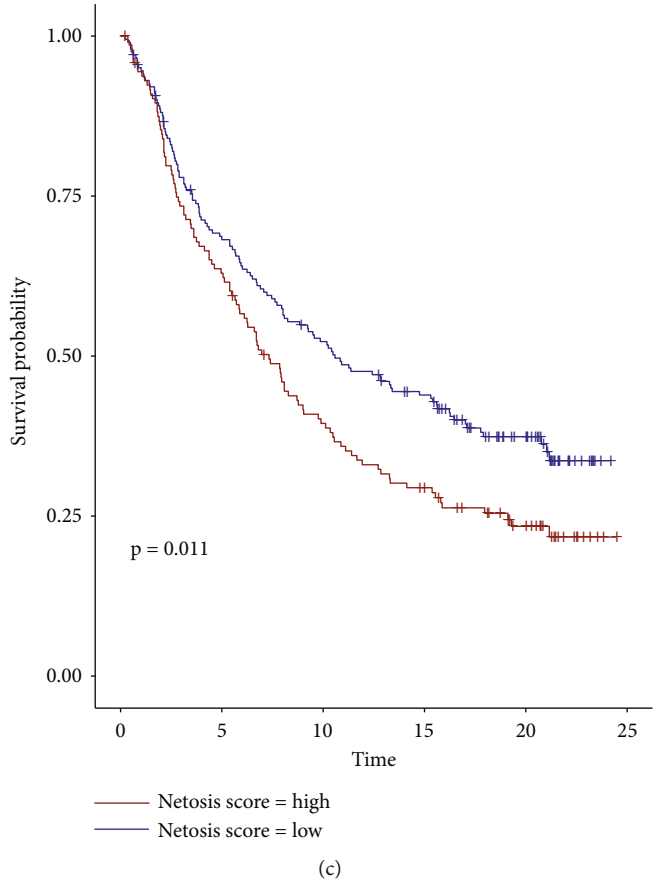

Figure 8: The prognostic value of NETosis score in patients with immunotherapy. (a) ssGSEA was used to calculate the level of NETosis between the high-risk and low-risk group. (b) Kaplan-Meier curves for the overall survival of patients in the David A. Braun et al.'s clear cell renal cell carcinoma cohort. (c) Kaplan-Meier curves for the overall survival of patients in the Sanjeev Mariathasan et al.'s urothelial cancer cohort.

employed to predict the chemotherapy response in both risk groups. A diminished estimated IC_{50} was documented by the low-risk patients vs. the high-risk ones in terms of these chemotherapy drugs: AKT inhibitor VIII, etoposide, JNK inhibitor VIII, metformin, methotrexate, rapamycin, shikonin, vorinostat, and elesclomol (Figures 9(a)–9(i)) ($P < 0.05$). The results showed that patients in the high-risk group had poorer outcomes vs. in the low-risk patients when receiving the above chemotherapy regimens.

3.10. lncRNA Expression from Our NETosis-Related lncRNA Signature In Vitro. There are five lncRNAs in our prognostic model, of which four are protective factors and one is a risk factor. The high-risk group documented an elevated expression of the risk factor with a diminished expression of protective factors. This led to whether tumor cell lines also document this similar expression as the high-risk group. We compared immortalized nasopharyngeal epithelial cell lines (NP69) and human nasopharyngeal carcinoma cell lines (CNE1, HNE1, and TW03). As we described above, protective factors include AC079336.5, AC087752.4, AL645933.2, and LINC00426, while LINC00623 is a risk factor. qPCR revealed lowered expression of LINC00426 in CNE1, HNE1, and TW03 than in NP69 and lowered expression of AC079336.5 and AL645933.2 in CNE1 and TW03 than in NP69, while the expression level of LINC00623 is inconsistent among control cell and tumor cell lines (Figures 10(a)–10(d)). The above results reflect the reliability of our model to a certain extent.

3.11. Verification the Effect of lncRNA on Proliferation and Migration In Vitro. To further investigate the role of LINC00426, we tested the effect of LINC00426 on the proliferation and migration of human nasopharyngeal carcinoma cell lines by transient transfection of overexpressing plasmids. The expression of mRNA was assessed by qPCR. We then investigated whether the cell proliferation and migration were inhibited upon LINC00426 overexpression in the nasopharyngeal carcinoma cell lines cells (CNE1 and SUNE1). However, cell proliferation assays showed that overexpression of LINC00426 did not affect cell viability compared to the negative group (Figure S2A and Figure S2C). There was also no change in colony formation ability after overexpression of LINC00426 in CNE1 and SUNE1 cells (Figure S2B and Figure S2D). In addition, the wound healing assay also showed that overexpression of LINC00426 did not affect the migration ability of CNE1 and SUNE1 cells (Figure S2E and Figure S2F).

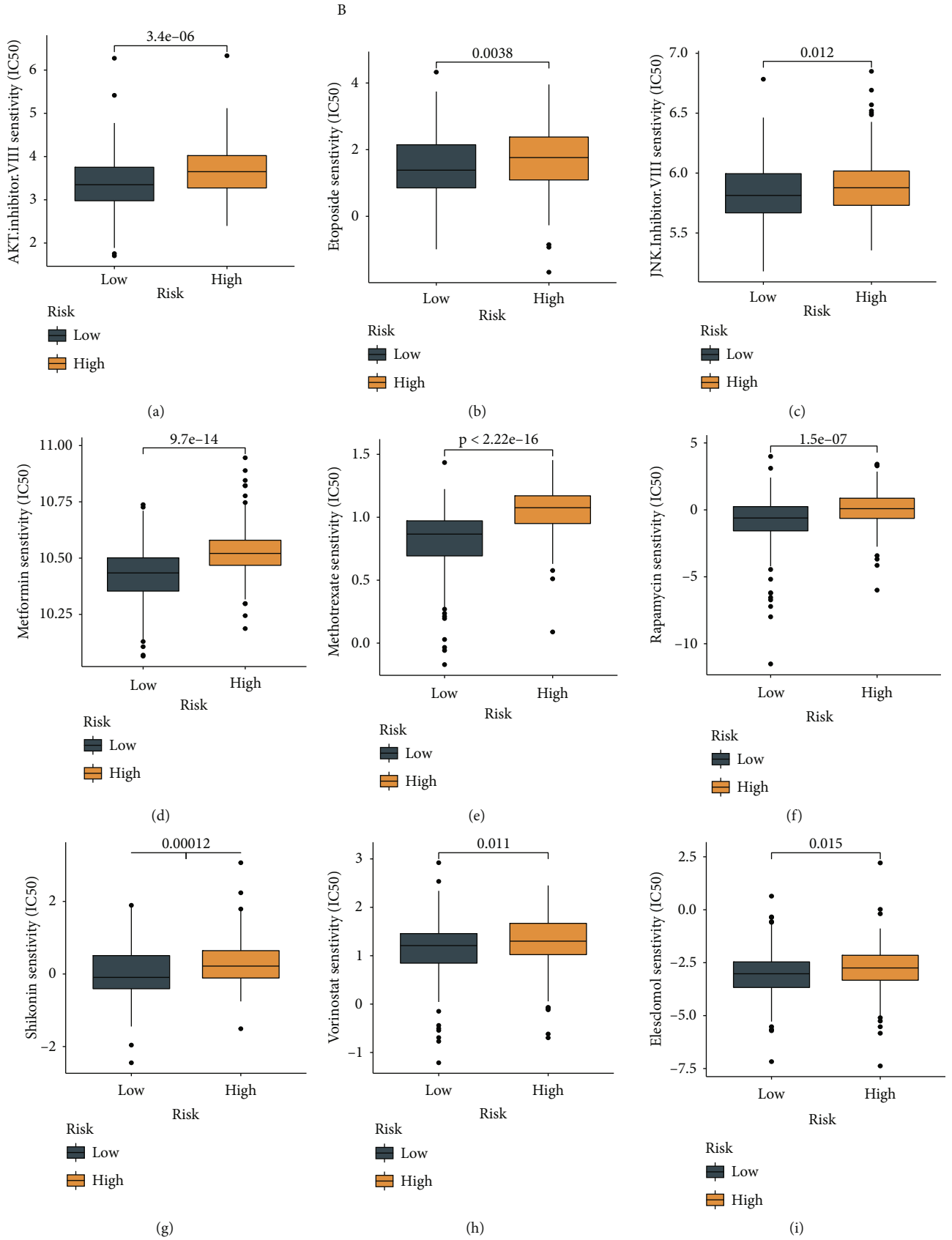

Figure 9: Evaluation of chemosensitivity by the risk model. The model showed that low-risk scores were associated with a lower half inhibitory centration (IC_{50}) for chemotherapeutics such as (a) AKT inhibitor, (b) etoposide, (c) JNK inhibitor V, (d) metformin, (e) methotrexate, (f) rapamycin, (g) shikonin, (h) vorinostat, and (i) elesclomol.

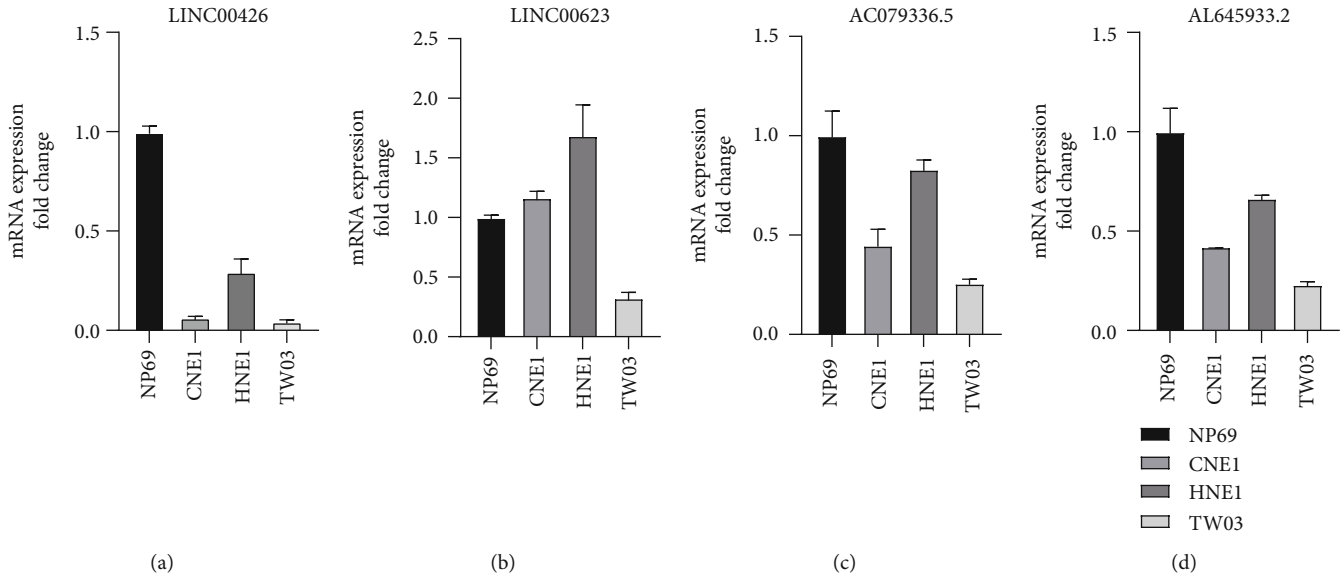

Figure 10: lncRNA expression from our NETosis-related lncRNA signature. (a) mRNA expression of LINC00426 in different cell lines. (b) mRNA expression of LINC00623 in different cell lines. (c) mRNA expression of AC079336.5 in different cell lines. (d) mRNA expression of AL645933.2 in different cell lines.

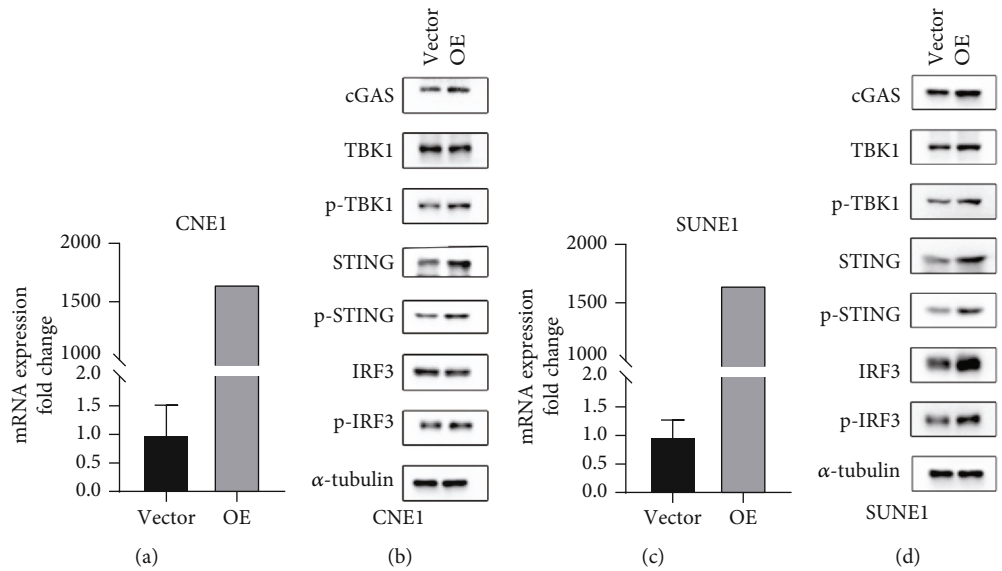

Figure 11: Changes in STING signaling pathway-related proteins in different cell lines transfected with or without LINC00426 overexpression plasmids. (a) mRNA expression of LINC00426 in CNE1 cells. (b) Western blot for cGAS, TBK1, STING, and IRF3 in CNE1 cells. (c) mRNA expression of LINC00426 in SUNE1 cells. (d) Western blot for cGAS, TBK1, STING, and IRF3 in SUNE1 cells.

3.12. LINC00426 Contributes to the STING Signaling Pathway. The prognostic model of lncRNA that we built was able to not only predict the prognosis of patients but also identify "hot" and "cold" tumors. Therefore, we try to explore the possibility of lncRNA regulation of immunity in vitro. We hypothesized that LINC00426 regulated immune cell infiltration; we overexpressed LINC00426 in CNE1 and SUNE1 cells (Figures 11(a) and 11(c)) and detected the expression of cGAS-STING-TBK1-IRF3 signaling pathway. The data exhibited that LINC00426 overexpressed significantly enhanced p-STING, p-TBK1, and p-IRF3 protein levels in both CNE1 and SUNE1 cells (Figures 11(b) and 11(d)). The activation of the STING signaling pathway is known to further promote the secretion of cytokines such as CXCL10, CCL5, ISG15, and ISG56, thereby recruiting B cells, T cells, and promoting immune cell infiltration. These data explain to some extent the role of our prognostic model in predicting "hot" and "cold" tumors.

4. Discussion

To our knowledge, our study was the first to probe a NETosis-related lncRNA signature to predict HSNCC prognosis and group a patient set into high-risk and low-risk

groups. An evident increase in anticancer immune pathways was documented in the low-risk group by functional enrichment analysis. In the meanwhile, a close association emerged for our lncRNA signature with the immune cell infiltration and NETosis profiles in HNSCC. To expound, an immunologically "cold" profile emerged in the high-risk group, which included diminished immune cell infiltration and activity, and dampened immune checkpoint molecule expression, while an immunologically "hot" profile emerged in the low-risk group. The putative potential of our signature was also corroborated in the two patient sets who received ICB as evidenced in the ssGSEA to predict the relevance of ICB in patients. The effective prediction of the response to select chemotherapy drugs by the signature was also documented in HNSCC patients.

The involvement of lncRNAs in NETosis has been demonstrated in several studies. For example, Li et al. reported that an upregulation of IL-12A due to lncRNA X-inactive specific transcript by binding to miR-21 stimulates NETosis and accelerates primary graft dysfunction subsequent to lung transplantation [36]. Gao and Zhang documented that diminishing of lncRNA MINCR inhibits NETosis and is involved in LPS-evoked acute injury and inflammatory response [37]. Nonetheless, there are few studies on elucidating lncRNAs connected with NETosis in oncogenesis and moreover HNSCC. There were many researches focusing on figuring out NETosis-associated gene; we employed Pearson's correlation analysis on these genes and lncRNAs to identify NETosis-related lncRNAs, which initially resulted in 113 NETosis-associated lncRNAs that regarded to be associated with the survival of HNSCC patients by univariate Cox regression. Further analyses narrowed down on five NETosis-related lncRNAs: AC079336.5, LINC00623, AC087752.4, AL645933.2, and LINC00426. Of these 5 lncRNAs in our prognostic signature, the involvement of LINC00426 in oncogenesis has been documented. For example, the regulation of miR-455-5p by LINC00426 to boost lung adenocarcinoma progression was demonstrated [38], while LINC00426 was downregulated in non-small-cell lung cancer patient tumor tissues and correlated with poor prognosis [39]. Another study documented that LINC00426 contributes to doxorubicin resistance by sponging miR-4319 in osteosarcoma [40]. Our results showed that LINC00426 overexpressed upregulated STING signaling pathway in HNSCC cell lines, which indicated that innate immunity was activated [41]. Our data explain to some extent the role of our prognostic model in predicting "hot" and "cold" tumors, which illustrated that our model is reliable. For the four remaining NET-related lncRNAs (AC079336.5, LINC00623, AC087752.4, and AL645933.2), research on their involvement in cancer has not yet been documented. We are not able to verify the function of the other four lncRNAs within severe constraints of time and money.

The involvement of NETosis in tumorigenesis and therapeutic approaches is being documented in several reports. The definition of NETosis entailed NET release and cell death involving ROS specifically in cells of hematopoietic origin [8]. Several signaling cascades are then stimulated by this NETosis production in tumors encompassing the malignancy itself with blood cells like leukocytes and platelets and establish an inflammatory microenvironment to boost tumor progression [42]. As outlined above, the involvement of this process and NETosis-related lncRNAs in the HNSCC immune microenvironment warrants scrutiny. This work documented a diminishing of crucial immune pathways involved in antitumor functioning like natural killer cell cytotoxicity, B cell/T cell receptor signaling, and elevated NETosis in the high-risk group in the relevant assays. This was suggestive of the plausible link between antitumor immunity and NETosis in HNSCC. Zhang et al. demonstrated the recruitment of neutrophils to trigger NETosis by IL17 to exclude cytotoxic CD8 T cells in pancreatic ductal adenocarcinoma. Interestingly, NET inhibition was documented in a recipient animal model with an arginine deiminase 4 gene (the enzyme PAD4, vitally involved in mediating NETosis from neutrophils) deletion with a better response to ICB in these murine systems emerging vs. those who expressed PAD4 and demonstrated NETs in the tumor microenvironment [43]. Another study has uncovered the inhibition of immune cytotoxicity by NETs via immune cell-target cell contact impairment and inhibition of NETosis by pharmacologically suppressing PAD4 augments tumor sensitivity to PD-1 + CTLA-4 dual checkpoint blockade in a syngeneic mouse model of breast cancer [9]. These results revealed a strong association between NETosis and antitumor immunity, which was consistent with our results.

In order to prove the hitherto unknown aspects of immune cell infiltration and NETosis in HNSCC, the former was scrutinized employing the algorithms listed earlier. A conspicuous diminishing of infiltration of cytotoxic cells inclusive of naive B cells and CD8+ T cells emerged in the high-risk patients vs. that of the low-risk patient set. The high-risk group also was demonstrative of diminished immune checkpoint molecule expression to be hence tagged as immunologically "cold" tumors to plausibly limit the response of ICB therapy as documented by our lncRNA signature. To corroborate this possibility, functional enrichment analysis was conducted, which revealed that anticancer immune pathways were significantly upregulated in the low-risk HNSCC group. Furthermore, probing of the cohorts with our NETosis-associated lncRNA signature unearthed an augmented survival post-ICB therapy in low-risk patients. These observations were indicative of the putative impact of our NETosis-related lncRNA signature to predict ICB response in patients to further guide treatments in the future.

An augmentation of NETosis emerged in the high-risk cohort as scrutinized by the "GSVA" package-based score. This leads us to hypothesize an augmented response to ICB therapy in this group by boosting immune cell infiltration by plausibly suppressing this NETosis in this high-risk group. The role of NETosis in anti-tumor immunity is being unearthed by ongoing work. Inhibition of NETosis is closely associated with antitumor immunity. Our research has provided the theoretical basis that high-risk HNSCC patients may benefit from the combination of ICB with NETosis inhibitors, which inhibit cell NETosis and increase immune cell infiltration to enhance the response to ICB therapy. This gains support with ongoing trials exploring the efficacy of

concurrent NETosis inhibitors with other therapeutic strategies. The suitability of the neutrophil/NET system and the CXCR1/2 and the IL-8 pathway is receiving the center stage as therapeutic targets given their crucial importance. Concurrent administration of ICB with some CXCR1 and 2 inhibitors has been subjected to clinical testing. For instance, a phase I study is probing a combination of SX-682 (a CXCR1/2 inhibitor) and nivolumab (anti-PD1) in metastatic pancreatic ductal adenocarcinoma (NCT04477343). The concurrent administration of pembrolizumab (anti-PD1) with navarixin (a CXCR1/2 inhibitor) in advanced/metastatic solid tumors is being probed in a phase II study (NCT03473925) [42]. Our study may help provide clues to identify high-risk patients who may benefit more from the combination of ICB and NETosis inhibitors.

This work encompasses a few limitations. More in vivo or in vitro basic experiments are warranted to corroborate the potential molecular mechanistic aspects of NETosis-related lncRNAs in prognosis. In addition, clinical trials are urgently required to confirm whether inhibiting NETosis could improve the efficacy of immunotherapy in human HNSCC patients.

In conclusion, we identified the suitability of a NETosis-based lncRNA signature in the prognosis of HNSCC patients. Further variation in the immune cell profile and immune checkpoint molecule expression between the high-risk and low-risk groups are also documented. Our study suggests that NETosis inhibition may emerge as a strategy to augment the efficacy of immunotherapy in HNSCC patients.

Abbreviations

AIC: Akaike information criterion
AUC: Area under time-dependent receiver operating characteristic curve
CYT: Cytolytic activity
GSEA: Gene set enrichment analysis
HNSCC: Head and neck squamous cell carcinoma
HPV: Human papillomavirus
ICB: Immune checkpoint blockade
KEGG: Kyoto Encyclopedia of Genes and Genomes
LASSO: Least absolute shrinkage and selection operator
lncRNAs: Long noncoding RNAs
NETs: Neutrophil extracellular traps
NK: Natural killer
OS: Overall survival
ROC: Receiver operating characteristic
TCGA: The Cancer Genome Atlas.

Data Availability

The RNA sequencing data and patient characteristics of HNSCC patients were sourced from the TCGA database (https://portal.gdc.cancer.gov/repository). lncRNA and protein-coding gene annotations were ensued in the Ensembl human genome browser GRCh38.p13 (http://asia.ensembl.org/index.html). Gene set enrichment analysis (GSEA) was performed by GSEA software (versionv4.1.0, http://www.gsea-msigdb.org/gsea/downloads).

Consent

Consent is not necessary.

Conflicts of Interest

The authors declare that they have no known competing financial interests or personal relationships that could have appeared to influence the work reported in this paper.

Authors' Contributions

XH, ZL, and XZ were responsible for the conception and design. SL and YX were responsible for the data acquisition. XH, SL, ZL, XZ, and RD were responsible for the data analysis and interpretation. SL, YX, ZL, XZ, and RD were responsible for the material support. XH, ZL, and XZ were responsible for the study supervision. YX was responsible for the in vitro experiments. XH and SL wrote the original draft. The final version is ensured and approved by all authors. Xiaohua He, Yinglu Xiao, and Shan Liu contributed equally to this work.

Supplementary Materials

Supplementary 1. Table S1: 24 NETosis-associated genes were identified from the literature.

Supplementary 2. Figure S1: the flow chart of our study. Figure S2: the effect of LINC00426 on nasopharyngeal carcinoma cell lines. (A) Cell proliferation assays showed that LINC00426 overexpression did not affect the viability of CNE1 cells. (B) Plate colony formation assay showed that LINC00426 overexpression did not affect the ability of colony formation in CNE1 cells. (C) Cell proliferation assays showed that LINC00426 overexpression did not affect the viability of SUNE1 cells. (D) Plate colony formation assay showed that LINC00426 overexpression did not affect the ability of colony formation in SUNE1 cells. Wound healing assay showed that LINC00426 overexpression did not affect the ability of migration both in CNE1 (E) and SUNE1 (F) cells.

References

[1] D. E. Johnson, B. Burtness, C. R. Leemans, V. W. Y. Lui, J. E. Bauman, and J. R. Grandis, "Head and neck squamous cell carcinoma," *Nature Reviews. Disease Primers*, vol. 6, no. 1, p. 92, 2020.

[2] A. J. Charap, T. Enokida, R. Brody et al., "Landscape of natural killer cell activity in head and neck squamous cell carcinoma," *Journal for Immunotherapy of Cancer*, vol. 8, no. 2, p. e001523, 2020.

[3] C. R. Leemans, P. J. F. Snijders, and R. H. Brakenhoff, "The molecular landscape of head and neck cancer," *Nature Reviews. Cancer*, vol. 18, no. 5, pp. 269–282, 2018.

[4] J. D. Cramer, B. Burtness, Q. T. Le, and R. L. Ferris, "The changing therapeutic landscape of head and neck cancer," *Nature Reviews. Clinical Oncology*, vol. 16, no. 11, pp. 669–683, 2019.

[5] W. Zhu, Z. Ye, L. Chen, H. Liang, and Q. Cai, "A pyroptosis-related lncRNA signature predicts prognosis and immune microenvironment in head and neck squamous cell carcinoma," *International Immunopharmacology*, vol. 101, no. Part B, p. 108268, 2021.

[6] S. K. Jorch and P. Kubes, "An emerging role for neutrophil extracellular traps in noninfectious disease," *Nature Medicine*, vol. 23, no. 3, pp. 279–287, 2017.

[7] Q. Ou, J. Q. Fang, Z. S. Zhang et al., "TcpC inhibits neutrophil extracellular trap formation by enhancing ubiquitination mediated degradation of peptidylarginine deiminase 4," *Nature Communications*, vol. 12, no. 1, p. 3481, 2021.

[8] C. I. Efrimescu, P. M. Buggy, and D. J. Buggy, "Neutrophil extracellular trapping role in cancer, metastases, and cancer-related thrombosis: a narrative review of the current evidence base," *Current Oncology Reports*, vol. 23, no. 10, p. 118, 2021.

[9] A. Teijeira, S. Garasa, M. Gato et al., "CXCR1 and CXCR2 chemokine receptor agonists produced by tumors induce neutrophil extracellular traps that interfere with immune cytotoxicity," *Immunity*, vol. 52, no. 5, pp. 856–871.e8, 2020, e8.

[10] B. M. Szczerba, F. Castro-Giner, M. Vetter et al., "Neutrophils escort circulating tumour cells to enable cell cycle progression," *Nature*, vol. 566, no. 7745, pp. 553–557, 2019.

[11] L. Yang, Q. Liu, X. Zhang et al., "DNA of neutrophil extracellular traps promotes cancer metastasis via CCDC25," *Nature*, vol. 583, no. 7814, pp. 133–138, 2020.

[12] B. Li, Y. Liu, T. Hu et al., "Neutrophil extracellular traps enhance procoagulant activity in patients with oral squamous cell carcinoma," *Journal of Cancer Research and Clinical Oncology*, vol. 145, no. 7, pp. 1695–1707, 2019.

[13] C. Fang, F. Liu, Y. Wang et al., "A innovative prognostic symbol based on neutrophil extracellular traps (NETs)-related lncRNA signature in non-small-cell lung cancer," *Aging (Albany NY)*, vol. 13, pp. 17864–17879, 2021.

[14] Y. Huang, "The novel regulatory role of lncRNA-miRNA-mRNA axis in cardiovascular diseases," *Journal of Cellular and Molecular Medicine*, vol. 22, no. 12, pp. 5768–5775, 2018.

[15] X. Le, R. Ferrarotto, T. Wise-Draper, and M. Gillison, "Evolving role of immunotherapy in recurrent metastatic head and neck cancer," *Journal of the National Comprehensive Cancer Network*, vol. 18, no. 7, pp. 899–906, 2020.

[16] M. W. Knitz, T. E. Bickett, L. B. Darragh et al., "Targeting resistance to radiation-immunotherapy in cold HNSCCs by modulating the Treg-dendritic cell axis," *Journal for Immunotherapy of Cancer*, vol. 9, no. 4, p. e001955, 2021.

[17] H. R. Thiam, S. L. Wong, D. D. Wagner, and C. M. Waterman, "Cellular mechanisms of NETosis," *Annual Review of Cell and Developmental Biology*, vol. 36, no. 1, pp. 191–218, 2020.

[18] D. M. Clancy, C. M. Henry, G. P. Sullivan, and S. J. Martin, "Neutrophil extracellular traps can serve as platforms for processing and activation of IL-1 family cytokines," *The FEBS Journal*, vol. 284, no. 11, pp. 1712–1725, 2017.

[19] D. Sarr, L. J. Oliveira, B. N. Russ et al., "Myeloperoxidase and other markers of neutrophil activation associate with malaria and malaria/HIV coinfection in the human placenta," *Frontiers in Immunology*, vol. 12, p. 682668, 2021.

[20] R. A. Gordon, J. S. Tilstra, A. Marinov, K. M. Nickerson, S. I. Bastacky, and M. J. Shlomchik, "Murine lupus is neutrophil elastase-independent in the MRL.Faslpr model," *PLoS One*, vol. 15, no. 4, article e0226396, 2020.

[21] G. Sollberger, A. Choidas, G. L. Burn et al., "Gasdermin D plays a vital role in the generation of neutrophil extracellular traps," *Science Immunology*, vol. 3, no. 26, 2018.

[22] E. Apostolidou, P. Skendros, K. Kambas et al., "Neutrophil extracellular traps regulate IL-1β-mediated inflammation in familial Mediterranean fever," *Annals of the Rheumatic Diseases*, vol. 75, no. 1, pp. 269–277, 2016.

[23] L. Jin, S. Batra, and S. Jeyaseelan, "Diminished neutrophil extracellular trap (NET) formation is a novel innate immune deficiency induced by acute ethanol exposure in polymicrobial sepsis, which can be rescued by CXCL1," *PLoS Pathogens*, vol. 13, no. 9, article e1006637, 2017.

[24] S. W. Kim and J. K. Lee, "Role of HMGB1 in the interplay between NETosis and thrombosis in ischemic stroke: a review," *Cell*, vol. 9, no. 8, 2020.

[25] H. T. Snoderly, B. A. Boone, and M. F. Bennewitz, "Neutrophil extracellular traps in breast cancer and beyond: current perspectives on NET stimuli, thrombosis and metastasis, and clinical utility for diagnosis and treatment," *Breast Cancer Research*, vol. 21, no. 1, pp. 1–13, 2019.

[26] F. Cunningham, P. Achuthan, W. Akanni et al., "Ensembl 2019," *Nucleic Acids Research*, vol. 47, no. D1, pp. D745–D751, 2019.

[27] A. M. Newman, C. L. Liu, M. R. Green et al., "Robust enumeration of cell subsets from tissue expression profiles," *Nature Methods*, vol. 12, no. 5, pp. 453–457, 2015.

[28] F. Finotello, C. Mayer, C. Plattner et al., "Molecular and pharmacological modulators of the tumor immune contexture revealed by deconvolution of RNA-seq data," *Genome Medicine*, vol. 11, no. 1, p. 34, 2019.

[29] D. Aran, Z. Hu, and A. J. Butte, "xCell: digitally portraying the tissue cellular heterogeneity landscape," *Genome Biology*, vol. 18, no. 1, p. 220, 2017.

[30] E. Becht, N. A. Giraldo, L. Lacroix et al., "Estimating the population abundance of tissue-infiltrating immune and stromal cell populations using gene expression," *Genome Biology*, vol. 17, no. 1, p. 218, 2016.

[31] J. Racle, K. de Jonge, P. Baumgaertner, D. E. Speiser, and D. Gfeller, "Simultaneous enumeration of cancer and immune cell types from bulk tumor gene expression data," *eLife*, vol. 6, 2017.

[32] T. Li, J. Fan, B. Wang et al., "TIMER: a web server for comprehensive analysis of tumor-infiltrating immune cells," *Cancer Research*, vol. 77, no. 21, pp. e108–e110, 2017.

[33] D. A. Braun, Y. Hou, Z. Bakouny et al., "Interplay of somatic alterations and immune infiltration modulates response to PD-1 blockade in advanced clear cell renal cell carcinoma," *Nature Medicine*, vol. 26, no. 6, pp. 909–918, 2020.

[34] S. Mariathasan, S. J. Turley, D. Nickles et al., "TGF beta attenuates tumour response to PD-L1 blockade by contributing to exclusion of T cells," *Nature*, vol. 554, no. 7693, pp. 544–548, 2018.

[35] P. Geeleher, N. Cox, and R. S. Huang, "pRRophetic: an R package for prediction of clinical chemotherapeutic response from tumor gene expression levels," *PLoS One*, vol. 9, no. 9, article e107468, 2014.

[36] J. Li, L. Wei, Z. Han, Z. Chen, and Q. Zhang, "Long noncoding RNA X-inactive specific transcript silencing ameliorates primary graft dysfunction following lung transplantation through microRNA-21-dependent mechanism," *eBioMedicine*, vol. 52, article 102600, 2020.

[37] W. Gao and Y. Zhang, "Depression of lncRNA MINCR antagonizes LPS-evoked acute injury and inflammatory response via miR-146b-5p and the TRAF6-NFkB signaling," *Molecular Medicine*, vol. 27, no. 1, p. 124, 2021.

[38] H. Li, Q. Mu, G. Zhang et al., "Linc00426 accelerates lung adenocarcinoma progression by regulating miR-455-5p as a molecular sponge," *Cell Death & Disease*, vol. 11, no. 12, p. 1051, 2020.

[39] W. Du, J. Sun, J. Gu, S. Zhang, and T. Zhang, "Bioinformatics analysis of LINC00426 expression in lung cancer and its correlation with patients' prognosis," *Thorac Cancer.*, vol. 11, no. 1, pp. 150–155, 2020.

[40] L. Wang, Y. Luo, Y. Zheng et al., "Long non-coding RNA LINC00426 contributes to doxorubicin resistance by sponging miR-4319 in osteosarcoma," *Biology Direct*, vol. 15, no. 1, p. 11, 2020.

[41] T. Li and Z. J. Chen, "The cGAS-cGAMP-STING pathway connects DNA damage to inflammation, senescence, and cancer," *Journal of Experimental Medicine*, vol. 215, no. 5, pp. 1287–1299, 2018.

[42] L. Ronchetti, N. S. Boubaker, M. Barba, P. Vici, A. Gurtner, and G. Piaggio, "Neutrophil extracellular traps in cancer: not only catching microbes," *Journal of Experimental & Clinical Cancer Research*, vol. 40, no. 1, p. 231, 2021.

[43] Y. Zhang, V. Chandra, E. Riquelme Sanchez et al., "Interleukin-17-induced neutrophil extracellular traps mediate resistance to checkpoint blockade in pancreatic cancer," *The Journal of Experimental Medicine*, vol. 217, no. 12, 2020.

Hindawi
BioMed Research International
Volume 2022, Article ID 3543948, 12 pages
https://doi.org/10.1155/2022/3543948

Research Article

Long Noncoding RNA LEMD1-AS1 Increases LEMD1 Expression and Activates PI3K-AKT Pathway to Promote Metastasis in Oral Squamous Cell Carcinoma

Zaiye Li,[1,2,3,4] **Jie Wang**,[5] **Jianjun Wu**,[1,2,3] **Ning Li**,[1,2,3] **and Canhua Jiang**[1,2,3]

[1]*Department of Oral and Maxillofacial Surgery, Center of Stomatology, Xiangya Hospital, Central South University, Changsha, China*
[2]*Research Center of Oral and Maxillofacial Tumor, Xiangya Hospital, Central South University, Changsha, China*
[3]*Institute of Oral Cancer and Precancerous Lesions, Central South University, Changsha, China*
[4]*State Key Laboratory of Oral Diseases, National Clinical Research Center for Oral Diseases, Chinese Academy of Medical Sciences Research Unit of Oral Carcinogenesis and Management, West China Hospital of Stomatology, Sichuan University, Chengdu, Sichuan 610041, China*
[5]*Department of Immunology, Xiangya School of Medicine, Central South University, Changsha, China*

Correspondence should be addressed to Canhua Jiang; canhuaj@csu.edu.cn

Received 20 May 2022; Accepted 7 July 2022; Published 9 August 2022

Academic Editor: Wei Han

Background. The survival rate of oral squamous cell carcinoma (OSCC) is only 50% due to a high incidence of metastasis. Long noncoding RNAs (lncRNAs) play a crucial role in OSCC genesis and progression, although their potential role in the metastasis of OSCC remains unclear. *Methods*. The transcriptome of 5 metastatic and 5 nonmetastatic OSCC samples were assessed by RNA sequencing. The biological functions and regulatory mechanisms of LEMD1-AS1 in OSCC were explored by in vitro and in vivo assays. *Results*. We identified 487 differentially expressed mRNAs (DEmRNAs) and 1507 differentially expressed lncRNAs (DElncRNAs) in OSCC with cervical lymph node (LN) metastasis relative to the nonmetastatic samples. In addition, both LEMD1-AS1 and its cognate LEMD1 were up-regulated in metastatic OSCC compared to nonmetastatic OSCC. Gain-of-function, loss-of-function, and rescue experiments indicated that LEMD1-AS1 upregulated LEMD1 to increase OSCC migration and invasion in vitro and in vivo. Mechanistically, LEMD1-AS1 stabilized LEMD1 and increased its mRNA and protein levels, and consequently activated the PI3K-AKT signaling pathway to facilitate OSCC metastasis. *Conclusions*. We established the lncRNA-mRNA landscape of metastatic OSCC, which indicated that LEMD1-AS1 enhanced OSCC metastasis by stabilizing its antisense transcript LEMD1. Thus, LEMD1-AS1 is a potential biomarker for predicting metastasis, as well as a therapeutic target of OSCC.

1. Background

Oral squamous cell carcinoma (OSCC) is one of the most commonly diagnosed malignancies worldwide [1–3] and is characterized by a high incidence of local invasion and cervical lymph node (LN) metastasis. Despite recent advances in surgery, chemoradiotherapy, and other targeted therapies, the overall survival of OSCC patients is still only 50% due to the high metastasis rates [4, 5]. Therefore, it is essential to identify the underlying mechanisms of OSCC metastasis in order to develop novel effective therapies.

Long noncoding RNAs (lncRNAs) are noncoding transcripts more than 200 nucleotides in length [6, 7] and are classified into the antisense, intronic, bidirectional, intergenic, and overlapping types. lncRNAs regulate gene expression via chromatin modification, miRNA quenching, direct modulation of mRNA stability, transcription, and translation, as well as protein stability control [8, 9], and are involved in tumor

initiation and progression. The antisense lncRNAs account for approximately 50–70% of all lncRNAs and can exert their function through *cis*- or *trans*-mechanisms [10]. The *cis*-acting antisense lncRNAs bind to genes in their vicinity, while the *trans*-lncRNAs modulate more distant genes on the same or even on different chromosomes. Furthermore, *cis*-antisense lncRNAs modulate gene expression at the pretranscriptional, transcriptional, and posttranscriptional levels through DNA–lncRNA, lncRNA–RNA, or protein–lncRNA interactions. lncRNA-RNA interactions in particular are common during cancer initiation and progression and involve hybridization of the sense and antisense sequences into RNA duplexes that regulate the posttranscriptional outcome. Zhao et al. reported that MACC1-AS1 promoted gastric cancer cell metabolic plasticity by stabilizing MACC1 mRNA [11]. In addition, lncRNA PXN-AS1-L acts as an oncogene in non-small-cell lung cancer (NSCLC) by increasing PXN expression [12]. Yuan et al. found that MUC5B-AS1 promoted lung adenocarcinoma metastasis by forming RNA-RNA duplex with MUC5B. However, little is known regarding the function of antisense lncRNAs in metastatic OSCC.

To this end, we performed next-generation sequencing analysis of human OSCC tissues in order to map the differentially expressed RNAs and establish a lncRNA-mRNA interaction network. Accordingly, we identified lncRNA LEMD1-AS1 and its target gene LEMD1, which acts as an oncogene in multiple cancers, and analyzed their biological role in OSCC via functional assays. Our findings provide new insights into OSCC metastasis and identify a novel biomarker for prognostic prediction and targeted therapy.

2. Results

2.1. Overview of RNA Sequencing Data. All raw data had been uploaded in GEO database (GSE145272, https://www.ncbi.nlm.nih.gov/geo/query/acc.cgi?acc=GSE145272). A total of 487 differentially expressed mRNAs (DEmRNAs) (319 upregulated and 168 downregulated) and 1507 differentially expressed lncRNAs (DElncRNAs) (971 upregulated and 536 downregulated) were identified in RNA-seq data using $|\log 2 \text{ fold change (FC)}| > 1.0$ and P value < 0.05 as the thresholds (Figure 1). The functional enrichment analysis (Additional Figure 1A) showed that 487 DEmRNAs were enriched in 520 biological process (BP), 13 cellular component (CC), and 21 molecular function (MF) terms, including cell-cell adhesion, receptor complex, channel complex, channel activity, and receptor activity. KEGG pathway analysis (Additional Figure 1B) indicated enrichment of 243 pathways, including the cAMP signaling pathway, calcium signal pathway, cytokine-cytokine receptor interaction, and cell adhesion molecules (CAMs).

2.2. DElncRNA-DEmRNA Interaction Network. Potential interactions between the DElncRNAs and DEmRNAs were predicted using the LncTar software and correlated via R software. The interacting pairs were screened using $\text{cor} \neq 0$ and P value < 0.05 as the thresholds. As shown in Additional Figure 2, 132 *cis*-regulation pairs and 165994 *trans*-regulation pairs were identified.

2.3. Validation of Dysregulated RNAs. To validate the RNA-seq data, we randomly selected five DERNAs (LEMD1-AS1, LEMD1, TBILA, LINC01133, and PURPL) from the top 50 DERNAs identified in 10 samples by qPCR. LEMD1-AS1, LEMD1, TBILA, and LINC01133 were significantly upregulated in metastatic versus nonmetastatic OSCC while PURPL was downregulated in the former (Figure 2).

2.4. LEMD1-AS1 and LEMD1 Are Overexpressed in Human OSCC Tissues and Cell Lines. Since both LEMD1-AS1 and LEMD1 were upregulated in the metastatic OSCC samples relative to the nonmetastatic samples, we hypothesized that LEMD1-AS1 promotes OSCC metastasis by upregulating its predicted target LEMD1. To confirm our hypothesis, we detected the expression levels of both in additional OSCC samples by qRT-PCR. Consistent with the bioinformatics results, the metastatic tumors expressed higher levels of both LEMD1-AS1 and LEMD1, which showed a significant positive correlation (Figure 2(f)). In addition, the metastatic OSCC cell lines UM1, OSC19, and CAL27 showed significantly higher LEMD1-AS1 levels compared to the nonmetastatic UM2 and OSC3 cells (Additional Figure 3). Taken together, the LEMD1-AS1 and LEMD1 interaction is prometastatic in OSCC.

2.5. LEMD1-AS1 Promoted Migration of OSCC Cells via LEMD1. FISH assay showed that LEMD1-AS1 was mainly localized in the cytoplasm of OSCC cells, and minimal signals were observed in the nucleus (Additional Figure 4). To further analyze the biological role of LEMD1-AS1 in OSCC cells, we knocked down its expression in the OSC19 and CAL27 cells using the smart silencer (Additional Figure 5A), and ectopically expressed it in the UM2 and OSC3 cells (Additional Figure 5B). The cells overexpressing LEMD1-AS1 had higher levels of LEMD1, while LEMD1-AS1 knockdown was associated with downregulation of LEMD1 (Additional Figure 5C-D). Neither LEMD1-AS1 silencing nor overexpression had any effect on the proliferation of the OSCC cells compared to the respective controls (Additional Figure 6). However, LEMD1-AS1 overexpression in UM2 and OSC3 cells significantly increased their migration abilities *in vitro* (Figure 3), whereas LEMD1-AS1 knockdown had the opposite effect in OSC19 and CAL27 cells. Taken together, LEMD1-AS1 is a prometastatic factor in OSCC. To determine whether LEMD1-AS1 mediated its effects in OSCC via LEMD1, we knocked down the latter in cells stably overexpressing LEMD1-AS1 (Additional Figure 7). As shown in Figure 4, the knockdown of LEMD1 abrogated the effects of LEMD1-AS1 overexpression on the migration and invasion abilities of OSCC cells. Thus, LEMD1-AS1/LEMD1 interaction is crucial for OSCC progression and metastasis.

2.6. LEMD1-AS1 Increased the Stability of LEMD1 mRNA by Forming a Protective RNA Duplex. The results so far indicated that LEMD1-AS1 regulated LEMD1 mRNA expression levels. Consistent with this, the LEMD1 protein levels were also increased in OSC3 cells stably overexpressing LEMD1-AS1 and decreased in LEMD1-AS1-knockdown

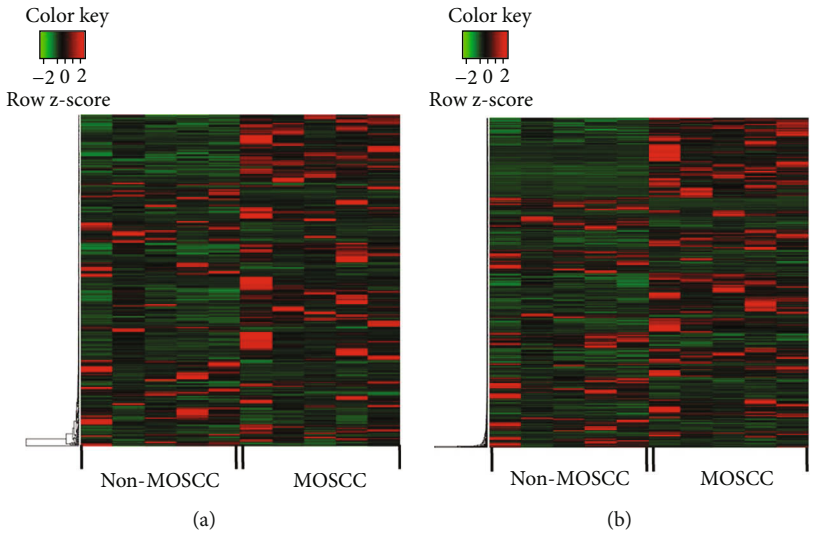

Figure 1: Heatmap of differentially expressed RNAs between metastatic OSCC and nonmetastatic OSCC. (a) mRNAs. (b) lncRNAs.

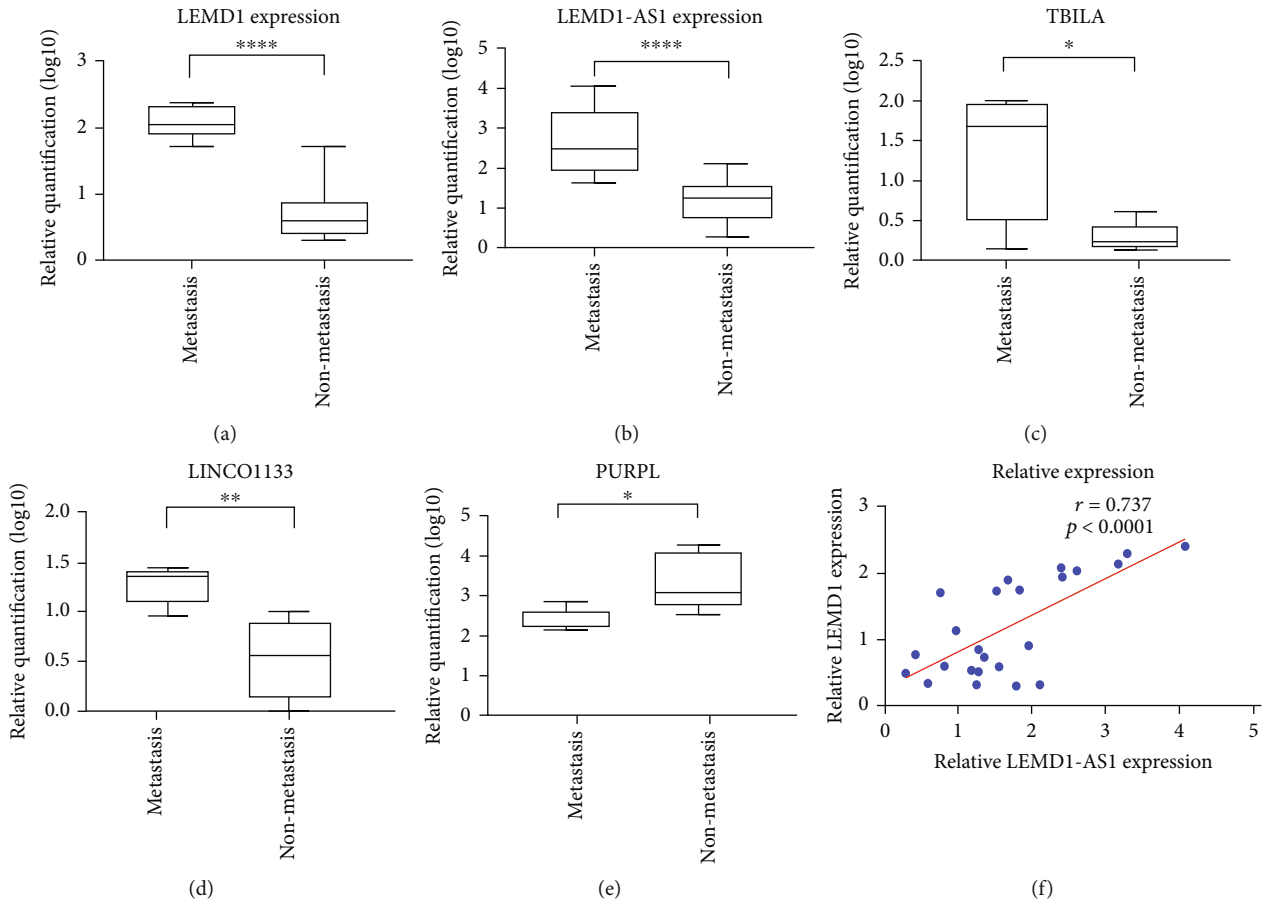

Figure 2: Validation of DERNA expression level in 10 OSCC samples included in next generation sequencing. (a) LEMD1. (b) LEMD1-AS1. (c) TBILA. (d) LINC01133. (e) PURPL. (f) Correlation between LEMD1-AS1 and LEMD1 mRNA expression in 24 OSCC tissues. $^{*}P < 0.05$; $^{**}P < 0.01$; $^{***}P < 0.001$; $P < 0.0001$.

cells (Figure 5). LEMD1-AS1 is localized at the antisense chain of the LEMD1 gene. In addition, antisense lncRNAs increase the stability of their cognate sense mRNAs by forming an RNA-RNA duplex, which also enhances the mRNA expression levels. Bioinformatics and gene sequence analysis revealed an overlapping (OL) region between LEMD1-AS1

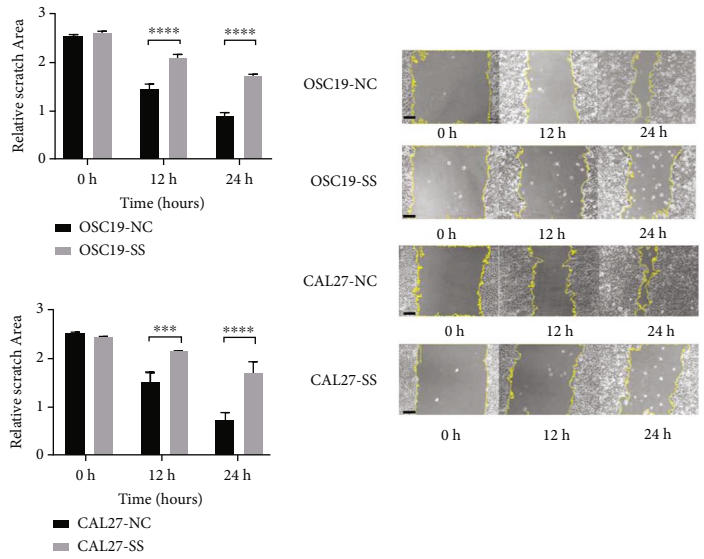

(a)

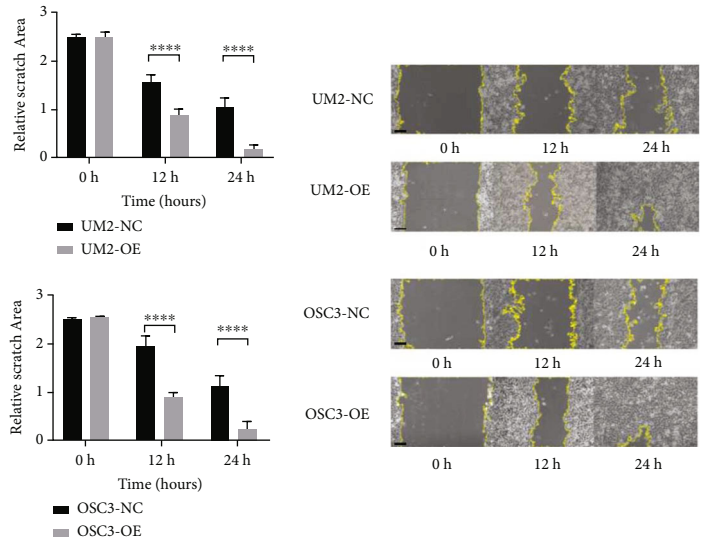

(b)

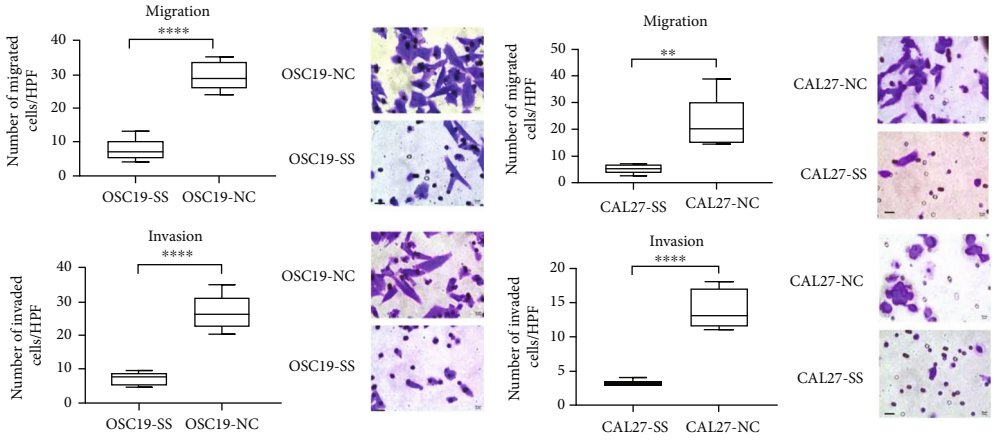

(c)

Figure 3: Continued.

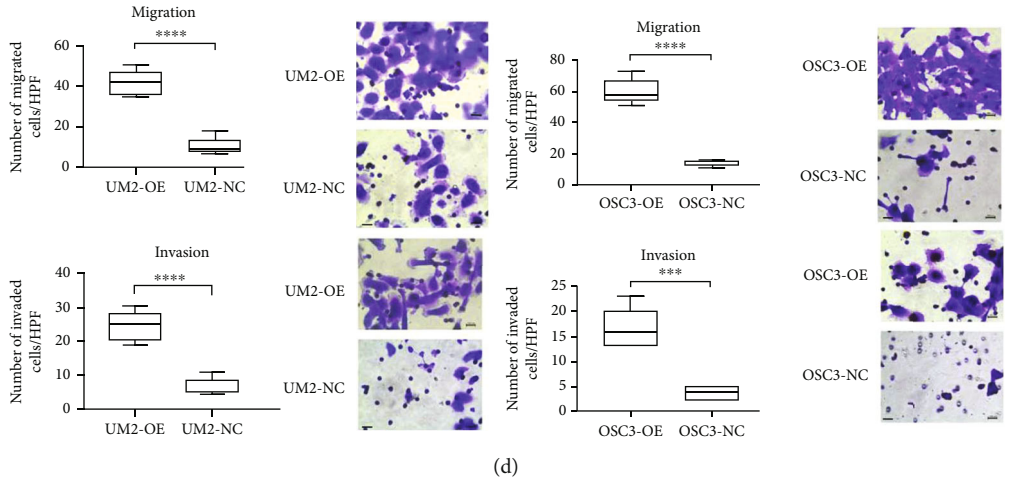

(d)

FIGURE 3: Wound healing assay showed that LEMD1-AS1 enhanced OSCC cells migration. The scope adumbrated by yellow line indicated the empty area calculated by ImageJ software. Data exhibited the mean of five biological replicates ± SE. (a) Downregulating LEMD1-AS1 expression significantly inhibited cell migration and invasion in OSC19 and CAL27 cells. (b) Upregulating LEMD1-AS1 expression highly promoted migration and invasion of UM2 and OSC3. (c) Transwell assay showed that up-regulating LEMD1-AS1 stimulated migration and invasion ability, while silencing LEMD1-AS1 repressed. The effect of LEMD1-AS1 in OSC19 and CAL27(C), UM2 and OSC3 (d). SS: LEMD1-AS1 Smart Silencer; NC: normal control. OE: LEMD1-AS1-overexpressing. Scale bar in wound healing assay = 100 μm. Scale bar in transwell assay = 20 μm.

and LEMD1. The RNase protection assay further showed that the remnant of the OL region between LEMD1-AS1 and LEMD1 was higher than the non-OL region, indicating that the OL region was partially protected from RNase degradation (Figure 6(a)). These results indicated that the stability of LEMD1 mRNA was increased by LEMD1-AS1. To functionally validate this surmise, we treated control or LEMD1-AS1-overexpressing OSC3 cells with the RNA polymerase II inhibitor α-amanitin to block new RNA synthesis and found that high levels of LEMD1-AS1 increased the stability of LEMD1 mRNA compared to that in control cells (Figure 6(b)). Thus, LEMD1-AS1 stabilizes and enhances the expression of LEMD1 mRNA in OSCC cells.

2.7. LEMD1-AS1 Activates the PI3K-AKT Pathway. On the basis of bioinformatics analysis and literature review, we analyzed the level of PI3K-AKT pathway-related proteins in the LEMD1-AS1-overexpressing OSCC cells. As shown in Additional Figure 8, p-PI3K and p-AKT were significantly upregulated in the OSC3 cells stably overexpressing LEMD1-AS1 compared to the control cells. Thus, LEMD1-AS1 might activate the PI3K-AKT pathway via increasing LEMD1 mRNA and protein levels.

2.8. LEMD1-AS1 Promoted Cervical LN and Hepatic Metastasis of OSCC In Vivo. To confirm the biological function of LEMD1-AS1 *in vivo*, we established cervical LN and hepatic metastasis models in B/C mice. LEMD1-AS1-overexpressing (OSC3-OE) or normal control (OSC3-NC) OSCC cells were injected into the mice FOM, and while 37.5% of the OSC3-OE mice had cervical LN metastasis, the OSC3-NC group did not show any metastasis (Additional Figure 9). Contradictory to the *in vitro* results, the volume of the orthotopic tumor was markedly larger in the OSC3-OE versus the OSC3-NC group, implying a greater proliferative capacity of the OSC3-OE cells *in vivo* (Figure 7).

3. Discussion

Recent studies have associated aberrant expression levels of lncRNAs with OSCC genesis and progression. However, little is known regarding the function of dysregulated lncRNAs in OSCC with regional LN metastasis [13, 14], which is the most pervasive cause of death in OSCC patients. To determine the role of lncRNAs and their target genes in cervical LN metastasis of OSCC, we identified the differentially expressed mRNAs and lncRNAs between primary OSCC samples with and without regional LN metastasis, since the expression pattern of primary tissues was similar to that of metastatic tissues according to the single cell sequencing result of head and neck squamous cell carcinoma in 2017 [15]. The DERNAs were enriched in GO components and KEGG pathways associated with tumor progression, migration and invasion, such as cell adhesion [16, 17], channel and receptor activity [18–20], cAMP signaling pathway [21], PI3K-AKT signaling pathway [22, 23], cytokine-cytokine receptor interaction, and CAMs [24]. The DElncRNA-DEmRNA network was subsequently constructed, and LEMD1-AS1 and its antisense mRNA LEMD1 were identified as a relevant pair in OSCC. LEMD1 [25] is a member of cancer–testis antigen (CTA) family and is located at chromosome 1q32.1. LEMD1-AS1 and LEMD1 were both upregulated in OSCC with LN metastasis compared to the nonmetastatic samples, indicating that LEMD1 and its reverse chain LEMD1-AS1 might enhance the migration and invasion abilities of OSCC cells.

Although LEMD1-AS1 gain/loss of function had no effect on OSCC cell growth, the LEMD1-AS1-overexpressing OSC3

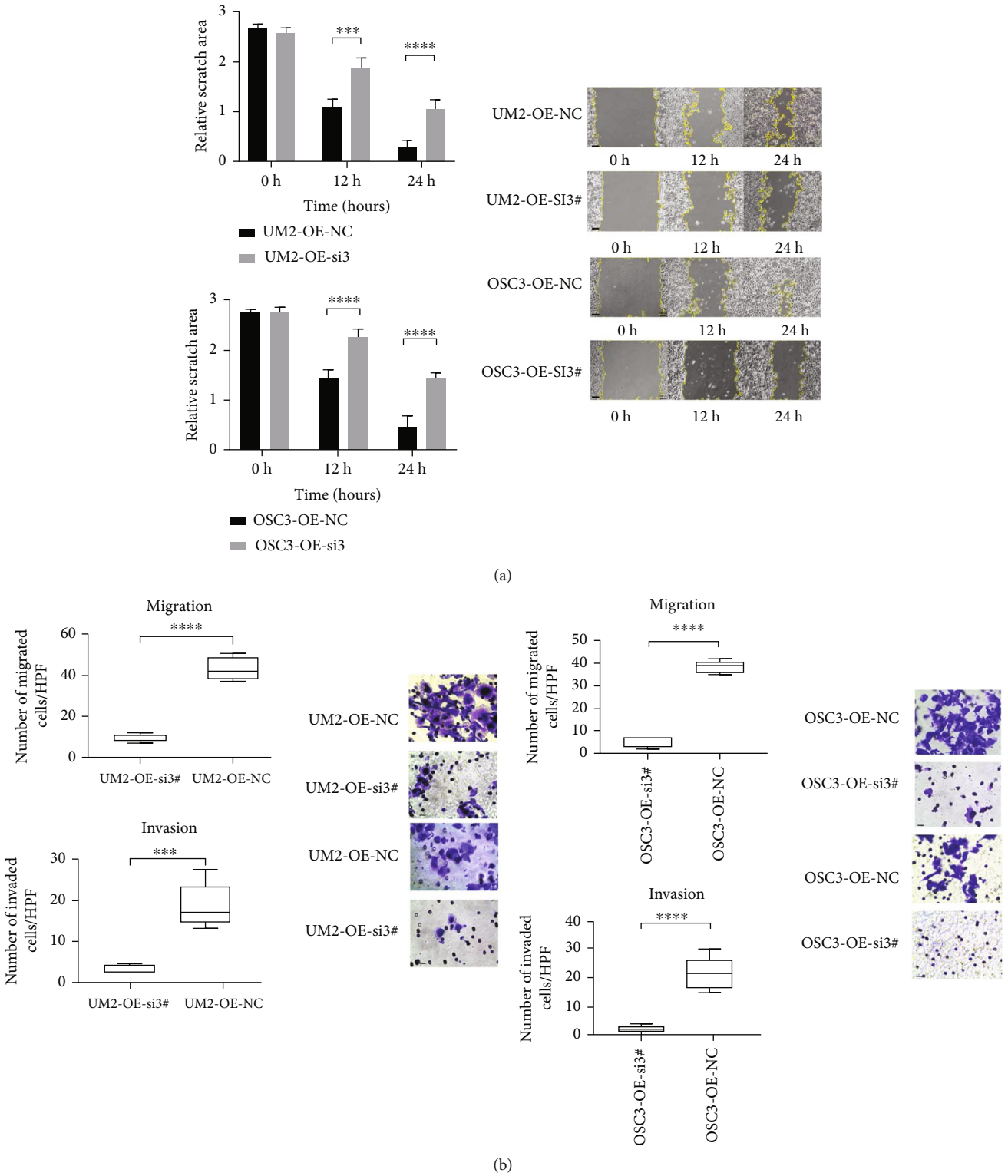

Figure 4: Silencing LEMD1 could rescue the phenotype in stably expressing LEMD1-AS1 OSCC cells. Wound healing assay in UM2 cell and OSC3 cell (a). Transwell assay in UM2 cells and OSC3 cells (b). si3#: LEMD1-si3#; NC: normal-control-si; OE: LEMD1-AS1-overexpressing. Scale bar in wound healing assay = 100 μm. Scale bar in transwell assay = 20 μm.

cells resulted in larger tumors compared to the control cells. This was likely due to the fact that increased invasiveness of these cells led to impingement of the orthotopic tumor into the mandibula and FOM muscle, which resulted in larger tumor volume. In the orthotopic OSCC model as well, OSC3-OE cells resulted in higher LN and hematogenous metastasis rates, which further verified the metastatic potential of LEMD1-AS1. Consistent with this, LEMD1-AS1

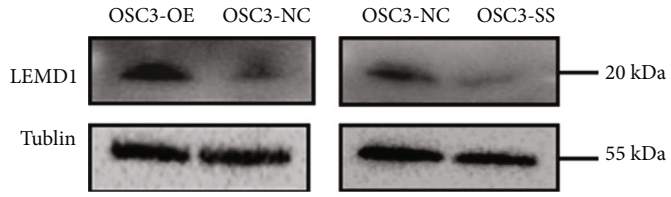

Figure 5: Western Blotting of LEMD1. After silencing LEMD1-AS1 for 48 hours in OSC3, the protein level of LEMD1 was diminished; and overexpression of LEMD1-AS1 increased LEMD1 expression at protein level. The samples were derived from the same experiment and that blots were processed in parallel. Full-length blots are presented in Supplementary Files.

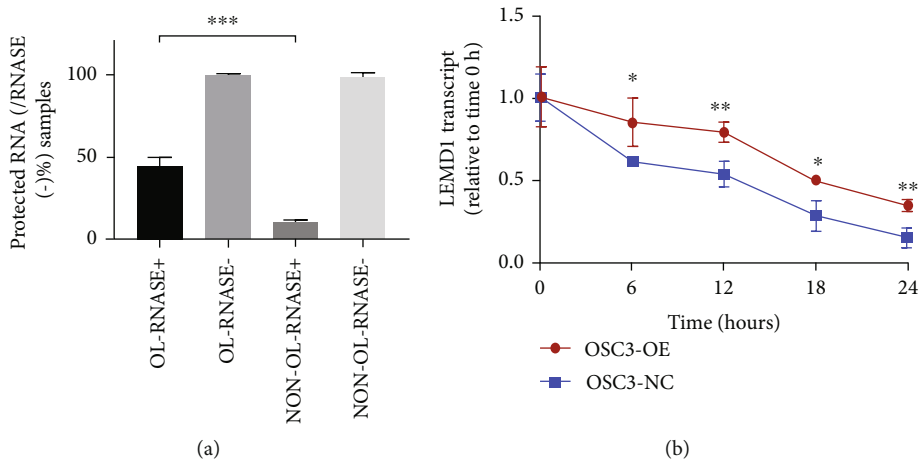

Figure 6: LEMD1-AS1 stabilized LEMD1 mRNA. (a) RNase protected assay indicated that the LEMD1-AS1 could protect OL region of LEMD1 from being depleted by RNase. (b) LEMD1-A1-overexpressing OSC3 cells were treated with 50 μM α-amanitin, and the LEMD mRNAs were detected by qPCR. High levels of LEMD1-AS1 increased the stability of LEMD1 mRNA compared to that in control cells. 18sRNA was applied as an internal control.

significantly promoted OSCC migration and invasion *in vitro*. Furthermore, LEMD1 silencing neutralized the pro-metastatic effects of LEMD1-AS1, indicating that LEMD1-AS1 directly targeted LEMD1 to increase OSCC cell invasiveness.

More than 63% of all transcripts in human cells possess antisense transcripts, which upon any perturbation can alter the expression of sense mRNAs [26–28]. Studies increasingly show that natural antisense lncRNA can stabilize its counterpart mRNA to increase its expression levels [29–31]. RNA-asRNA interactions are the result of the formation of RNA-RNA hybrid, partial physical binding [32, 33] or activating polysomes [27]. Bioinformatics analysis revealed that LEMD1-AS1 and LEMD1 formed a "tail-to-tail" paring pattern with a 183 bp OL region. In addition, LEMD1-AS1 was localized in the cytoplasm, indicating the possibility of duplex formation between LEMD1 and its antisense lncRNA. Furthermore, the OL region on LEMD1 mRNA was protected from RNase digestion, which depleted most of the non-OL region. Finally, overexpression of LEMD1-AS1 increased stability of LEMD1 mRNA even in the presence of the RNA polymerase II inhibitor α-amanitin. Thus, LEMD1-AS1 can stabilize LEMD1 mRNA and protect it from RNase via RNA-RNA interaction.

CTAs are upregulated in male germ cells and various cancer tissues, but not in normal tissues [34]. This protein cluster promotes epithelial mesenchymal transition (EMT) [35] and metastasis [36], invasion, and carcinogenesis. Not surprisingly, CTAs are attractive diagnostic biomarkers and therapeutic targets in cancer. LEMD1 also promotes the initiation and progression of various cancers like colorectal cancer [25, 37, 38] and prostate cancer [39]. Sasahira et al. [40] identified LEMD1 as a novel oncogene in OSCC and supported its diagnostic and therapeutic potential. LEMD1 is also the target gene of microRNA-135 in anaplastic large cell lymphoma [41]. We have elucidated the regulatory interaction between LEMD1-AS1 and LEMD1 for the first time, which provides novel insights into the mechanism of CTAs in cancer.

The PI3K-AKT pathway is crucial for cancer initiation and progression, and is frequently disrupted in solid tumors [22, 42]. Mutation or alterations in the PI3K-AKT pathway have been identified in OSCC [24, 43–45]. Consistent with a previous study in gastric cancer [46], we found that the PI3K-AKT pathway was activated in OSC3 cells stably overexpressing LEMD1-AS1. We surmise therefore that LEMD1-AS1 upregulates LEMD1 to activate the PI3K-AKT pathway, which promotes OSCC migration and invasion.

Regional LN metastasis is the most common cause of the poor survival rate among OSCC patients. We identified 487 DEmRNAs and 1507 DElncRNAs in the metastatic versus nonmetastatic OSCC samples and characterized LEMD1-AS1/LEMD1 interaction as a promoter of OSCC metastasis

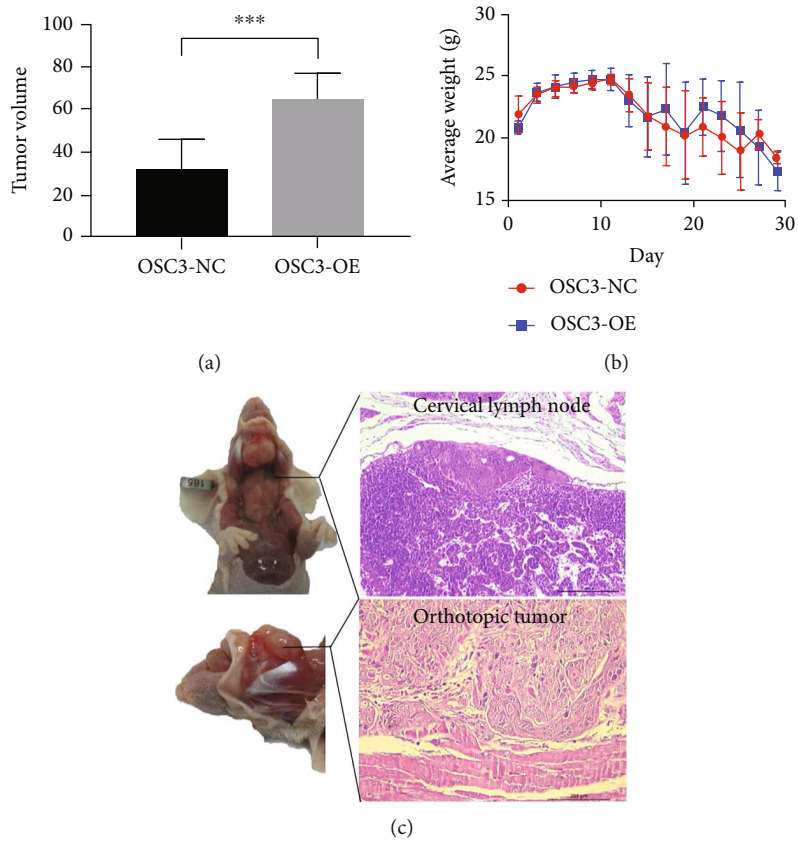

Figure 7: (a) The volume of the orthotopic tumor was markedly larger in the OSC3-OE compared to the OSC3-NC group. (b) However, there was no significant difference of weight between two groups. (c) Histochemical images of the orthotopic tumor and the metastatic lymph nodes.

for the first time. Mechanistically, LEMD1-AS1 activates the PI3K-AKT pathway by stabilizing and upregulating LEMD1. However, survival analysis related to LEMD1-AS1 expression was not possible due to the short follow-up time. In addition, the exact regulatory axis between LEMD1-AS1, LEMD1, and PI3K-AKT pathway in OSCC progression remains to be elucidated. Besides, the targeted genes of LEMD1-AS1 might not be only LEMD1; the relationship between its targeted genes should be further investigated. Our findings have to be validated on larger cohorts with longer follow-up.

4. Conclusions

LEMD1-AS1 was substantially increased in metastatic OSCC tissues and cell lines and promoted OSCC migration and invasion *in vitro* and *in vivo* by stabilizing its antisense transcript LEMD1, which is a potential activator of the PI3K-AKT signaling pathway. Therefore, LEMD1-AS1 is a novel diagnostic biomarker and immunotherapeutic target for metastatic OSCC.

5. Methods

5.1. Human Tissue Samples. Tumor tissues were collected from OSCC patients who underwent surgery at the Xiangya Hospital of Central South University. The patients that received radiotherapy or chemotherapy prior to the surgery were excluded. The baseline data of recruited patients is present in Table 1. All primary tumor tissue samples were confirmed by two experienced pathologists and stored at -80°C for RNA extraction. The clinical characteristics of the included patients were also recorded. The informed consent was obtained from all subjects. This study was approved by the ethics committee of the Xiangya Hospital (No. 201907790).

5.2. Next-Generation RNA Sequencing and Bioinformatics Analysis. Total RNA was isolated from 5 patients with cervical LN metastasis and 5 patients without cervical LN metastasis using the TRIzol reagent (Invitrogen, CA, USA) according to the manufacturer's instructions. The quality of RNA was evaluated by Qubit, Nanodrop, and Agilent 2100 Bioanalyzer. RNA sequencing libraries were prepared using TruSeq Stranded Total RNA Library Prep Kit according to manufacturer's specifications. The rRNAs were then removed, and the remaining transcripts were purified and fragmented. First-strand cDNA synthesis was performed using random primers, followed by second-strand cDNA synthesis and end repair. The 3′ ends of the cDNAs were adenylated and ligated to Illumina Truseq adaptors for PCR. The cDNA libraries were sequenced by Illumina Hiseq 2500. All bioinformatical analysis were performed by R and

Table 1: Baseline data of the patients recruited.

No.	Gender	Age (year)	Location	TNM stage	Differentiation level	Drinking	Smoking (*n*/day)
1	Male	52	Tongue	T1N2M0	High	+	10-20
2	Male	29	Tongue	T1N2M0	Moderate-high	—	<5
3	Male	50	Tongue	T1N1M0	High	+	0
4	Male	39	Bucal	T1N1M0	Moderate-high	+	10-20
5	Male	48	Tongue	T1N1M0	High	+	0
6	Male	52	Buccal mucosa	T3N0M0	High	—	10-20
7	Male	65	Tongue	T3N0M0	High	+	10-20
8	Male	47	Buccal mucosa	T3N0M0	High	+	10-20
9	Male	55	Buccal mucosa	T3N0M0	Moderate-high	—	<5
10	Male	55	Tongue	T3N0M0	High	+	<5

Table 2: Primers used for qRT-PCR.

Gene	Forward primer	Reverse primer
LEMD1-AS1	TGCAGCTCAGTCAGACCAAA	AGGCAGACGTGGGAGGAT
LEMD1	GAGCACCAAGCACCAGAATCA	ACCAAGCACAGCAAGCTTCA
LEMD1-OL	TGGACCCAGAGAGCTGGATG	TGCGTTTAGTGGTGGAAGCC
LEMD1-non-OL	ACTTCTATCATCATGGTGGATG	GATCTGTGAGAGCAGCACAG
GAPDH	AGTGGTCGTTGAGGGCAAT	GCATCCTGGGCTACACTGAG
18sRNA	GTAACCCGTTGAACCCCATT	CCATCCAATCGGTAGTAGCG
PURPL	GGCATGATCTCGGCTCACTA	CAGATCACGAGGTCAGGAGA
TBILA	TGACTTTCAAAGCACAGGAGG	CCATGATTCCTGTCCCGAGA
LINC01133	TGGTATTTTCATCATTGTGGTGT	TCAGGGTAGTGTTTTGGTTCTTT

LncTar software. *P* value was adjusted for multiple testing adopting the false discovery rated method, and $|\log 2 \text{ fold change (FC)}| > 1.0$ and *P* value< 0.05 were set as the cutoff criteria.

5.3. OSCC Cell Lines and Animals. OSCC cell lines including UM1, UM2, OSC3, OSC19, and CAL27 were cultured in high-glucose DMEM (Gibco, CA, USA) supplemented with 10% fetal bovine serum (Gibco, CA, USA), 100 U/ml penicillin, and 100 mg/ml streptomycin (Gibco, CA, USA) at 37% in a humidified incubator containing 5% CO_2. BALB/c-nude mice (5-week-old) were obtained from the Experiment Animal Center of Central South University. All animal experiments were approved by the Institutional Animal Care Committee of Central South University (No.2019sydw0116).

5.4. qRT-PCR Analysis. Total RNA was isolated using TRIzol reagent (Invitrogen, CA, USA) as described above, and reverse transcribed to cDNA by HiScript III RT SuperMix (Vazyme, Nanjing, China). Real-time PCR was performed on QuaintStudio 7 Flex System (Thermo Fisher, CA, USA) using the SYBR All-in-One qPCR mix (GeneCopoeia, Guangzhou, China), and relative gene expression was calculated using $2^{-\Delta\Delta CT}$ method normalized to that of GAPDH or 18sRNA. Primer sequences are listed in Table 2.

5.5. Fluorescent in Situ Hybridization. RNA fluorescence in situ hybridization (RNA-FISH) was performed using a FISH kit (Ribobio, Guangzhou, China) according to the manufacturer's instruction. Briefly, the suitably treated cells were fixed with 4% formaldehyde for 10 min, permeabilized with 0.5% Triton X-100 in PBS, and subsequently blocked through prehybridization at 37°C for 30 minutes. The cells were then incubated overnight with 50 nM FISH probe (Ribobio Co.) in 100 μl hybridization buffer at 37°C. The slides were washed with a gradient of hybridization wash buffer (4 × SCC with 0.1% Tween-20, 2 × SCC, 1 × SCC) at 42°C for 5 min, respectively, and air-dried. After counterstaining with 4′,6-diamidino-2-phenylindole (DAPI), the slides were imaged under a fluorescence microscope.

Table 3: Sequences of Smart Silencer for LEMD1-AS1 and siRNA for LEMD1.

Name	Targeted Sequence (5′-3′)
LEMD1-AS1 Smart Silencer	GACCAAACCTCTCTGAATA GACAGAACAAGAAGCACAA CTCTACATATCCATCACAT TCCAGCGCCCACTTTCTCAG GTCAGGACACAACAATAGAG ACAGCTCCTAGGCAATCAAA
LEMD1-siRNA1#	GAATCACATATGGGACTAT
LEMD1-siRNA2#	CGGAAGACCAGACTATCGA
LEMD1-siRNA3#	GCTGGAGAGAAGAAGGTTT

5.6. Transfection. The Ribo™ Smart Silencer targeting LEMD1-AS1 was obtained from RiboBio (Guangzhou, China) and included three siRNA and three antisense oligonucleotides targeting different sequences. The siRNAs for human LEMD1 were designed and synthesized by RiboBio (China). Cells were transfected with the respective siRNAs using Lipofectamine3000 Reagent (Invitrogen, CA, USA). In addition, OSCC cells were transduced with LEMD1-AS1 expressing lentivirus (GENECHEM, Shanghai, China) with specific MOI (multiplicity of infection). The siRNA sequences are listed in Table 3.

5.7. CCK-8 Assay. Cell growth was monitored using the 2-(2-methoxy-4-nitrophenyl)-3-(4-nitrophenyl)-5-(2,4-disulfothenyl)-2H-tetrazolium reagent (CCK-8, Meilunbio, Dalian, China) assay according to manufacturer's instruction. The transient and stable transfectants were seeded in 96-well plates at the density of 3000 cells/well with 5 replicates per sample. CCK-8 reagent was added to each well after 1, 2, and 3 days of culture, and the absorbance of each well was measured at 450 nm.

5.8. Wound Healing Assay. Suitably treated cells were seeded in six-well plates and grown till confluency. The monolayer was scratched across the plate using a sterile 10 μl pipette tip, and the dislodged cells were washed. The wounded regions were photographed at 0, 12, and 24 hours after scratching, and the scratch area was calculated by ImageJ software.

5.9. Transwell Assay. Cells harvested 36~48 hours after transient or stable transfection were seeded into the upper chambers of a transwell insert (Corning (3422, 354480), NY, USA) at the density of 8×10^4 cells/well in 200 μl serum-free high-glucose DMEM. The lower chambers were filled with 400 μl DMEM supplemented with 20% FBS. After a 24 h culture, the migrated cells were fixed with 4% paraformaldehyde for 30 minutes, stained with crystal violet for 30 minutes, and counted.

5.10. Western Blotting. Protein was extracted by lysing the cells in RIPA buffer (Abcam, NY, USA) supplemented with protease inhibitors and phosphate inhibitors, separated by SDS-PAGE and transferred onto a PVDF membrane. After blocking in 5% skimmed milk for 1 hour, the gels were incubated overnight with the primary antibodies (Abcam, MA, USA and CST, MA, USA), followed by the HRP-conjugated IgG secondary antibody. The bands were visualized using ECL Substrates (SAB, MD, USA). Tubulin was used as the loading control.

5.11. RNase Protection Assay. RNA duplex formation between LEMD1-AS1 and LEMD1 was assessed with the RNase A+T cocktail (Invitrogen, CA, USA) that can only digest single-stranded and not duplex RNAs. Briefly, the samples were incubated with the enzyme cocktail at 37°C for 30 minutes, and the remaining double-stranded RNA was extracted using RNeasy Kit (Tianmo, Beijing, China) and analyzed by qRT-PCR.

5.12. Stability and α-Amanitin Treatment. OSC3 cells stably expressing LEMD1-AS1 or the empty vector were seeded into 6-well plates and treated with 50 μM of the RNA synthesis blocker α-amanitin. The cells were harvested 0, 6, 12, 18, and 24 hours posttreatment and analyzed by qRT-PCR. The 18s RNA was used as the internal control since it is stable after α-amanitin treatment.

5.13. Animal Experiments. An orthotopic oral tumor model was established in mice by injecting control or LEMD1-AS1-overexpressing 2×10^5 OSC3 cells ($n = 8$ per group) in 100 μl DMEM into the floor of mouth (FOM) via submental to the space between the FOM muscles (around 5 mm). The mice were sacrificed on day 30 after implantation or when their weight was reduced to 16 grams (g) or less. The tongue and cervical LNs were collected and fixed in 10% paraformaldehyde immediately for HE staining. The volume of the orthotopic tumor was calculated as length × width^2/2. All tissue staining results were examined by two expert pathologists.

5.14. Statistical Analysis. All data were analyzed using the SPSS 22.0 statistical software package (SPSS Inc., Chicago, IL, USA) and visualized with Graphpad Prism 7. The results were expressed as the mean ± SD of three experiments. Two or multiple groups were compared using two-tailed Student's t-test and One-way ANOVA, respectively. Pearson's correlation coefficient was used to analyze the correlation between LEMD1-AS1 and LEMD1 expression levels. P value < 0.05 was considered statistically significant.

Data Availability

The data used to support the findings of this study are included within the article and the supplementary information files.

Ethical Approval

This study was approved by the Ethics Committee of the Xiangya Hospital (No. 201907790) and the Institutional Animal Care Committee of Central South University (No. 2019sydw0116).

Consent

The informed consent was obtained from all subjects. All methods were carried out in accordance with relevant guidelines and regulations (for both humans and animals).

Conflicts of Interest

The authors declare that they have no competing interests.

Authors' Contributions

Zaiye Li and Canhua Jiang did the conceptualization. Zaiye Li is assigned to the methodology. Zaiye Li is assigned to the software. Ning Li and Jianjun Wu did the validation. Jie Wang did the formal analysis and investigation. Jianjun Wu is assigned to the resources. Zaiye Li, Jianjun Wu and

Canhua Jiang curated the data. Zaiye Li and Jie Wang did the writing—original draft preparation. Jie Wang and Canhua Jiang did the writing—review and editing. Jianjun Wu worked on visualization. Jie Wang and Canhua Jiang worked on supervision. Canhua Jiang is responsible for the project administration. Canhua Jiang and Zaiye Li acquired funding. All authors have read and agreed to the published version of the manuscript.

Acknowledgments

This study was supported by the Natural Science Foundation of Hunan Province, China (Grant No. 2020JJ4881), and the Fundamental Research Funds for Central Universities of the Central South University (2019zzts795).

Supplementary Materials

Additional Figure 1: functional enrichment analysis of DEmRNAs. (A) The bar plot of GO analyses. Purple for MF, orange for CC, and yellow for BP. (B) The top 10 enrichment scores in KEGG pathway. Additional Figure 2: DElncRNA-DEmRNA interaction network in *cis*- and *trans*-way. Circles indicate mRNAs, and rectangles indicate lncRNAs. Red nodes mean upregulation in metastatic OSCC samples, while green nodes represent downregulation. (A) *Cis*-way. (B) *Trans*-way. Additional Figure 3: expression of LEMD1-AS1 in OSCC cell lines. Five OSCC cell lines were examined. The metastatic OSCC cell lines UM1, OSC19, and CAL27 showed significantly higher LEMD-AS1 levels compared to the nonmetastatic UM2 and OSC3 cells. The red $*$ indicated statistical difference with OSC3, and blue one indicated that with UM1. Additional Figure 4: subcellular location of LEMD1-AS1. Fish assay revealed that LEMD1-AS1 mainly is located in the cytoplasm, while a few in the nucleus. Red shows LEMD1-AS1, and blue shows nucleus; scale bar = 50 μm. Additional Figure 5: expression of LEMD1AS1 and LEMD1 in transfectants. (A) LEMD1-AS1 knockdown efficiency in OSC19 and CAL27 with Smart Silencer. (B) LEMD1-AS1 overexpression efficiency in UM2 and OSC3 with lentivirus. (C) LEMD1 mRNA expression level was decreased in LEMD1-AS1-knockdown OSCC cells. (D) LEMD1 mRNA expression level was elevated in LEMD1-AS1-overexpressing OSCC cells. Additional Figure 6: CCK8 assay implied that LEMD1-AS1 was not able to influence the cell growth in OSCC cells. (A) Knockdown of LEMD1-AS1 in OSC19 and CAL27 cells did not affect cell growth. (B) Overexpression of LEMD1-AS1 in UM2 and OSC3 cells did not change the ability of growth. SS: LEMD1-AS1 Smart Silencer; NC: normal control; OE: LEMD1-AS1-overexpressing. Additional Figure 7: apply 3 sequences of siRNA to inhibit LEMD1 expression. Among these, si3# had the highest transfection efficiency. Additional Figure 8: Western Blotting showed that the level of PI3K-AKT pathway-related proteins was increased in LEMD1-AS1-overexpressing OSC3 cells compared to the control cells. Additional Figure 9: the metastasis ratio of two groups (LEMD1-AS1-overexpressing and normal control (NC)). *(Supplementary Materials)*

References

[1] R. L. Siegel, K. D. Miller, and A. Jemal, "Cancer statistics, 2019," *CA: a cancer journal for clinicians*, vol. 69, no. 1, pp. 7–34, 2019.

[2] M. Du, R. Nair, L. Jamieson, Z. Liu, and P. Bi, "Incidence trends of lip, oral cavity, and pharyngeal cancers: global burden of disease 1990-2017," *Journal of dental research*, vol. 99, no. 2, pp. 143–151, 2020.

[3] R. L. Siegel, K. D. Miller, H. E. Fuchs, and A. Jemal, "Cancer statistics, 2021," *CA: a cancer journal for clinicians*, vol. 71, no. 1, pp. 7–33, 2021.

[4] S. Warnakulasuriya, "Global epidemiology of oral and oropharyngeal cancer," *Oral oncology*, vol. 45, no. 4-5, pp. 309–316, 2009.

[5] C. Rivera and B. Venegas, "Histological and molecular aspects of oral squamous cell carcinoma (review)," *Oncology letters*, vol. 8, no. 1, pp. 7–11, 2014.

[6] C. P. Ponting, P. L. Oliver, and W. Reik, "Evolution and functions of long noncoding RNAs," *Cell*, vol. 136, no. 4, pp. 629–641, 2009.

[7] J. S. Mattick and J. L. Rinn, "Discovery and annotation of long noncoding RNAs," *Nature structural & molecular biology*, vol. 22, no. 1, pp. 5–7, 2015.

[8] X. Luo, Y. Qiu, Y. Jiang et al., "Long non-coding RNA implicated in the invasion and metastasis of head and neck cancer: possible function and mechanisms," *Molecular cancer*, vol. 17, no. 1, p. 14, 2018.

[9] S. Ghafouri-Fard, H. Mohammad-Rahimi, M. Jazaeri, and M. Taheri, "Expression and function of long non-coding RNAs in head and neck squamous cell carcinoma," *Experimental and Molecular Pathology*, vol. 112, article 104353, 2020.

[10] M. Guttman and J. L. Rinn, "Modular regulatory principles of large non-coding RNAs," *Nature*, vol. 482, no. 7385, pp. 339–346, 2012.

[11] Y. Zhao, Y. Liu, L. Lin et al., "The lncRNA MACC1-AS1 promotes gastric cancer cell metabolic plasticity via AMPK/Lin28 mediated mRNA stability of MACC1," *Molecular cancer*, vol. 17, no. 1, p. 69, 2018.

[12] Z. Zhang, Z. Peng, J. Cao et al., "Long noncoding RNA PXN-AS1-L promotes non-small cell lung cancer progression via regulating PXN," *Cancer cell international*, vol. 19, no. 1, p. 20, 2019.

[13] Y. Wang, X. Zhang, Z. Wang et al., "LncRNA-p23154 promotes the invasion-metastasis potential of oral squamous cell carcinoma by regulating Glut1-mediated glycolysis," *Cancer letters*, vol. 434, pp. 172–183, 2018.

[14] Y. L. Qiu, Y. H. Liu, J. D. Ban et al., "Pathway analysis of a genome-wide association study on a long non-coding RNA expression profile in oral squamous cell carcinoma," *Oncology reports*, vol. 41, no. 2, pp. 895–907, 2019.

[15] S. V. Puram, I. Tirosh, A. S. Parikh et al., "Single-cell transcriptomic analysis of primary and metastatic tumor ecosystems in head and neck cancer," *Cell*, vol. 171, no. 7, pp. 1611–24.e24, 2017.

[16] E. Bonastre, E. Brambilla, and M. Sanchez-Cespedes, "Cell adhesion and polarity in squamous cell carcinoma of the lung," *The Journal of pathology*, vol. 238, no. 5, pp. 606–616, 2016.

[17] F. Ramadan, A. Fahs, S. E. Ghayad, and R. Saab, "Signaling pathways in rhabdomyosarcoma invasion and metastasis," *Cancer Metastasis Reviews*, vol. 39, no. 1, pp. 287–301, 2020.

[18] H. Wang, L. Zou, K. Ma et al., "Cell-specific mechanisms of TMEM16A Ca^{2+}-activated chloride channel in cancer," *Molecular cancer*, vol. 16, no. 1, p. 152, 2017.

[19] N. Deliot and B. Constantin, "Plasma membrane calcium channels in cancer: alterations and consequences for cell proliferation and migration," *Biochimica et Biophysica Acta*, vol. 1848, no. 10, pp. 2512–2522, 2015.

[20] C. S. Hinrichs, "Molecular pathways: breaking the epithelial cancer barrier for chimeric antigen receptor and T-cell receptor gene therapy," *Clinical cancer research : an official journal of the American Association for Cancer Research*, vol. 22, no. 7, pp. 1559–1564, 2016.

[21] J. Li, M. A. Duran, N. Dhanota et al., "Metastasis and immune evasion from extracellular cGAMP hydrolysis," *Cancer Discovery*, vol. 11, no. 5, pp. 1212–1227, 2021.

[22] D. Tewari, P. Patni, A. Bishayee, A. N. Sah, and A. Bishayee, "Natural products targeting the PI3K-Akt-mTOR signaling pathway in cancer: a novel therapeutic strategy," *Seminars in cancer biology*, 2019.

[23] B. Yang, L. Li, G. Tong et al., "Circular RNA circ_001422 promotes the progression and metastasis of osteosarcoma via the miR-195-5p/FGF2/PI3K/Akt axis," *Journal of Experimental & Clinical Cancer Research*, vol. 40, no. 1, p. 235, 2021.

[24] Z. Li, C. Jiang, and Y. Yuan, "TCGA based integrated genomic analyses of ceRNA network and novel subtypes revealing potential biomarkers for the prognosis and target therapy of tongue squamous cell carcinoma," *PLoS One*, vol. 14, no. 5, article e0216834, 2019.

[25] D. Yuki, Y. M. Lin, Y. Fujii, Y. Nakamura, and Y. Furukawa, "Isolation of LEM domain-containing 1, a novel testis-specific gene expressed in colorectal cancers," *Oncology reports*, vol. 12, no. 2, pp. 275–280, 2004.

[26] S. Katayama, Y. Tomaru, T. Kasukawa et al., "Antisense transcription in the mammalian transcriptome," *Science*, vol. 309, no. 5740, pp. 1564–1566, 2005.

[27] C. Carrieri, L. Cimatti, M. Biagioli et al., "Long non-coding antisense RNA controls _Uchl1_ translation through an embedded SINEB2 repeat," *Nature*, vol. 491, no. 7424, pp. 454–457, 2012.

[28] R. Yelin, D. Dahary, R. Sorek et al., "Widespread occurrence of antisense transcription in the human genome," *Nature biotechnology*, vol. 21, no. 4, pp. 379–386, 2003.

[29] K. Matsui, M. Nishizawa, T. Ozaki et al., "Natural antisense transcript stabilizes inducible nitric oxide synthase messenger RNA in rat hepatocytes," *Hepatology*, vol. 47, no. 2, pp. 686–697, 2008.

[30] C. L. Zhang, K. P. Zhu, and X. L. Ma, "Antisense lncRNA FOXC2-AS1 promotes doxorubicin resistance in osteosarcoma by increasing the expression of FOXC2," *Cancer letters*, vol. 396, pp. 66–75, 2017.

[31] B. Huang, J. H. Song, Y. Cheng et al., "Long non-coding antisense RNA KRT7-AS is activated in gastric cancers and supports cancer cell progression by increasing KRT7 expression," *Oncogene*, vol. 35, no. 37, pp. 4927–4936, 2016.

[32] G. Gao, W. Li, S. Liu et al., "The positive feedback loop between ILF3 and lncRNA ILF3-AS1 promotes melanoma proliferation, migration, and invasion," *Cancer management and research*, vol. Volume 10, pp. 6791–6802, 2018.

[33] J. Sun, X. Wang, C. Fu et al., "Long noncoding RNA FGFR3-AS1 promotes osteosarcoma growth through regulating its natural antisense transcript FGFR3," *Molecular biology reports*, vol. 43, no. 5, pp. 427–436, 2016.

[34] M. J. Scanlan, A. O. Gure, A. A. Jungbluth, L. J. Old, and Y. T. Chen, "Cancer/testis antigens: an expanding family of targets for cancer immunotherapy," *Immunological Reviews*, vol. 188, no. 1, pp. 22–32, 2002.

[35] P. Yang, Z. Huo, H. Liao, and Q. Zhou, "Cancer/testis antigens trigger epithelial-mesenchymal transition and genesis of cancer stem-like cells," *Current pharmaceutical design*, vol. 21, no. 10, pp. 1292–1300, 2015.

[36] B. Shang, A. Gao, Y. Pan et al., "CT45A1 acts as a new proto-oncogene to trigger tumorigenesis and cancer metastasis," *Cell death & disease*, vol. 5, no. 6, article e1285, 2014.

[37] R. Takeda, Y. Hirohashi, M. Shen et al., "Identification and functional analysis of variants of a cancer/testis antigen LEMD1 in colorectal cancer stem-like cells," *Biochemical and biophysical research communications*, vol. 485, no. 3, pp. 651–657, 2017.

[38] D. Li, D. Wang, H. Liu, and X. Jiang, "LEM domain containing 1 (LEMD1) transcriptionally activated by SRY-related high-mobility-group box 4 (SOX4) accelerates the progression of colon cancer by upregulating phosphatidylinositol 3-kinase (PI3K)/protein kinase B (Akt) signaling pathway," *Bioengineered*, vol. 13, no. 4, pp. 8087–8100, 2022.

[39] S. Ghafouri-Fard, Z. Ousati Ashtiani, B. Sabah Golian, S. M. Hasheminasab, and M. H. Modarressi, "Expression of two testis-specific genes, SPATA19 and LEMD1, in prostate cancer," *Archives of Medical Research*, vol. 41, no. 3, pp. 195–200, 2010.

[40] T. Sasahira, M. Kurihara, C. Nakashima, T. Kirita, and H. Kuniyasu, "LEM domain containing 1 promotes oral squamous cell carcinoma invasion and endothelial transmigration," *British journal of cancer*, vol. 115, no. 1, pp. 52–58, 2016.

[41] H. Matsuyama, H. I. Suzuki, H. Nishimori et al., "miR-135b mediates NPM-ALK-driven oncogenicity and renders IL-17-producing immunophenotype to anaplastic large cell lymphoma," *Blood*, vol. 118, no. 26, pp. 6881–6892, 2011.

[42] J. A. Engelman, J. Luo, and L. C. Cantley, "The evolution of phosphatidylinositol 3-kinases as regulators of growth and metabolism," *Nature reviews Genetics*, vol. 7, no. 8, pp. 606–619, 2006.

[43] D. R. Simpson, L. K. Mell, and E. E. Cohen, "Targeting the PI3K/AKT/mTOR pathway in squamous cell carcinoma of the head and neck," *Oral oncology*, vol. 51, no. 4, pp. 291–298, 2015.

[44] R. Vander Broek, S. Mohan, D. F. Eytan, Z. Chen, and C. Van Waes, "The PI3K/Akt/mTOR axis in head and neck cancer: functions, aberrations, cross- talk, and therapies," *Oral diseases*, vol. 21, no. 7, pp. 815–825, 2015.

[45] F. E. Marquard and M. Jucker, "PI3K/AKT/mTOR signaling as a molecular target in head and neck cancer," *Biochemical Pharmacology*, vol. 172, article 113729, 2020.

[46] Q. Li, Y. Ge, X. Chen et al., "LEM domain containing 1 promotes proliferation via activating the PI3K/Akt signaling pathway in gastric cancer," *Journal of Cellular Biochemistry*, vol. 120, no. 9, pp. 15190–15201, 2019.

Hindawi
BioMed Research International
Volume 2022, Article ID 8506242, 8 pages
https://doi.org/10.1155/2022/8506242

Research Article

PCR Detection of Epstein-Barr Virus (EBV) DNA in Patients with Head and Neck Squamous Cell Carcinoma, in Patients with Chronic Tonsillitis, and in Healthy Individuals

Joanna Katarzyna Strzelczyk,[1] **Agata Świętek**,[1] **Krzysztof Biernacki**,[1] **Karolina Gołąbek**,[1] **Jadwiga Gaździcka**,[1] **Katarzyna Miśkiewicz-Orczyk**,[2] **Wojciech Ścierski**,[2] **Janusz Strzelczyk**,[3] **Rafał Fiolka**,[4] **and Maciej Misiołek**[2]

[1]*Department of Medical and Molecular Biology, Faculty of Medical Sciences in Zabrze, Medical University of Silesia in Katowice, 19 Jordana St., 41-808 Zabrze, Poland*
[2]*Department of Otorhinolaryngology and Oncological Laryngology, Faculty of Medical Sciences in Zabrze, Medical University of Silesia in Katowice, 10 C Skłodowskiej St., 41-800 Zabrze, Poland*
[3]*Department of Endocrinology and Neuroendocrine Tumors, Department of Pathophysiology and Endocrinology, Faculty of Medical Sciences in Zabrze, Medical University of Silesia in Katowice, 35 Ceglana St., 40-514 Katowice, Poland*
[4]*Doctoral School, Faculty of Medical Sciences in Zabrze, Medical University of Silesia in Katowice, 40-055 Katowice, Poland*

Correspondence should be addressed to Joanna Katarzyna Strzelczyk; jstrzelczyk@sum.edu.pl

Received 25 May 2022; Revised 24 June 2022; Accepted 27 July 2022; Published 8 August 2022

Academic Editor: Jing Zhang

Epstein-Barr virus (EBV) is a common virus worldwide that is an etiologic agent in the development of many diseases, including cancer. Recent reports have shown the association of EBV with tumorigenesis in head and neck squamous cell carcinoma (HNSCC). Moreover, EBV has been reported to be present in tonsillar tissues, which suggests a close relationship between viral infections and tonsillar diseases, including chronic tonsillitis. The aim of the study was to analyze the prevalence of EBV DNA in 86 patients with HNSCC, in 70 patients with chronic tonsillitis, and in 144 healthy individuals (control group) and the associations between EBV infection and clinicopathological and demographic characteristics and the use of stimulants in all study groups. The objective of this study was also to analyze the prevalence of coinfection with human papillomavirus (HPV). After prior DNA isolation, EBV detection was performed using an EBV kit by real-time polymerase chain reaction. The prevalence of EBV infection in patients with HNSCC, patients with chronic tonsillitis, and the control group was 47.7%, 60%, and 24.3%, respectively. Compared to controls, a significantly higher prevalence of EBV in patients with chronic tonsillitis and HNSCC may suggest that EBV is a potential risk factor. No association was found between EBV infection and demographic or clinical data. Further studies are warranted due to inconclusive reports that were mainly related to geographic distribution, sample type, and detection technique. Considering the prevalence of the virus and the risk of serious diseases, attention should be paid to screening diagnosis and prevention of the infection.

1. Introduction

Epstein-Barr virus belongs to the gammaherpesviruses and is composed of an icosahedral capsid of more than 100 nm in diameter, consisting of 162 capsomeres, which envelops a double-stranded deoxyribonucleic acid (DNA) molecule [1]. Moreover, there are two EBV types, namely, EBV-1 and EBV-2 (previously known as EBV-A and EBV-B). The virus is spread through body fluids, mainly saliva, blood, and semen [2]. The symptoms of EBV infection may vary, depending on age and immunity. They are mostly mild benign in younger individuals [3]. According to various sources, 90-95% of the adult population is infected with EBV, regardless of socioeconomic status and place of

residence. Recently, interest in EBV has increased significantly due to the reports on the potentially oncogenic nature of the virus [4, 5]. Studies showed that EBV could be involved in initiating and/or enhancing epithelial-mesenchymal transition (EMT), which is important in cancer progression and metastasis [6–9]. It has been reported that among oncogenic viruses, EBV may be associated with the development of tumors in head and neck squamous cell carcinoma (HNSCC) [10].

HNSCC is a disease related to important anatomical regions such as the oral cavity, the nasopharyngeal cavity, and the larynx [11]. HNSCC is the sixth most prevalent cancer worldwide (890,000 new cases and approximately 450,000 deaths annually) [12]. About 90% of all cancers of the head and neck region originate from squamous cells [13]. The occurrence of these cancers is strongly related to environmental factors and lifestyle. Studies have shown that increased risk factors for HNSCC include tobacco exposure and alcohol abuse [14–16].

The term "chronic tonsillitis" is not clearly defined, and it usually refers to a sore throat lasting more than 3 months accompanied by the inflammation of the tonsils with lymph node reaction [17]. Most chronic inflammation occurs in the palatine and/or pharyngeal tonsils [18]. Inflamed tonsils are a focus of infection that can have a significant impact on other organs. In chronic inflammation, tonsillectomy is usually performed [19].

The aim of the study was to analyze the prevalence of EBV DNA in patients with HNSCC, in patients with chronic tonsillitis, and in healthy individuals and the associations between EBV infection and clinicopathological and demographic characteristics and the use of stimulants in all study groups. The objective of this study was also to analyze the prevalence of coinfection with human papillomavirus (HPV).

2. Material and Methods

2.1. Study Population and Specimen Collection. The study was approved by the Bioethics Committee (Institutional Review Board on Medical Ethics, No. KNW/0022/KB1/49/16 and No. KNW/0022/KB1/49/II/16/17). All volunteers gave written informed consent before participating in the study.

The study was comprised of 300 patients, including 86 subjects with HNSCC and 70 patients with chronic tonsillitis. The control group consisted of 144 healthy individuals. Information on demographic variables including age, sex, and the use of stimulants such as alcohol and tobacco was collected from all patients and healthy individuals. Patients in the study groups were diagnosed in the Department of Otorhinolaryngology and Oncological Laryngology in Zabrze, Medical University of Silesia in Katowice. Cancer samples were obtained during surgical resection and tonsillar tissue samples during tonsillectomy.

The diagnosis of HNSCC in the tumor tissues was made by routine histological assessment after surgical resection. In the group with chronic tonsillitis, the samples were histologically verified by a pathologist after sampling during tonsillectomy. The samples from both groups were stored at -80°C until further analysis after being frozen in liquid nitrogen.

Buccal epithelial scrapings were collected from healthy volunteers. The oral mucosa of cheeks was scraped with a cotton swab stick followed by the DNA extraction. All molecular analyses were performed at the Department of Medical and Molecular Biology, Faculty of Medical Sciences in Zabrze, Medical University of Silesia. Moreover, the HPV infection status of all study participants was obtained from our previous study to analyze coinfections [20].

2.2. Study Groups. The HNSCC group consisted of 86 patients (mean age 57.9 ± 11.7 years); this group consisted of 28 (32.6%) women and 58 (67.4%) men (Table 1). In 86 patients, the anatomical sites of tumors were as follows: the tongue ($n = 42$, 48.8%), the floor of the mouth ($n = 16$, 18.6%), the mandible ($n = 15$, 17.4%), the left palatine tonsil ($n = 7$, 8.1%), the cheek and the soft palate ($n = 6$, 7.0%), and the right palatine tonsil ($n = 5$, 5.8%). One case of HNSCC was found in the retromolar trigone (1.2%). In addition, in 22 patients (25.6%), tumors were detected in more than one location. Radiation therapy or chemotherapy was not administered to any patient prior to tumor excision surgery. The clinical stage of tumors was characterized according to the TNM classification of the American Joint Committee on Cancer (AJCC) 8th edition [21]. The detailed clinical data, including T-classification (T), lymph node status (N), and histological grade (G), are given in Table 2.

The chronic tonsillitis group was composed of 70 patients (mean age 33.3 ± 11.2 years); this group included 36 (51.4%) women and 34 (48.6%) men (Table 1).

The healthy control group consisted of 144 individuals (mean age 40.8 ± 16.6 years); this group was composed of 91 (63.2%) women and 53 (36.8%) men (Table 1).

2.3. DNA Preparation. All tumor and tonsillar tissue samples were slowly thawed and homogenized with Lysing Matrix A ceramic beads in FastPrep®-24 (MP Biomedicals, Irvin, California, USA), and then, DNA was isolated using a Gene Matrix Tissue DNA Purification Kit (EURx, Gdańsk, Poland) according to the standard procedures. In case of a control group, DNA was isolated from buccal epithelial cells using a GeneMATRIX Swab-Extract DNA Purification Kit (EURx, Gdańsk, Poland) according to the manufacturer's instructions. The quantity and quality of the extracted DNA were analyzed using a spectrophotometer (NanoPhotometer Pearl, Implen, Germany).

2.4. EBV Detection by Polymerase Chain Reaction. EBV detection was performed with EBV PCR Kit (EBV/ISEX/100, GeneProof, Brno, Czech Republic) using real-time PCR according to the manufacturer's protocol using QuantStudio 5 (Thermo Fisher Scientific, Waltham, Massachusetts, USA). The method consists in amplifying a specific conserved DNA sequence of a single copy gene encoding nuclear antigen 1 (EBNA1) and measuring the increase in fluorescence. The presence of EBV is indicated by the increase in fluorescence of the FAM fluorophore. An internal standard (IS) was included in the reaction mixture,

Table 1: Summary of the main characteristics of the study participants.

		HNSCC *n* (%)	Chronic tonsillitis *n* (%)	Control *n* (%)	All *n* (%)
Sex	Female	28 (32.56%)	36 (51.43%)	91 (63.19%)	155 (51.67%)
	Male	58 (67.44%)	34 (48.57%)	53 (36.81%)	145 (48.33%)
Smoking	Yes	59 (69.41%)	10 (14.29%)	25 (17.36%)	94 (31.44%)
	No	26 (30.59%)	60 (85.71%)	119 (82.64%)	205 (68.56%)
Occasional drinking	Yes	56 (65.12%)	21 (30%)	107 (74.31%)	184 (61.33%)
	No	30 (34.88%)	49 (70%)	37 (25.69%)	116 (38.67%)
Regular drinking	Yes	42 (48.84%)	2 (2.86%)	10 (6.94%)	54 (18%)
	No	44 (51.16%)	68 (97.14%)	134 (93.06%)	246 (82%)
Both smoking and drinking	Yes	43 (50%)	6 (8.57%)	23 (15.97%)	72 (24%)
	No	43 (50%)	64 (91.43%)	121 (84.03%)	228 (76%)

Table 2: Clinical data of the HNSCC group.

	n	(%)
Clinical T-classification	86	(100.00)
T1	10	(11.6)
T2	22	(25.6)
T3	26	(30.2)
T4	28	(32.6)
T1+T2	32	(37.2)
T3+T4	54	(62.8)
Lymph node status	86	(100.00)
N0	39	(43.3)
N1	21	(24.4)
N2	23	(26.7)
N3	3	(3.5)
N1+N2	44	(51.2)
Histological grade	86	(100.00)
G1	13	(15.1)
G2	54	(62.8)
G3	19	(22.1)
G1+G2	66	(76.7)

which also controls the quality of the DNA extraction process. Positive IS amplification was detected in the fluorescence channel of the HEX fluorophore.

2.5. HPV Detection and HPV Type Determination. HPV infection status of all study participants was obtained from our previous study [20]. HPV detection and identification of subtypes were performed by GenoFlow HPV (Human Papillomavirus) Array Test Kits (DiagCor Bioscience Inc., Hong Kong). Colored dots on the membrane indicated positivity and were recorded by scanning (CapturePro Image, CaptureREAD 3.1.; DiagCor Bioscience Inc., Hong Kong). All runs included positive and negative controls and amplification and hybridization controls.

2.6. Statistical Analysis. The Kruskal-Wallis test and the Fisher exact test were used to compare the groups based on the EBV status and age, sex, smoking, occasional/regular alcohol consumption, and both alcohol and tobacco use. The EBV status and EBV and HPV coinfection impact on clinical T-classification (T), lymph node status (N), histological grade (G), and localization of the primary tumor were assessed using the Kruskal-Wallis and Fisher exact tests. All statistical analyses were performed using the STATISTICA 13.3 software (StatSoft. Inc., Tulsa, Oklahoma, USA) with the significance level of $\alpha < 0.05$ for complete sets of clinical data. Therefore, some patients or controls were excluded from the study.

3. Results

3.1. The Prevalence of EBV in All Study Groups. EBV was present in 60% (42/70) of patients with chronic tonsillitis, which was significantly higher ($p < 0.05$) than in the control group (24.3%, 35/144). However, it was not significantly ($p = 0.13$) more prevalent than in the HNSCC group (47.7%, 41/86). EBV-positive status was significantly more prevalent in the HNSCC group and chronic tonsillitis group than in the healthy control group ($p < 0.05$, Figure 1).

Coinfection of HPV and EBV was the most prevalent in the group with chronic tonsillitis (15.7%). In the HNSCC group, coinfection occurred in 11.6% of patients while in the control group only in 7.6% (Figure 1). Coinfection of EBV with HPV was significantly higher in HNSCC patients with lymph node status N2 (Table S1). This effect could only be observed in patients with coinfection. No other significant differences were observed in terms of the prevalence of coinfection.

3.2. Clinical and Demographic Data, the Use of Stimulants, and the EBV Status in the Groups with HNSCC and Chronic Tonsillitis and in the Control Group. No significant association was found between the EBV status and age, sex, smoking, occasional/regular alcohol consumption, or both alcohol consumption and smoking in groups with HNSCC and chronical tonsillitis or in the control group. Additionally, no significant association was found between the EBV status and clinical T-classification (T), lymph node status (N), histological grade (G), or the location of the

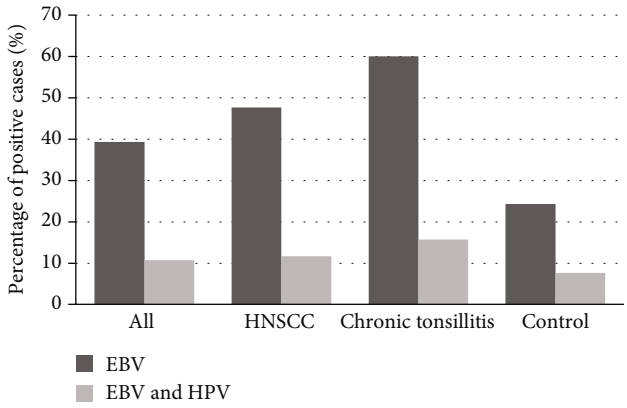

Figure 1: Percentage of positive EBV cases and coinfection of EBV and HPV in all study groups.

primary tumor in HNSCC patients. When analyzing all samples ($n = 300$), we found only one significant association, which was the lower prevalence of EBV infections in the group of occasional and regular alcohol users (Table S2).

4. Discussion

Epstein-Barr virus (EBV) is the first herpesvirus to be linked to cancer and is known to infect most of the adult human population. The EBV life cycle is divided into a lytic phase and a latent phase. Expression of latent EBV genes in infected epithelial cells is probably associated with their transformation into cancer cells [22].

The aim of the study is to clarify whether EBV has any impact on the biological behaviour of HNSCC carcinogenesis and chronic inflammation process by analyzing EBV prevalence and clinicopathological and demographic characteristics in HNSCC patients, in patients with chronic tonsillitis, and in healthy individuals. Our analysis also focuses on external environmental factors, such as alcohol use and cigarette smoking, and coinfection with human papillomavirus (HPV).

Polz-Gruszka et al. [23] conducted a study on a Polish population and reported that EBV was detected in 57.5% (46/80) of samples, including 60% (30/50) of laryngeal carcinomas and 53.3% (16/30) of oropharyngeal carcinomas. In addition, the virus has been reported more frequently in patients over 50 years of age (66.7%) [24]. In another study by Polz-Gruszka et al. [24], which included 154 patients with primary oral squamous cell carcinoma (OSCC) and oropharyngeal squamous cell carcinoma (OPSCC) in the Polish population, it was shown that 27.3% of all tested specimens were positive for EBV, in oropharyngeal 29.1%, and in oral cavity 26.1% [24]. In a study involving 78 patients with histologically confirmed OPSCC and 40 healthy controls from Poland, EBV DNA was detected in 51.3% of tumor samples and 20% of controls [25]. In a subsequent study based on 146 Polish patients, the prevalence of EBV infection was 34.3% in oropharyngeal cancer and 8.6% in cancer of the oral cavity [26]. In our study, EBV was present in 47.7% of cases in HNSCC. Such different results of EBV detection may be related to the differences in the HNSCC groups, particularly connected with various locations of primary tumors. She et al. conducted an important meta-analysis to examine the association of EBV with OSCC [27]. The results of 13 studies [28–40] suggested a positive association between EBV infection and the risk of OSCC. The total number of participants was 686 patients and 433 controls. Nine studies used paraffin-embedded tissues and four studies used fresh frozen tissues. Different detection techniques such as PCR, nested PCR, RT-qPCR, IHC (immunohistochemistry), and ISH (*in situ* hybridization) were used to detect EBV [27]. These tests showed differential detection of EBV. Therefore, adopting adequate methodology and techniques is crucial in the detection of EBV. There is still no gold standard in this type of research. Moreover, data suggests that the role of EBV in OSCC might depend on the geographical location [41]. Jalolulu et al. [42] detected EBV in the samples of OSCC from 8 different countries (Norway, UK, Sweden, USA, Sri Lanka, India, Sudan, and Yemen). Of the 155 oral carcinomas, 85 (55%) were positive for EBV. EBV-positive samples (80%) were the most prevalent among the UK patients.

In our study in HNSCC cases, coinfection of EBV and HPV occurred in 11.6% of patients. Moreover, coinfection was associated with pathoclinical features. In the group of patients with the lymph node status of N2, coinfection of EBV and HPV was observed more frequently. In a study by Polz-Gruszka et al. [24] conducted on the Polish population, coinfection with EBV and HPV was detected in 15% of samples [24]. In another study by Polz-Gruszka et al. [24], which was conducted on the Polish population of 154 patients with primary OSCC and OPSCC, the coinfection of HPV and EBV was detected in 7.8% (12/154) of the patients, 9.7% (6/62) among oropharyngeal patients, and 6.5% (6/92) among oral cavity patients. No correlation was found between HPV or EBV infection and age or tobacco smoking [24]. In another study, which was aimed at analyzing the prevalence of coinfection with HPV, EBV, and polyoma BK virus (BKPyV) in oral, oropharyngeal, and laryngeal squamous cell carcinomas in 146 Polish patients, a single infection was detected in 43.8% of the samples and mixed infections in 56.2%. Coinfections for HPV/EBV, HPV/BKV, and EBV/BKV were detected in 34.1%, 22%, and 23.2% of samples, respectively. All three tested viruses were present in 17 specimens. HPV was more often detected in oral cavity cancer patients (44.5%) while EBV in oropharyngeal cancer (57.1%). EBV was also detected in laryngeal cancer (34.3%) and in oral cavity cancer (8.6%) patients. Grade G3 and stages N1 and N2 were the most common in patients with HPV/EBV coinfection. Stages N1 and N2 were characteristic of infection with all three viruses. Grade G3 was present four times higher in HPV/EBV coinfection, five times higher in EBV/BKV coinfection, and ten times higher in samples with all three viruses in contrast to only EBV detection [26]. Jiang et al. suggested that the presence of EBV infection may promote the invasiveness of HPV-positive OPSCC tumors [43]. On the other hand, the presence of HPV may increase the pathogenic effects of EBV in the oral cavity by affecting epithelial cells and prolonging EBV cell cycle [44]. Contrary to that study, Guidry et al. [45] showed

a change in the life cycle of EBV after infection with HPV of the immortalized epithelial tissue. HPV-related cell changes contributed to the formation of a latent EBV infection [45].

Some authors showed that EBV was also detected in tonsillar diseases, including chronic tonsillitis [46–50]. In our study population, we observed statistically significant differences in the incidence of EBV-positive cases between the group with chronic tonsillitis and the control group ($p < 0.05$; 60% vs. 24.3%). Some authors indicated a differential frequency of the virus in recurrent tonsillitis and hypertrophic tonsillitis ranging from 26 to 43% [48, 51–54]. It is reported that the prevalence of EBV associated with tonsillitis varied depending on the method [48]. Higher detection of EBV in tonsillar tissues was demonstrated in studies using PCR, which is considered a rapid, specific, and sensitive method to detect minimal amount of viral DNA as reported by Peiper et al. [55]. Using this method, our study showed the presence of EBV in the tonsillar tissues of patients with chronic tonsillitis in 42/70 (60%) cases. Similarly, other studies related to chronic tonsillitis indicated the presence of EBV in 54.1% of cases (13/24) [47] and in 46% of cases (23/50) [49]. Other reports of noncancerous tonsillitis detected the virus in most cases, i.e., in 53.6% [56] and 58% in chronic hyperplasic tonsillitis [57] and in 64% in tonsils of acute infectious mononucleosis [58]. It is suggested that oral and pharyngeal epithelial cells, particularly the tonsillar tissue, are considered the main reservoir of EBV [48, 57]. Furthermore, other studies suggested tonsil lymphocytes as the site of virus replication [49, 50, 53].

Gonzalez-Lucano [49] reported that younger age of patients with chronic tonsillitis was associated with higher presence of EBV [49]. Such reports were also confirmed by other studies on noncancerous tonsillar tissue, such as recurrent and hypertrophic tonsillitis [46, 48, 51]. It is suspected that EBV may infect the tonsils of children and thus contribute to the development of recurrent and hypertrophic tonsillitis [48]. Another hypothesis is that overuse of antibiotics leads to changes in the tonsillar microbiome and increases the risk of viral infections of tonsils [47]. In our study, we did not observe a correlation between the age of patients with chronic tonsillitis and an increased prevalence of EBV. In our study group, it can be explained by the absence of children, who usually have high EBV copy number. However, time and maturation of virus-specific immunity are essential factors in suppression [56].

In addition, our study showed 15.7% EBV/HPV coinfection in the chronic tonsillitis group. A search of databases (PubMed and Medline) revealed no other reports suggesting coinfection in chronic tonsillitis. Xue et al. who examined samples of children with tonsillar or adenoid hypertrophy demonstrated EBV infection in 45% of tonsillar tissues but found no EBV/HPV coinfection in any patient [59]. Similar results were obtained by Jiang [43], who observed EBV infection in 20% of noncancer base of tongue samples. However, HPV was not confirmed [43]. In a study of patients with nonmalignant tonsils, of the above viruses, only DNA-EBV was detected in more than half of the samples. The authors concluded that HPV and EBV infected independently of each other [60]. Interestingly, *in vitro* studies suggest that in the case of coinfection in oral squamous epithelial cells, the presence of HPV may increase the pathogenesis of EBV [44].

To conclude, it seems that the etiology of chronic tonsillitis can be related to EBV. Further research should focus on explaining the role of EBV infection in chronic tonsillitis in a larger population. The data could be useful in designing public health strategies, including clinical examination and EBV testing.

The prevalence of EBV in healthy individuals ranges from 0 to 90%. In our case-control study, we detected 24.3% (35/109) cases of EBV in oral swab specimens, which is in line with other reports in which EBV was detected in 18.1% (17/94) of samples of exfoliated oral cells [61], in 22% (34/157) of throat washings [62], and in 20% (4/20) of samples of squamous epithelial cells collected by scraping [63]. EBV DNA was found in saliva in more than 30% of cases [64, 65], which is in line with Mao and Smith [66] who reported that 25% (15/60) of nonsmokers and occasional alcohol users showed EBV positivity [66]. No association was found between the EBV status and demographic factors or the use of stimulants, including smoking and drinking alcohol, which is in line with other studies [66, 67]. However, Kuri et al. reported more frequent EBV seropositivity in women [68]. Mao and Smith [66] showed a statistically insignificant relationship between older age (>60 years) and the prevalence of EBV [66]. Several studies found that the prevalence of EBV increased with age [64, 68]. Contrary to these reports, Gupta et al. observed EBV most frequently in the age group of 30-39 years [69]. Another study reported no effect of older age on the prevalence of EBV [38]. The virus was also detected in serum samples in 61% [69] and 85.3% of cases [68]. Significantly higher results were shown in a study in which the virus was detected in 90% (43/48) of throat washings of adult patients, which coincides with the overall data on EBV seropositivity in the Japanese population [64].

In our study, we detected viral coinfection in 7.6% of healthy volunteers. A similarly low result of several percent was obtained by McCormick et al. (13.3%) [70] and Lattario et al. (15%) [71] for cervical samples from healthy individuals. In a Polish study, the authors reported HPV (2.5%) and EBV (20%) infection in serum and saliva samples [25]. In the Tunisian study by Kahla et al., no HPV or EBV infection was detected in cervical biopsies of the control group [72]. Further research into the mechanisms related to HPV and EBV cooccurrence, as well as screening of healthy individuals for early detection of oncogenic viruses that affect the risk of cancer progression, is important [72].

Rapid advances in scientific fields such as molecular biology, genetic engineering, and virology have contributed to the development of new vaccine options, both for the prevention of primary infections and subsequent chronic diseases. Because EBV is related with many malignancies including HNSCC, development of EBV vaccine is also required.

5. Conclusion

In conclusion, the prevalence of EBV in HNSCC and chronic tonsillitis was significantly higher than in the control group, which suggests that EBV may be defined as a potential risk factor for these diseases. The findings showed that

oncogenic viruses, including EBV, are not the only risk factors in the development of HNSCC but may promote carcinogenesis with other etiological factors. Considering the prevalence of the virus and the risk of a serious disease, attention should be paid to screening diagnosis and prevention of the infection. In addition to the need for widely available rapid methods to effectively detect EBV, a prophylactic EBV vaccine would be promising in the prevention of EBV-associated cancers.

Abbreviations

AJCC: American Joint Committee on Cancer
BNLF: Brain-derived neurotrophic factor
EBERs: Epstein-Barr virus-encoded small RNAs
EBNA: Epstein-Barr nuclear antigen
EBV: Epstein-Barr virus
EMT: Epithelial-mesenchymal transition
HHV-4: Human gammaherpesvirus 4
HIV: Human immunodeficiency viruses
HNSCC: Head and neck squamous cell carcinoma
HPV: Human papillomavirus
IHC: Immunohistochemistry
ISH: *In situ* hybridization
LMP: Epstein-Barr virus latent membrane protein
miRNA: MicroRNA
NPC: Nasopharyngeal carcinoma
OPSCC: Oropharyngeal squamous cell carcinoma
OSCC: Oral squamous cell carcinoma
PCR: Polymerase chain reaction
PTEN: Phosphatase and tensin homolog
STAT3: Signal transducer and activator of transcription 3
TNBC: Triple-negative breast cancer.

Data Availability

The data used to support the findings of this study are available from the corresponding author upon request.

Conflicts of Interest

The authors declare that there is no conflict of interest.

Acknowledgments

This work was supported by the Ministry of Science and Higher Education (no. KNW-1-037/N/8/0).

Supplementary Materials

Supplementary 1. Table S1: association of EBV infection and coinfection of EBV and HPV and clinical parameters.

Supplementary 2. Table S2: association between EBV infection and coinfection of EBV and HPV and demographic parameters and smoking and alcohol consumption.

References

[1] G. S. Taylor, H. M. Long, J. M. Brooks, A. B. Rickinson, and A. D. Hislop, "The immunology of Epstein-Barr virus-induced disease," *Annual Review of Immunology*, vol. 33, no. 1, pp. 787–821, 2015.

[2] W. Amon, U. K. Binné, H. Bryant, P. J. Jenkins, C. E. Karstegl, and P. J. Farrell, "Lytic cycle gene regulation of Epstein-Barr virus," *Journal of Virology*, vol. 78, no. 24, pp. 13460–13469, 2004.

[3] A. Nowalk and M. Green, "Epstein-Barr virus," *Microbiology Spectrum*, vol. 4, no. 3, 2016.

[4] D. Germini, F. B. Sall, A. Shmakova et al., "Oncogenic properties of the EBV ZEBRA protein," *Cancers (Basel)*, vol. 12, no. 6, p. 1479, 2020.

[5] H. Yin, J. Qu, Q. Peng, and R. Gan, "Molecular mechanisms of EBV-driven cell cycle progression and oncogenesis," *Medical Microbiology and Immunology*, vol. 208, no. 5, pp. 573–583, 2019.

[6] X. Chen, A. M. Bode, Z. Dong, and Y. Cao, "The epithelial-mesenchymal transition (EMT) is regulated by oncoviruses in cancer," *FASEB journal : Official Publication of the Federation of American Societies for Experimental Biology*, vol. 30, no. 9, pp. 3001–3010, 2016.

[7] F. S. Cyprian, H. F. Al-Farsi, S. Vranic, S. Akhtar, and A. E. Al Moustafa, "Epstein-Barr virus and human papillomaviruses interactions and their roles in the initiation of epithelial-mesenchymal transition and cancer progression," *Frontiers in Oncology*, vol. 8, pp. 8–111, 2018.

[8] D. Elgui de Oliveira, B. G. Müller-Coan, and J. S. Pagano, "Viral carcinogenesis beyond malignant transformation: EBV in the progression of human cancers," *Trends in Microbiology*, vol. 24, no. 8, pp. 649–664, 2016.

[9] Q. Fernandes, I. Gupta, S. Vranic, and A. E. Al Moustafa, "Human papillomaviruses and Epstein-Barr virus interactions in colorectal cancer: a brief review," *Pathogens*, vol. 9, no. 4, p. 300, 2020.

[10] O. Kaidar-Person, Z. Gil, and S. Billan, "Precision medicine in head and neck cancer," *Drug Resistance Updates*, vol. 40, pp. 13–16, 2018.

[11] R. Sanderson and J. Ironside, "Clinical review Squamous cell carcinomas of the head and neck commentary: head and neck carcinomas in the developing world," *BMJ*, vol. 325, no. 7368, pp. 822–827, 2002.

[12] D. E. Johnson, B. Burtness, C. R. Leemans, V. W. Y. Lui, J. E. Bauman, and J. R. Grandis, "Head and neck squamous cell carcinoma," *Nature Reviews. Disease Primers*, vol. 6, no. 1, p. 92, 2020.

[13] Y. Suh, I. Amelio, T. Guerrero Urbano, and M. Tavassoli, "Clinical update on cancer: molecular oncology of head and neck cancer," *Cell Death & Disease*, vol. 5, no. 1, article e1018, 2014.

[14] A. R. Jethwa and S. S. Khariwala, "Tobacco-related carcinogenesis in head and neck cancer," *Cancer Metastasis Reviews*, vol. 36, no. 3, pp. 411–423, 2017.

[15] D. Kawakita and K. Matsuo, "Alcohol and head and neck cancer," *Cancer Metastasis Reviews*, vol. 36, no. 3, pp. 425–434, 2017.

[16] S. M. Thomas and J. R. Grandis, "The current state of head and neck cancer gene therapy," *Human Gene Therapy*, vol. 20, no. 12, pp. 1565–1575, 2009.

[17] S. Bathala and R. Eccles, "A review on the mechanism of sore throat in tonsillitis," *The Journal of Laryngology and Otology*, vol. 127, no. 3, pp. 227–232, 2013.

[18] L. Plank, "Infectious mononucleosis, tonsils," in *Head and Neck Pathology*, Encyclopedia of Pathology, M. Volavšek, Ed., pp. 153–157, Springer, Cham, 2016.

[19] J. E. R. E. Wong Chung, P. P. G. van Benthem, and H. M. Blom, "Tonsillotomy versus tonsillectomy in adults suffering from tonsil-related afflictions: a systematic review," *Acta Oto-Laryngologica*, vol. 138, no. 5, pp. 492–501, 2018.

[20] J. K. Strzelczyk, K. Biernacki, J. Gaździcka et al., "The prevalence of high- and low-risk types of HPV in patients with squamous cell carcinoma of the head and neck, patients with chronic tonsillitis, and healthy individuals living in Poland," *Diagnostics (Basel)*, vol. 11, no. 12, p. 2180, 2021.

[21] W. M. Lydiatt, S. G. Patel, B. O'Sullivan et al., "Head and neck cancers-major changes in the American Joint Committee on cancer eighth edition cancer staging manual," *CA: a Cancer Journal for Clinicians*, vol. 67, no. 2, pp. 122–137, 2017.

[22] S. W. Tsao, C. M. Tsang, and K. W. Lo, "Epstein-Barr virus infection and nasopharyngeal carcinoma," *Philosophical Transactions of the Royal Society of London. Series B, Biological Sciences*, vol. 372, no. 1732, 2017.

[23] D. Polz-Gruszka, K. Morshed, A. Stec, and M. Polz-Dacewicz, "Prevalence of human papillomavirus (HPV) and Epstein-Barr virus (EBV) in oral and oropharyngeal squamous cell carcinoma in South-Eastern Poland," *Infectious Agents and Cancer*, vol. 10, no. 1, p. 37, 2015.

[24] D. Polz-Gruszka, A. Stec, J. Dworzański, and M. Polz-Dacewicz, "EBV, HSV, CMV and HPV in laryngeal and oropharyngeal carcinoma in Polish patients," *Anticancer Research*, vol. 35, no. 3, pp. 1657–1661, 2015.

[25] M. Polz-Dacewicz, M. Strycharz-Dudziak, J. Dworzański, A. Stec, and J. Kocot, "Salivary and serum IL-10, TNF-α, TGF-β, VEGF levels in oropharyngeal squamous cell carcinoma and correlation with HPV and EBV infections," *Infectious Agents and Cancer*, vol. 11, no. 1, p. 45, 2016.

[26] B. Drop, M. Strycharz-Dudziak, E. Kliszczewska, and M. Polz-Dacewicz, "Coinfection with Epstein-Barr virus (EBV), human papilloma virus (HPV) and polyoma BK virus (BKPyV) in laryngeal, oropharyngeal and oral cavity cancer," *International Journal of Molecular Sciences*, vol. 18, no. 12, p. 2752, 2017.

[27] Y. She, X. Nong, M. Zhang, and M. Wang, "Epstein-Barr virus infection and oral squamous cell carcinoma risk: a meta-analysis," *PLoS One*, vol. 12, no. 10, article 0186860, 2017.

[28] W. E. van Heerden, E. J. van Rensburg, S. Engelbrecht, and E. J. Raubenheimer, "Prevalence of EBV in oral squamous cell carcinomas in young patients," *Anticancer Research*, vol. 15, no. 5B, pp. 2335–2339, 1995.

[29] E. J. van Rensburg, S. Engelbrecht, W. Van Heerden, E. Raubenheimer, and B. D. Schoub, "Detection of EBV DNA in oral squamous cell carcinomas in a Black African population sample," *In Vivo (Athens, Greece)*, vol. 9, no. 3, pp. 199–202, 1995.

[30] I. Cruz, A. J. Van den Brule, R. D. Steenbergen et al., "Prevalence of Epstein—Barr virus in oral squamous cell carcinomas, premalignant lesions and normal mucosa—a study using the polymerase chain reaction," *Oral oncology*, vol. 33, no. 3, pp. 182–188, 1997.

[31] J. V. Bagan, Y. Jiménez, J. Murillo et al., "Epstein-Barr virus in oral proliferative verrucous leukoplakia and squamous cell carcinoma: a preliminary study," *Medicina Oral, Patología Oral y Cirugía Bucal*, vol. 13, no. 2, pp. 110–113, 2008.

[32] W. L. Chen, L. W. Tong, and Q. L. Deng, "Human papillomavirus type 16 and Epstein-Barr virus relative to oral squamous cell carcinoma," *Journal of Oral and Maxillofacial Surgery*, vol. 8, pp. 23–25, 1998.

[33] J. D'Costa, D. Saranath, V. Sanghvi, and A. R. Mehta, "Epstein-Barr virus in tobacco-induced oral cancers and oral lesions in patients from India," *Journal of Oral Pathology & Medicine*, vol. 27, no. 2, pp. 78–82, 1998.

[34] X. Q. Ding and Z. Y. Zhu, "Relationship between Epstein-Barr virus infection and oral squamous cell carcinoma," *Acad J SUM S*, vol. 18, pp. 140-141, 1997.

[35] R. Jiang, X. Gu, T. N. Moore-Medlin, C. A. Nathan, and L. M. Hutt-Fletcher, "Oral dysplasia and squamous cell carcinoma: correlation between increased expression of CD21, Epstein-Barr virus and CK19," *Oral Oncology*, vol. 48, no. 9, pp. 836–841, 2012.

[36] K. Kikuchi, Y. Noguchi, M. W. de Rivera et al., "Detection of Epstein-Barr virus genome and latent infection gene expression in normal epithelia, epithelial dysplasia, and squamous cell carcinoma of the oral cavity," *Tumour Biology*, vol. 37, no. 3, pp. 3389–3404, 2016.

[37] A. Kis, E. Fehér, T. Gáll et al., "Epstein–Barr virus prevalence in oral squamous cell cancer and in potentially malignant oral disorders in an eastern Hungarian population," *European Journal of Oral Sciences*, vol. 117, no. 5, pp. 536–540, 2009.

[38] L. P. Sand, J. Jalouli, P. A. Larsson, and J. M. Hirsch, "Prevalence of Epstein-Barr virus in oral squamous cell carcinoma, oral lichen planus, and normal oral mucosa," *Oral Surgery, Oral Medicine, Oral Pathology, Oral Radiology, and Endodontics*, vol. 93, no. 5, pp. 586–592, 2002.

[39] A. A. Shamaa, M. M. Zyada, M. Wagner, S. S. Awad, M. M. Osman, and A. A. Abdel Azeem, "The significance of Epstein Barr virus (EBV) & DNA topoisomerase II alpha (DNA-Topo II alpha) immunoreactivity in normal oral mucosa, oral epithelial dysplasia (OED) and oral squamous cell carcinoma (OSCC)," *Diagnostic Pathology*, vol. 3, no. 1, p. 45, 2008.

[40] M. Shimakage, K. Horii, A. Tempaku, K. Kakudo, T. Shirasaka, and T. Sasagawa, "Association of Epstein-Barr virus with oral cancers," *Human Pathology*, vol. 33, no. 6, pp. 608–614, 2002.

[41] L. Sand, M. Wallström, and J. M. Hirsch, "Smokeless tobacco, viruses and oral cancer," *Oral Health and Dental Management*, vol. 13, no. 2, pp. 372–378, 2014.

[42] J. Jalouli, M. M. Jalouli, D. Sapkota, S. O. Ibrahim, P. A. Larsson, and L. Sand, "Human papilloma virus, herpes simplex virus and Epstein Barr virus in oral squamous cell carcinoma from eight different countries," *Anticancer Research*, vol. 32, no. 2, pp. 571–580, 2012.

[43] R. Jiang, O. Ekshyyan, T. Moore-Medlin et al., "Association between human papilloma virus/Epstein–Barr virus coinfection and oral carcinogenesis," *Journal of Oral Pathology & Medicine*, vol. 44, no. 1, pp. 28–36, 2015.

[44] K. R. Makielski, D. Lee, L. D. Lorenz et al., "Human papillomavirus promotes Epstein-Barr virus maintenance and lytic reactivation in immortalized oral keratinocytes," *Virology*, vol. 495, pp. 52–62, 2016.

[45] J. T. Guidry, J. E. Myers, M. Bienkowska-Haba et al., "Inhibition of Epstein-Barr virus replication in human papillomavirus-immortalized keratinocytes," *Journal of Virology*, vol. 93, no. 2, pp. 1216–1218, 2019.

[46] C. A. Chagas, L. H. Endo, W. L. Dos-Santos et al., "Is there a relationship between the detection of human herpesvirus 8 and Epstein-Barr virus in Waldeyer's ring tissues?," *International Journal of Pediatric Otorhinolaryngology*, vol. 70, no. 11, pp. 1923–1927, 2006.

[47] E. P. Dias, M. L. Rocha, M. O. Carvalho, and L. M. Amorim, "Detection of Epstein-Barr virus in recurrent tonsillitis," *Brazilian Journal of Otorhinolaryngology*, vol. 75, no. 1, pp. 30–34, 2009.

[48] L. H. Endo, D. Ferreira, M. C. Montenegro et al., "Detection of Epstein-Barr virus in tonsillar tissue of children and the relationship with recurrent tonsillitis[1]," *International Journal of Pediatric Otorhinolaryngology*, vol. 58, no. 1, pp. 9–15, 2001.

[49] L. R. Gonzalez-Lucano, G. V. Vasquez-Armenta, A. L. Pereira-Suarez, A. Ramirez-de Arellano, S. Ramirez-de Los Santos, and E. I. Lopez-Pulido, "Prevalence of Epstein-Barr virus DNA in tonsillar tissue from patients with chronic tonsillitis in Mexican population," *Journal of Infection in Developing Countries*, vol. 13, no. 8, pp. 764–767, 2019.

[50] T. Ikeda, R. Kobayashi, M. Horiuchi et al., "Detection of lymphocytes productively infected with Epstein-Barr virus in non-neoplastic tonsils," *The Journal of General Virology*, vol. 81, Part 5, pp. 1211–1216, 2000.

[51] S. Al-Salam, S. A. Dhaheri, A. Awwad, S. Daoud, A. Shams, and M. A. Ashari, "Prevalence of Epstein-Barr virus in tonsils and adenoids of United Arab Emirates nationals," *International Journal of Pediatric Otorhinolaryngology*, vol. 75, no. 9, pp. 1160–1166, 2011.

[52] P. A. Chabay and M. V. Preciado, "EBV primary infection in childhood and its relation to B-cell lymphoma development: a mini-review from a developing region," *International Journal of Cancer*, vol. 133, no. 6, pp. 1286–1292, 2013.

[53] R. Kobayashi, H. Takeuchi, M. Sasaki, M. Hasegawa, and K. Hirai, "Detection of Epstein–Barr virus infection in the epithelial cells and lymphocytes of non-neoplastic tonsils by in situ hybridization and in situ PCR," *Archives of Virology*, vol. 143, no. 4, pp. 803–813, 1998.

[54] K. Yoda, H. Aramaki, Y. Yamauchi, Y. Sato, and T. Kurata, *Detection of herpes simplex and Epstein–Barr viruses in patient with acute tonsillitis*, Sapporo, Japan, Abstracts III International Symposium on Tonsils, 1995.

[55] S. C. Peiper, J. L. Myers, E. E. Broussard, and J. W. Sixbey, "Detection of Epstein-Barr virus genomes in archival tissues by polymerase chain reaction," *Archives of Pathology & Laboratory Medicine*, vol. 114, no. 7, pp. 711–714, 1990.

[56] F. Sahiner, R. Gümral, Ü. Yildizoğlu et al., "Coexistence of Epstein-Barr virus and parvovirus B19 in tonsillar tissue samples: quantitative measurement by real-time PCR," *International Journal of Pediatric Otorhinolaryngology*, vol. 78, no. 8, pp. 1288–1293, 2014.

[57] P. C. Pai, N. M. Tsang, C. K. Tseng et al., "Prevalence of LMP-1 gene in tonsils and non-neoplastic nasopharynxes by nest-polymerase chain reaction in Taiwan," *Head & Neck*, vol. 26, no. 7, pp. 619–624, 2004.

[58] G. Niedobitek, H. Herbst, L. S. Young et al., "Patterns of Epstein-Barr virus infection in non-neoplastic lymphoid tissue," *Blood*, vol. 79, no. 10, pp. 2520–2526, 1992.

[59] X. C. Xue, X. P. Chen, W. H. Yao, Y. Zhang, G. B. Sun, and X. J. Tan, "Prevalence of human papillomavirus and Epstein–Barr virus DNA in Chinese children with tonsillar and/or adenoidal hypertrophy," *Journal of Medical Virology*, vol. 86, no. 6, pp. 963–967, 2014.

[60] A. Holm, A. Schindele, A. Allard et al., "Mapping of human papilloma virus, p16, and epstein-barr virus in non-malignant tonsillar disease," *Laryngoscope Investigative Otolaryngology*, vol. 4, no. 3, pp. 285–291, 2019.

[61] S. Acharya, T. Ekalaksananan, P. Vatanasapt et al., "Association of Epstein-Barr virus infection with oral squamous cell carcinoma in a case–control study," *Journal of Oral Pathology & Medicine*, vol. 44, no. 4, pp. 252–257, 2015.

[62] J. W. Sixbey, P. Shirley, P. J. Chesney, D. M. Buntin, and L. Resnick, "Detection of a second widespread strain of Epstein-Barr virus," *Lancet*, vol. 2, no. 8666, pp. 761–765, 1989.

[63] C. Scully, S. R. Porter, L. Di Alberti, M. Jalal, and N. Maitland, "Detection of Epstein-Barr virus in oral scrapes in HIV infection, in hairy leukoplakia, and in healthy non-HIV-infected people," *Journal of Oral Pathology & Medicine*, vol. 27, no. 10, pp. 480–482, 1998.

[64] K. Ikuta, Y. Satoh, Y. Hoshikawa, and T. Sairenji, "Detection of Epstein-Barr virus in salivas and throat washings in healthy adults and children," *Microbes and Infection*, vol. 2, no. 2, pp. 115–120, 2000.

[65] E. Lucht, P. Biberfeld, and A. Linde, "Epstein-Barr virus (EBV) DNA in saliva and EBV serology of HIV-1-infected persons with and without hairy leukoplakia," *The Journal of Infection*, vol. 31, no. 3, pp. 189–194, 1995.

[66] E. J. Mao and C. J. Smith, "Detection of Epstein-Barr virus (EBV) DNA by the polymerase chain reaction (PCR) in oral smears from healthy individuals and patients with squamous cell carcinoma," *Journal of Oral Pathology & Medicine*, vol. 22, no. 1, pp. 12–17, 1993.

[67] L. Sand, M. Wallström, J. Jalouli, P. A. Larsson, and J. M. Hirsch, "Epstein-Barr virus and human papillomavirus in snuff-induced lesions of the oral mucosa," *Acta Oto-Laryngologica*, vol. 120, no. 7, pp. 880–884, 2000.

[68] A. Kuri, B. M. Jacobs, N. Vickaryous et al., "Epidemiology of Epstein-Barr virus infection and infectious mononucleosis in the United Kingdom," *BMC Public Health*, vol. 20, no. 1, p. 912, 2020.

[69] I. Gupta, G. K. Nasrallah, A. Sharma et al., "Co-prevalence of human papillomaviruses (HPV) and Epstein-Barr virus (EBV) in healthy blood donors from diverse nationalities in Qatar," *Cancer Cell International*, vol. 20, no. 1, p. 107, 2020.

[70] T. M. McCormick, N. H. Canedo, Y. L. Furtado et al., "Association between human papillomavirus and Epstein - Barr virus DNA and gene promoter methylation of RB1 and CDH1 in the cervical lesions: a transversal study," *Diagnostic Pathology*, vol. 10, no. 1, p. 59, 2015.

[71] F. Lattario, Y. L. Furtado, F. A. Silveira, I. C. do Val, G. Almeida, and M. da Gloria da Costa Carvalho, "Evaluation of DAPK gene methylation and HPV and EBV infection in cervical cells from patients with normal cytology and colposcopy," *Archives of Gynecology and Obstetrics*, vol. 277, no. 6, pp. 505–509, 2008.

[72] S. Kahla, S. Oueslati, M. Achour et al., "Correlation between EBV co-infection and HPV16 genome integrity in Tunisian cervical cancer patients," *Brazilian Journal of Microbiology*, vol. 43, no. 2, pp. 744–753, 2012.

Hindawi
BioMed Research International
Volume 2022, Article ID 8677309, 24 pages
https://doi.org/10.1155/2022/8677309

Research Article

Construction and Validation of a UPR-Associated Gene Prognostic Model for Head and Neck Squamous Cell Carcinoma

Tao Wang,[1] Lingling Chen,[1] Fuping Xie,[1] Shiqi Lin,[2] Yuhan Lin,[2] Jiamin Chen,[1] Huanhuan Liu,[1] and Ye Wu[1]

[1]*Fujian Key Laboratory of Oral Diseases and Fujian Provincial Engineering Research Center of Oral Biomaterial and Stomatological Key Lab of Fujian College and University, School and Hospital of Stomatology, Fujian Medical University, China*
[2]*School of Stomatology, Fujian Medical University, China*

Correspondence should be addressed to Ye Wu; wuye@fjmu.edu.cn

Received 2 March 2022; Accepted 12 May 2022; Published 6 June 2022

Academic Editor: Jinjun Shao

Our study is aimed at constructing and validating a UPR-associated gene signature to predict HNSCC prognosis. We obtained 544 samples of RNA sequencing data and clinical characteristics from TCGA database and randomly grouped the samples into training and testing cohorts (1 : 1 ratio). After identifying 14 UPR-associated genes with LASSO and univariate Cox regression analysis, HNSCC samples were categorized into low-risk (LR) and high-risk (HR) subgroups depending on the risk score. Our analyses indicated that low-risk patients had a much better prognosis in the training and testing cohorts. To predict the HNSCC prognosis with the 14 UPR-associated gene signatures, we incorporated the UPR gene risk score, N stage, M stage, and age into a nomogram model. We further explored the sensitivity to anticancer drugs by using the IC50 analysis in two subgroups from the Cancer Genome Project database. The outcomes showed that the AKT inhibitor III and sorafenib were sensitive anticancer drugs in HR and LR patients, respectively. The immune cell infiltration analysis and GSEA provided strong evidence for elucidating the molecular mechanisms of UPR-associated genes affecting HNSCC. In conclusion, the UPR-associated gene risk score, N stage, M stage, and age can serve as a robust model for predicting prognosis and can improve decision-making at the individual patient level.

1. Introduction

Head and neck squamous cell carcinoma (HNSCC) is the seventh most common malignant neoplasm globally. There were an estimated 931.7 thousand new cases of HNSCC worldwide in 2020, and more than 467,100 individuals died of this disease [1–3]. Smoking, alcohol abuse, and areca nut chewing are risk factors for HNSCC. Recent studies have shown that viruses may be extremely associated with an increased risk of HNSCC development, together with persistent infections by EBV and HPV [4–7]. HNSCC is characterized by a high degree of malignancy, high metastasis rate, and poor clinical prognosis [8]. The 5-year survival rate of HNSCC is less than 50% [4, 6, 9]. The prognosis of HNSCC is connected directly to the tumor stage, cervical lymph node, and distant metastasis. The TNM staging system of the AJCC is widely used to evaluate the prognosis of HNSCC clinically. However, there is a common phenomenon in clinical practice: patients with similar clinical stages show different prognostic outcomes to some extent, which suggests that TNM staging is not an accurate predictor of survival. Therefore, it is urgent to find an effective and reliable biomarker to help doctors assess the prognosis of patients accurately and formulate a personalized diagnosis and treatment plans.

Activation of the unfolded protein response (UPR) plays an essential role in tumor transformation. The UPR is chronically activated in general tumor cells, and it is believed that this state is a mechanism that leads to antiapoptosis and drug resistance of tumor cells [10–14]. When cancer cells suffer from internal and external challenges such as oncogene activation and hypoxia, misfolded proteins accumulate in the endoplasmic reticulum (ER) lumen [15]. To maintain the ER in a stable environment under this condition, cells initiate signaling cascades that reduce protein synthesis,

upregulate the expression of chaperones and folding enzymes, and induce accelerated degradation of misfolded proteins. Adaptive changes in cells make up the UPR [16].

Cells may adapt to adversity and survive by initiating autophagy via the UPR. However, the UPR transforms from a cellular protective response to a cytotoxic response that promotes apoptosis when ER stress is not alleviated [10]. Cancer cells hijack the UPR by activating UPR sensors, such as ATF6, IRE1a, and PERK, and their main regulatory factors, such as GRP78, allow drug resistance. Therefore, inhibiting the UPR pathway makes cancer cells more sensitive to conventional/targeted drug therapy [16, 17]. A recent study [18] found that tumor cells escaped the immune response by modulating immune cell activity in the tumor microenvironment via the UPR. Consequently, the UPR may provide a new way to judge the prognosis of patients with HNSCC. However, few investigations have explored whether the UPR is associated with survival outcomes in HNSCC.

Our study screened UPR-associated genes that were strongly connected with the prognosis of HNSCC. Fourteen UPR-associated genes were verified as prognostic biomarkers by survival analysis. The half-maximal inhibitory concentration (IC50) analysis, immune infiltration analysis, and a prognostic nomogram were carried out to help improve the understanding of survival prediction for HNSCC patients. Our study elucidated the molecular mechanism of UPR-associated genes affecting HNSCC, and UPR-associated gene may provide prognostic guidance for clinical diagnosis and treatment.

2. Materials and Methods

2.1. Data Acquisition of HNSCC Datasets. We downloaded and extracted the clinical and raw RNA-seq info of 500 HNSCC patient samples and 44 paracancerous samples from TCGA database. HNSCC patients were randomized to training and testing cohorts (1 : 1 ratio). The microarray expression and clinical data of a tongue cancer patient cohort (GSE41613) were used for external verification of signatures, which were obtained from the GEO database.

2.2. ssGSEA. The HNSCC RNA-seq expression data were analyzed by using the ssGSEA method with the GSVA [19] package according to the hallmark gene set. The univariate Cox regression was carried out according to ssGSEA values and HNSCC clinical information. The hallmark items were ultimately filtered for subsequent analysis according to the Cox results. Considering the criteria of $p < 0.05$ and maximum HR value, we selected UPR for subsequent analysis.

We performed WGCNA [20] with the WGCNA R package based on the HNSCC RNA-seq data of each gene and screened target genes. The correlation between the screened hallmark ssGSEA value and each coexpression module was calculated. The modular genes with the best correlation (the largest absolute value of the correlation coefficient) were selected for subsequent analysis.

The genes in the selected coexpression module had the best correlations with the ssGSEA value of the specified item. According to the clinical data, the survival [21] package was applied for the univariate Cox regression analysis on each gene, and genes with $p < 0.01$ were selected for LASSO model construction.

2.3. Construction and Validation of the UPR-Associated Gene Prognostic Signature. The glmnet [22] package was used to perform the LASSO regression analysis on the basis of the gene expression and clinical data acquired from the training group corresponding to the above screening results. After calculating the regression coefficients corresponding to each gene, the marker gene with regression coefficients not equal to 0 was determined. Survival and receiver operating characteristic (ROC) analyses were performed to verify the impact of the risk score on the prognosis of HNSCC patients and generate ROC curves based on the risk score and clinical information. According to the LASSO model and the expression level of each gene, the predict.cv.glmnet function was used to compute the risk score of each sample in the two groups.

Samples in the training and testing groups were divided into HR and LR groups according to the median risk score for survival analysis. ROC curve analysis was carried out to verify the LASSO regression model results. Combining the training and testing group data, we verified the LASSO regression model results and performed ROC analysis again. The GSE41613 dataset was used for external validation. The Cox regression model obtained from the training group was used to predict the risk of each sample in GSE41613, in which unrecorded genes were replaced by 0 values.

We grouped TCGA cohort by T stage, N stage, M stage, sex, age, histological grade, and pathological group. The Wilcox.test function in the R package was used to test the risk score in the above groups, and the correlation between some clinical data and the risk score was calculated.

2.4. Analysis of Sensitivity to Anticancer Drugs. According to the CGP database and the expression levels of UPR-associated genes in each HNSCC sample, the pRRophetic R package [23] was used for the IC50 test. After dividing the samples into HR and LR groups of UPR-associated gene expression by the median risk score, we calculated the IC50 score between the two groups with the limma [24] R package.

2.5. Analysis of Immune Infiltration. The CIBERSORT [25] software was used to score the immune infiltration of each sample according to the expression values of genes. The correlations between the scores of all 22 immune cells were estimated. The Wilcoxon test was applied to test the differences in immune scores between the HR and LR groups.

2.6. Construction and Verification of the Nomogram Model. We developed a nomogram using the rms package and combined the risk score with various clinical factors obtained in the LASSO analysis to perform a nomogram analysis. Afterward, the nomogram risk score of each sample was calculated. The survival, ROC, and Cox analyses were finally verified.

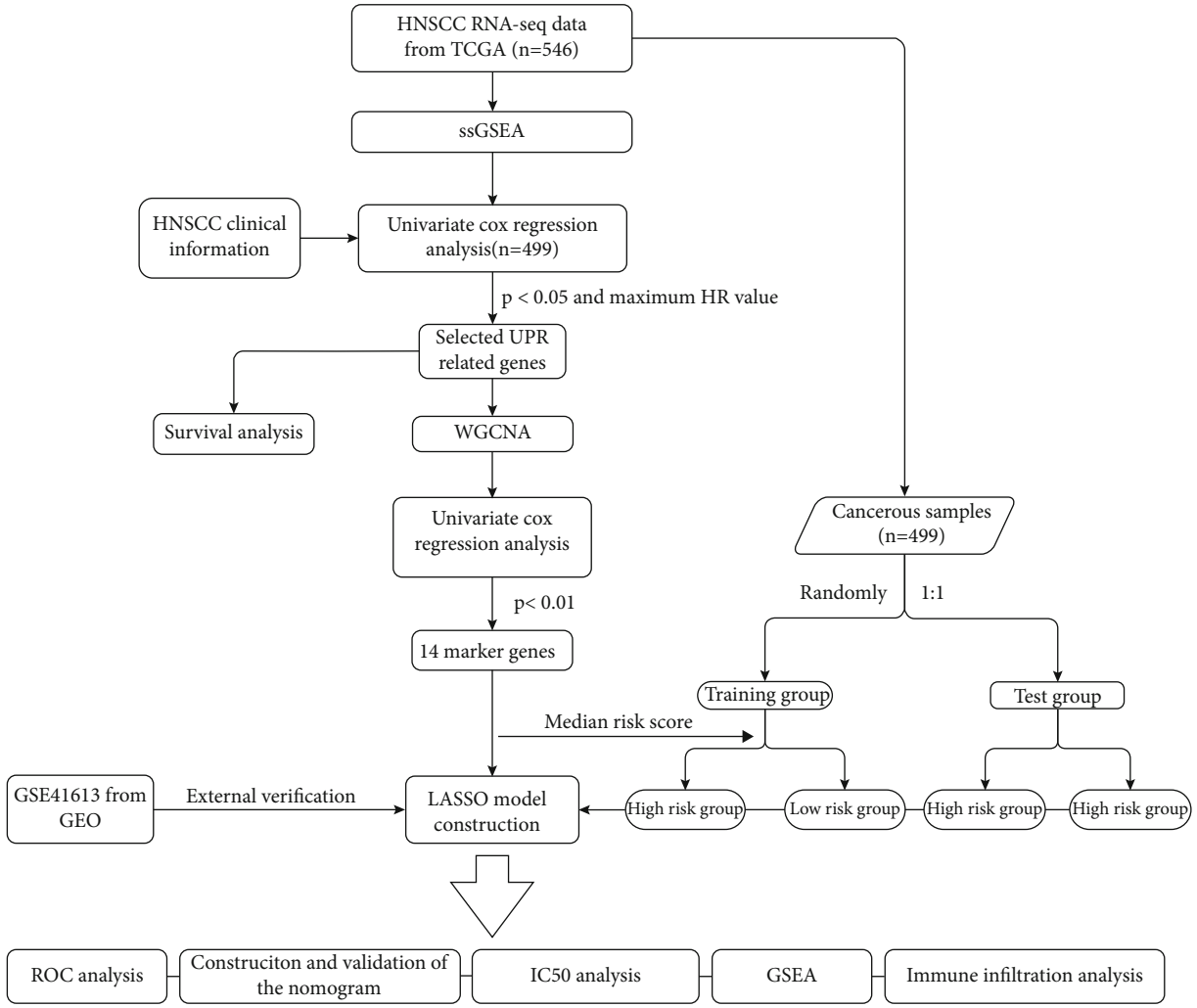

Figure 1: Flow diagram for developing and validating a UPR-associated gene prognostic model.

3. Results and Discussion

3.1. Construction of the UPR-Associated Gene-Bas Prognostic Signature. The workflow of our investigation is demonstrated in Figure 1. First, we enrolled a total of 544 samples with RNA-seq data and clinical information, including 44 paracancerous samples from TCGA database. After ssGSEA with the GSVA package according to the hallmark gene set, the HNSCC cohort samples were subjected to the univariate Cox regression analysis to explore pathways associated with prognosis. A total of 499 cancerous samples with survival information were used in this procedure. Considering the criteria of $p < 0.05$ and maximum HR value, we selected UPR-associated genes for subsequent analysis (Figures 2(a) and 2(b) and Table 1). According to the median ssGSEA scores in the UPR gene set, the HNSCC cohort samples were divided into HR and LR groups, and survival analysis was performed. The overall survival (OS) and disease-free survival (DFS) of HNSCC were significantly different between the two groups (Figures 2(c) and 2(d)). ROC curves from 1 year to 10.5 years (Figures 2(e) and 2(f)) revealed that the areas under the curve (AUCs) were all greater than 0.5, and the best cutoff value was 0.607 (5 years). The results indicate that the UPR-associated gene signature may predict long-term survival in patients with HNSCC.

A coexpression analysis was applied using the WGCNA package, and the correlations between the ssGSEA score of the hallmark UPR-associated gene and each coexpression module were calculated. Genes in the module with the best correlations were selected for subsequent analysis. According to clinical data, the survival package was used for the Cox regression analysis of the selected genes, and candidate genes ($p < 0.01$) were used in the LASSO model construction.

At a 1 : 1 ratio, 499 samples were randomly divided into test and training groups. Based on the expression of these candidate genes in the training group and clinical data in TCGA database, the LASSO regression analysis was conducted. Genes with regression coefficients that were not equal to 0 in the LASSO regression analysis (lambda = 0.0489, min = 0.0276) were selected as marker genes (Figures 3(a) and 3(b)), and we obtained 14 marker genes (Figure 3(c)). A risk score was calculated for each sample using the predict.cv.glmnet function based on the Cox regression model and the expression levels of each gene (Figure 3(d)).

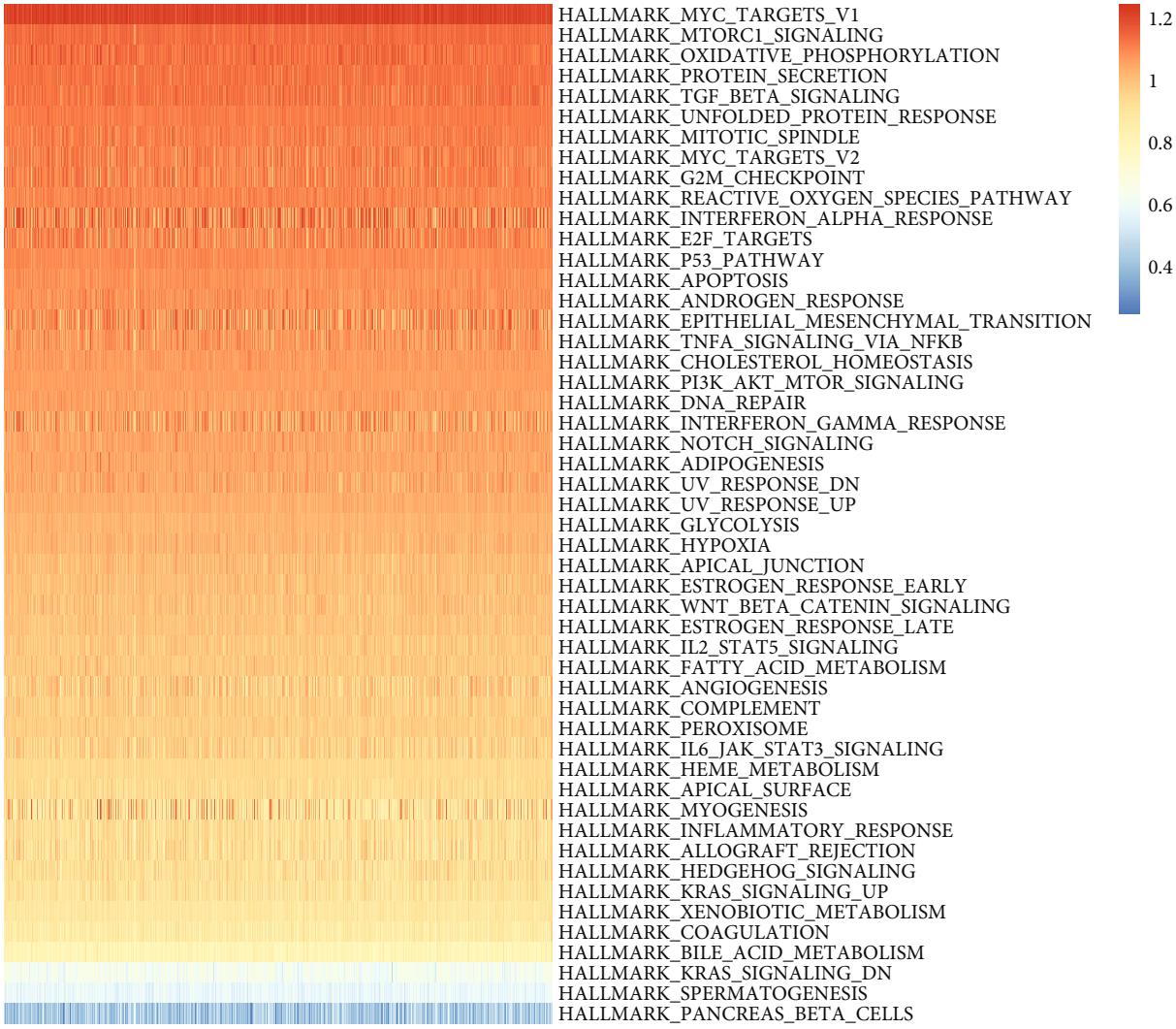

(a)

Figure 2: Continued.

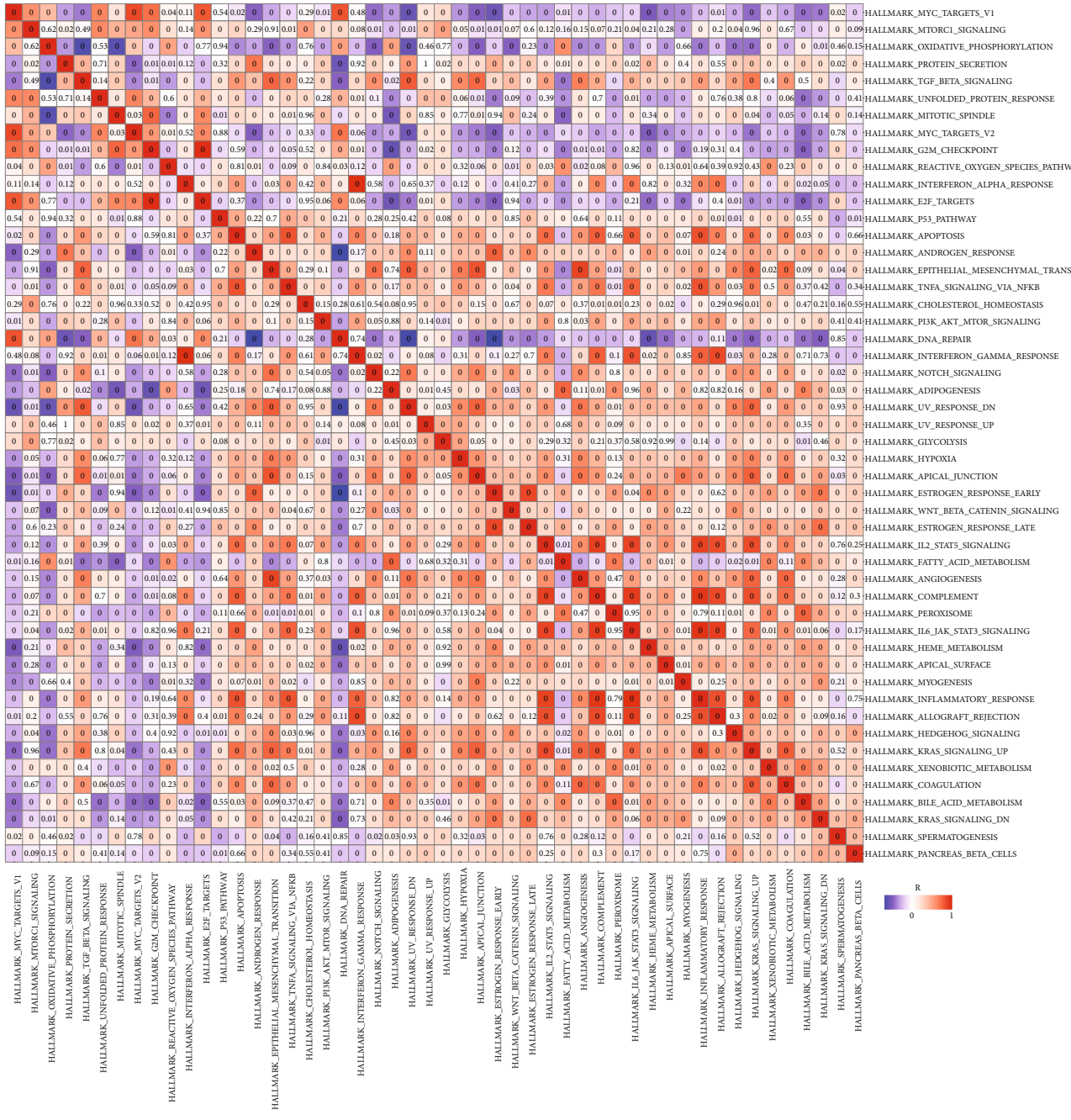

(b)

Figure 2: Continued.

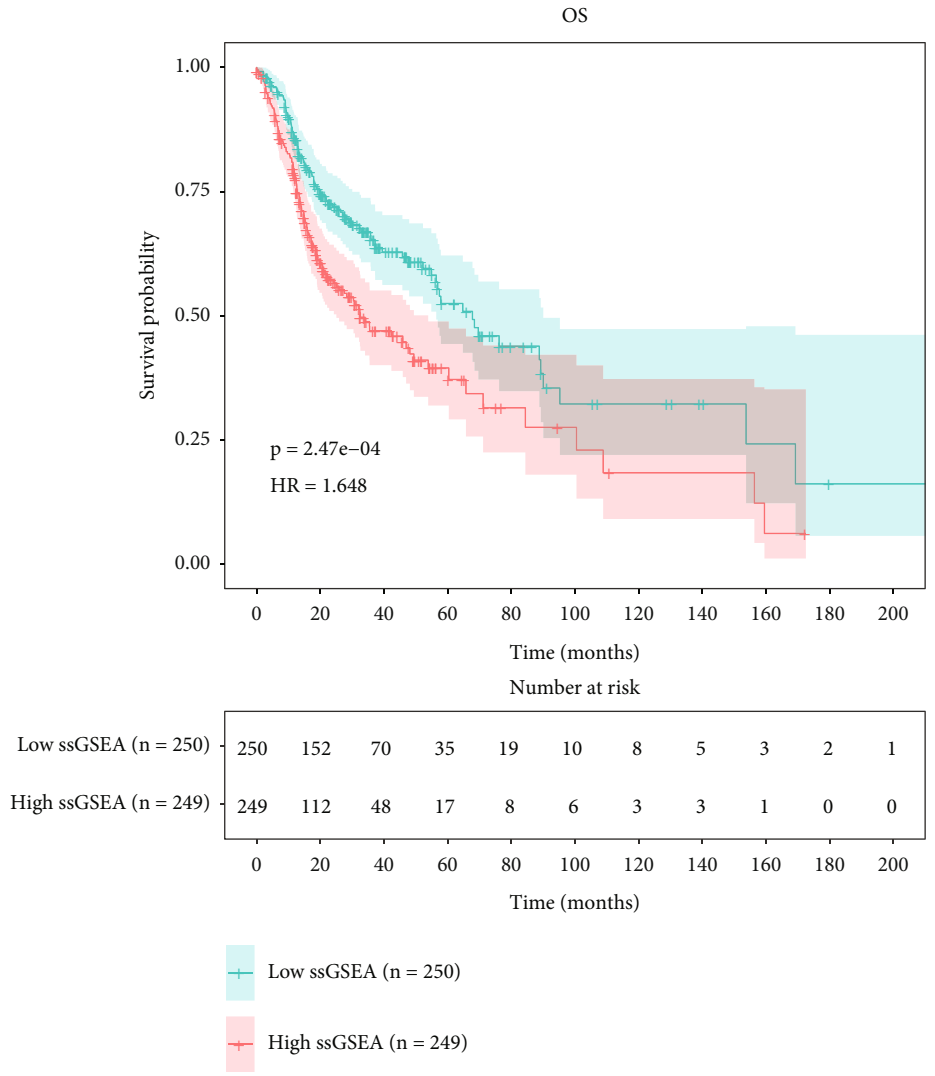

(c)

Figure 2: Continued.

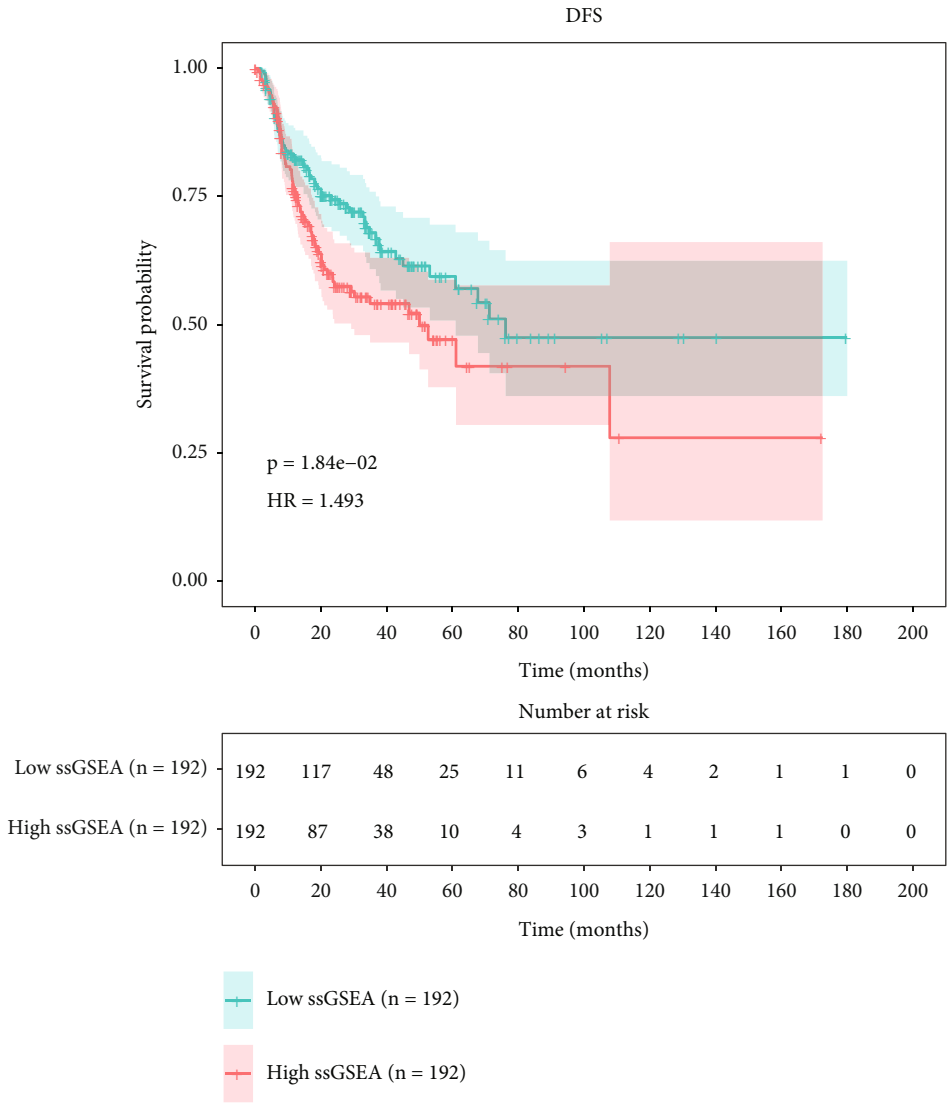

(d)

Figure 2: Continued.

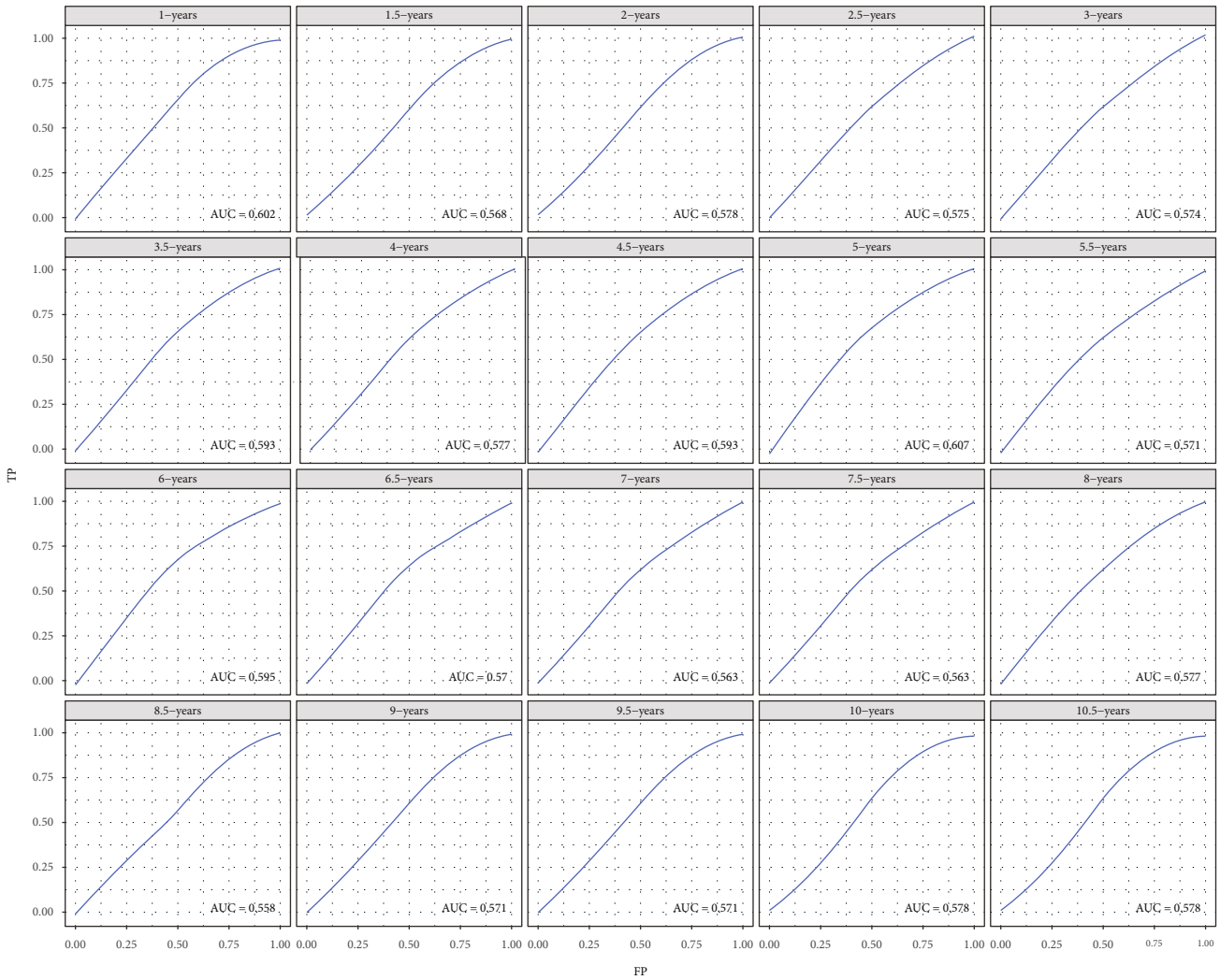

(e)

Figure 2: Continued.

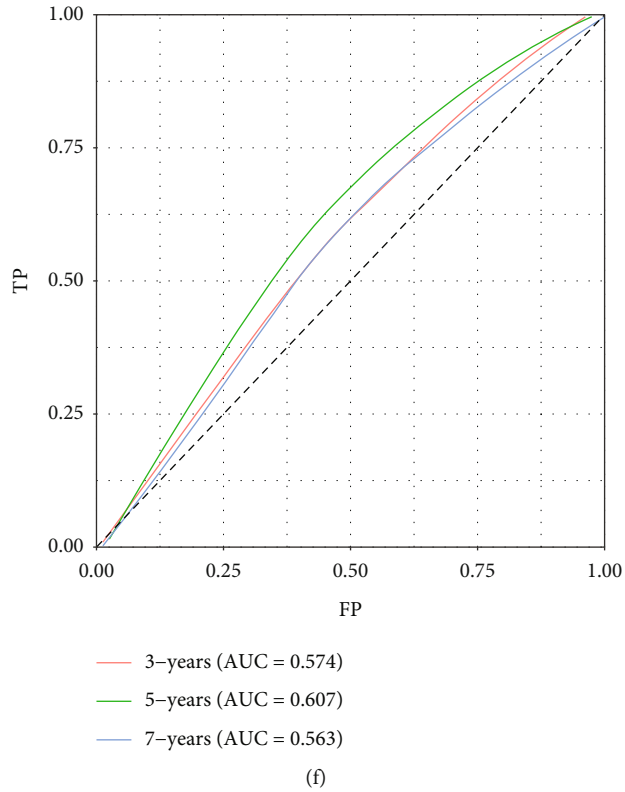

Figure 2: A prognostic signature based on genes associated with UPR. (a) Heatmap of the ssGSEA score of each item. (b) Heatmap of ssGSEA score correlations between items. (c) OS of the HR and LR groups. (d) DFS of the HR and LR groups. (e) Time-dependent ROC curves of the UPR-associated gene signature from 1 year to 10.5 years. (f) ROC curves for 3, 5, and 7 years.

Table 1: Cox regression results of hallmark items.

Term	p value	HR
HALLMARK_MYC_TARGETS_V1	0.011703	179594.1
HALLMARK_MTORC1_SIGNALING	$4.29E-05$	$1.59E+10$
HALLMARK_OXIDATIVE_PHOSPHORYLATION	0.030742	1266.05
HALLMARK_PROTEIN_SECRETION	0.018633	141007.4
HALLMARK_TGF_BETA_SIGNALING	0.067779	381.6219
HALLMARK_UNFOLDED_PROTEIN_RESPONSE	$3.63E-05$	$5.51E+12$
HALLMARK_MITOTIC_SPINDLE	0.736746	0.291637
HALLMARK_MYC_TARGETS_V2	0.05255	122.3036
HALLMARK_G2M_CHECKPOINT	0.495757	5.585005
HALLMARK_REACTIVE_OXYGEN_SPECIES_PATHWAY	0.061818	2061.022

3.2. Evaluation of the UPR-Associated Gene Prognostic Signature in the Internal and External Validation Cohorts. Based on the median risk score, we divided the training and testing groups into HR and LR groups for the validation of the LASSO Cox regression results. The results demonstrated that the difference in OS was significant between the HR and LR groups (Figures 4(a) and 4(c)). The 10-year AUC of the training group was 0.772, and the 10-year AUC of the test group was 0.727 (Figures 4(b) and 4(d)). After merging the data, the results also showed the same trends for the HR and LR groups ($p = 2.31E-12$, HR = 2.704), and the 10-year AUC was 0.74 (Figures 4(e) and 4(f)). Our results indicated that low-risk patients had a better prognosis in the training (HR vs. LR patients; 5-year OS: 8.8% vs. 14.4%; $p < 0.001$) and testing (HR vs. LR patients; 5-year OS: 5.6% vs. 12.8%; $p < 0.001$) cohorts.

External validation was performed with the GSE41613 dataset. The ROC analysis revealed a 5-year AUC of 0.607 (Figures 4(g) and 4(h)), and there was a significant difference in OS between the HR and LR groups ($p = 3.33E-01$, HR = 1.312). LR patients also had a better prognosis (HR vs. LR patients; 5-year OS: 29.2% vs. 49.0%; $p < 0.001$). The

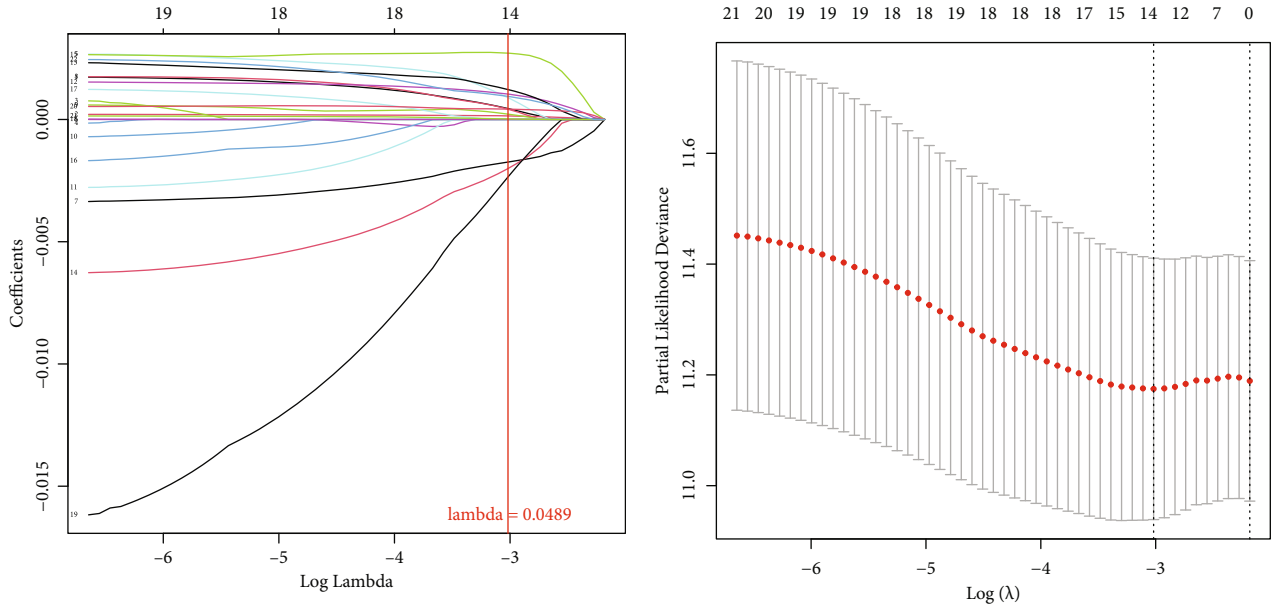

Variable	HR	95% CI	p_value
ADGRG1	1	1 – 1	0.00253
ALDOA	1	1 – 1	0.00546
ERP44	1.01	1 – 1.01	0.00144
GAK	0.992	0.987 – 0.997	0.00188
GARS1	1	1 – 1.01	0.000105
GHITM	1	1 – 1	0.00922
MYH11	1	1 – 1	0.00404
PFKM	1	1 – 1.01	0.00482
PKD1	0.993	0.988 – 0.998	0.00362
RDH11	1	1 – 1.01	0.00698
TJP3	0.985	0.974 – 0.996	0.00954
TPM3	1	1 – 1	0.00486
TPT1	1	1 – 1	0.00612
VDAC1	1	1 – 1	0.00478

Figure 3: An analysis of the LASSO Cox and univariate Cox regression of the UPR gene signature. (a) LASSO regression results, $\lambda = 0.0489$. (b) Cross-validation diagram of LASSO regression results. (c) The univariate Cox regression diagram of marker genes. (d) Heatmap of marker genes, selected from the univariate Cox regression.

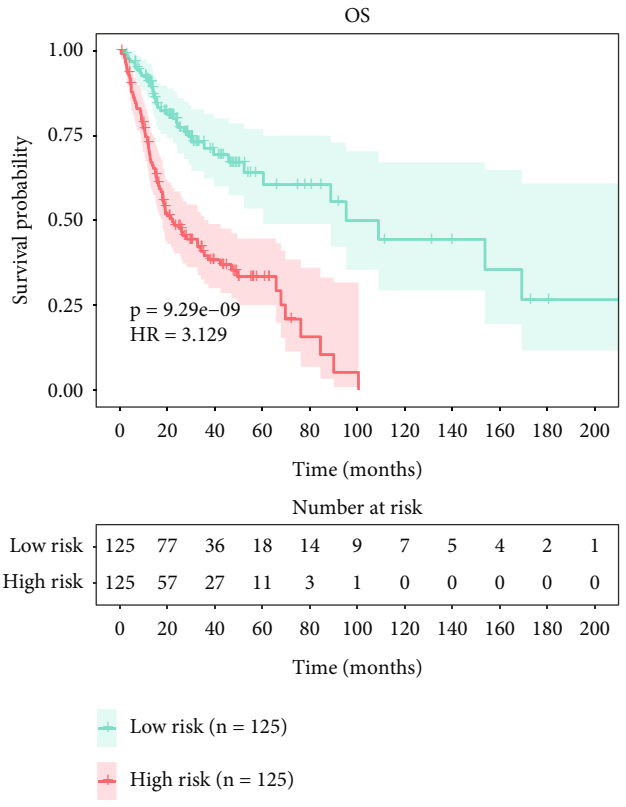

(a)

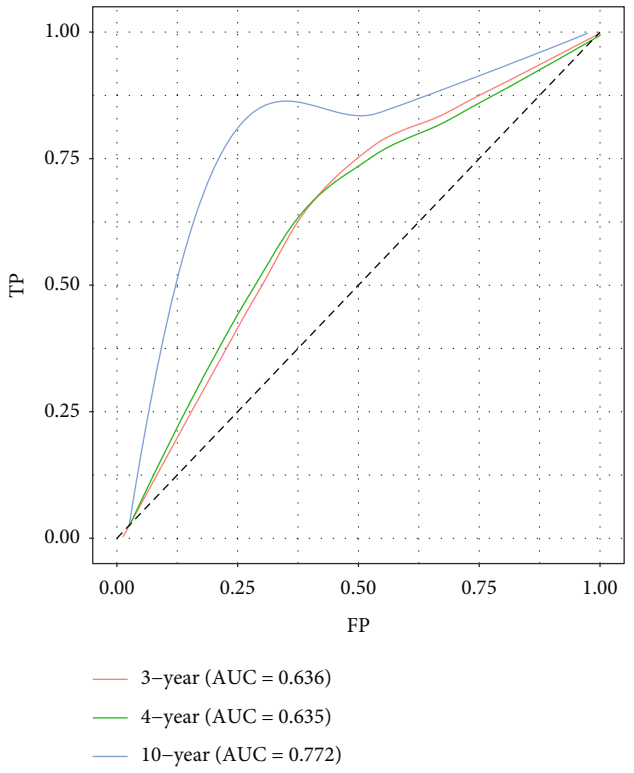

(b)

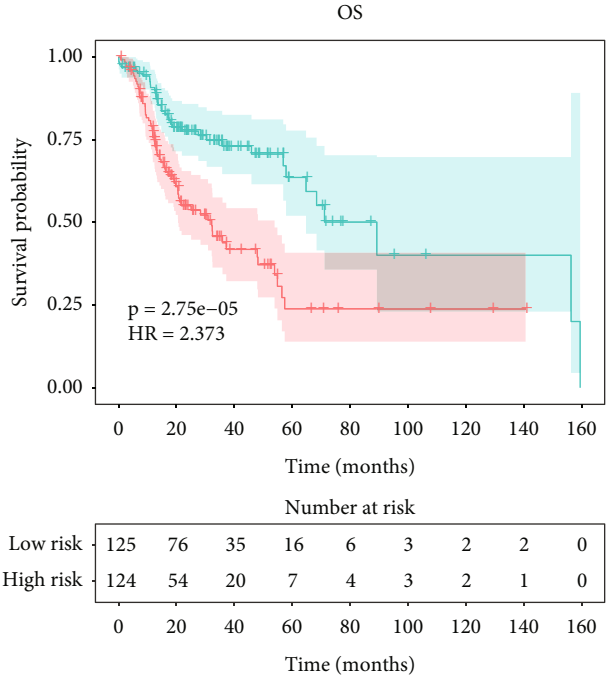

(c)

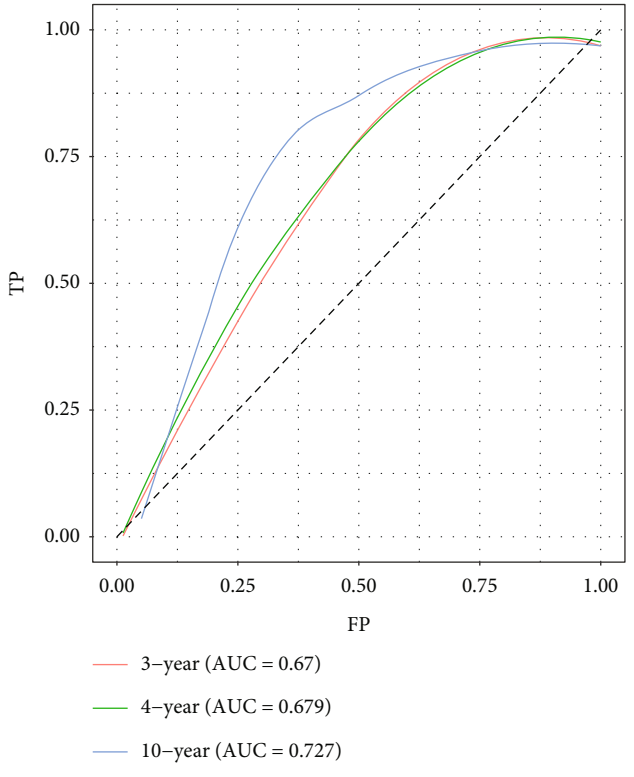

(d)

Figure 4: Continued.

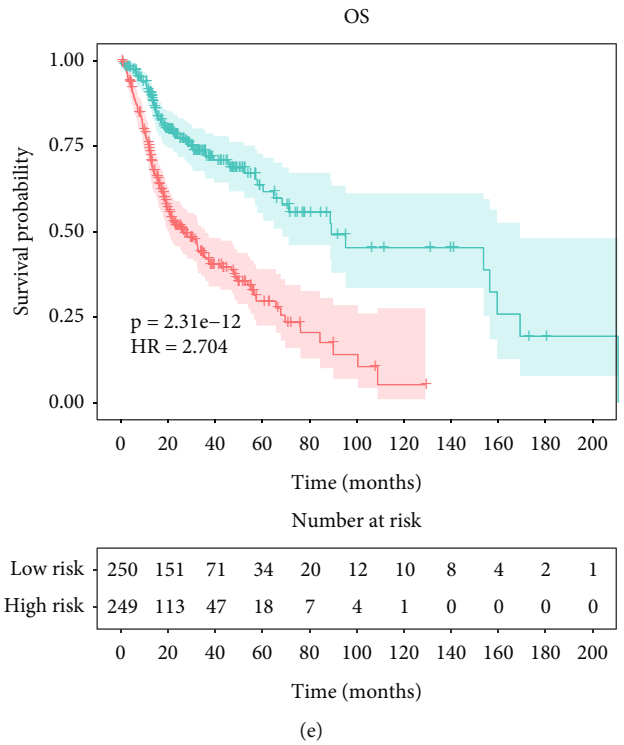

(e)

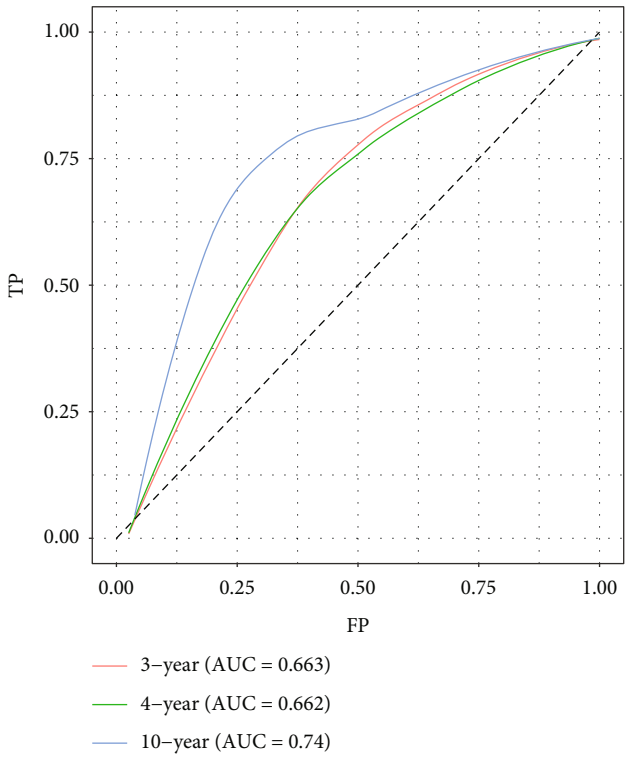

(f)

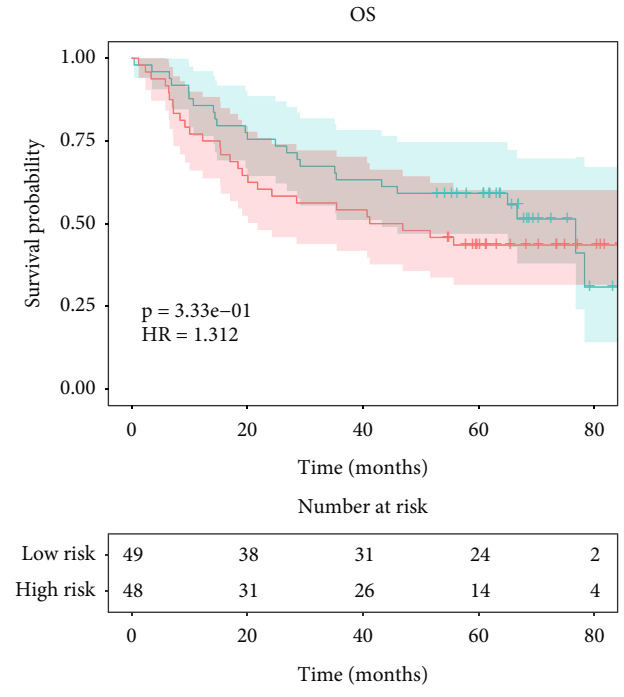

(g)

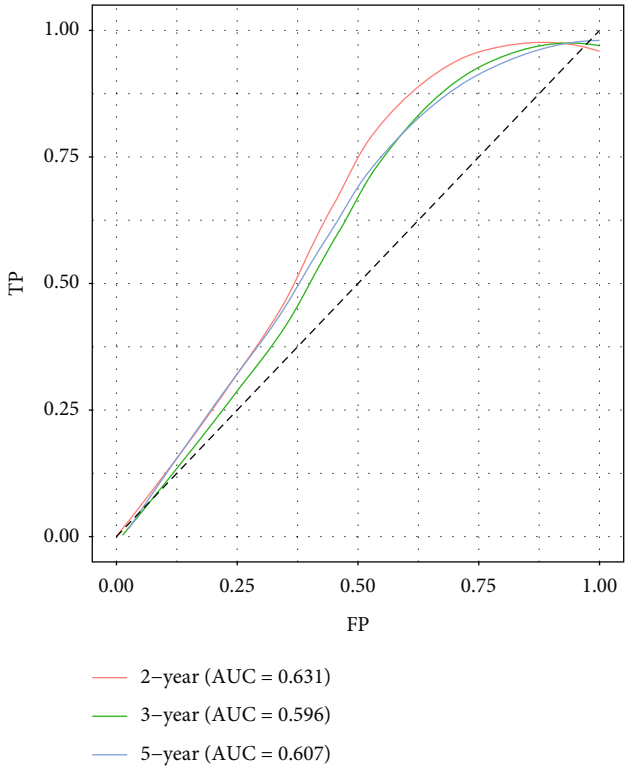

(h)

Figure 4: LASSO regression verification. (a, b) OS and ROC curves of the training group. (c, d) OS and ROC curves of the testing group. (e, f) OS and ROC curves of the total data of the training and testing groups. (g, h) OS and ROC curves of the external data (GSE41613).

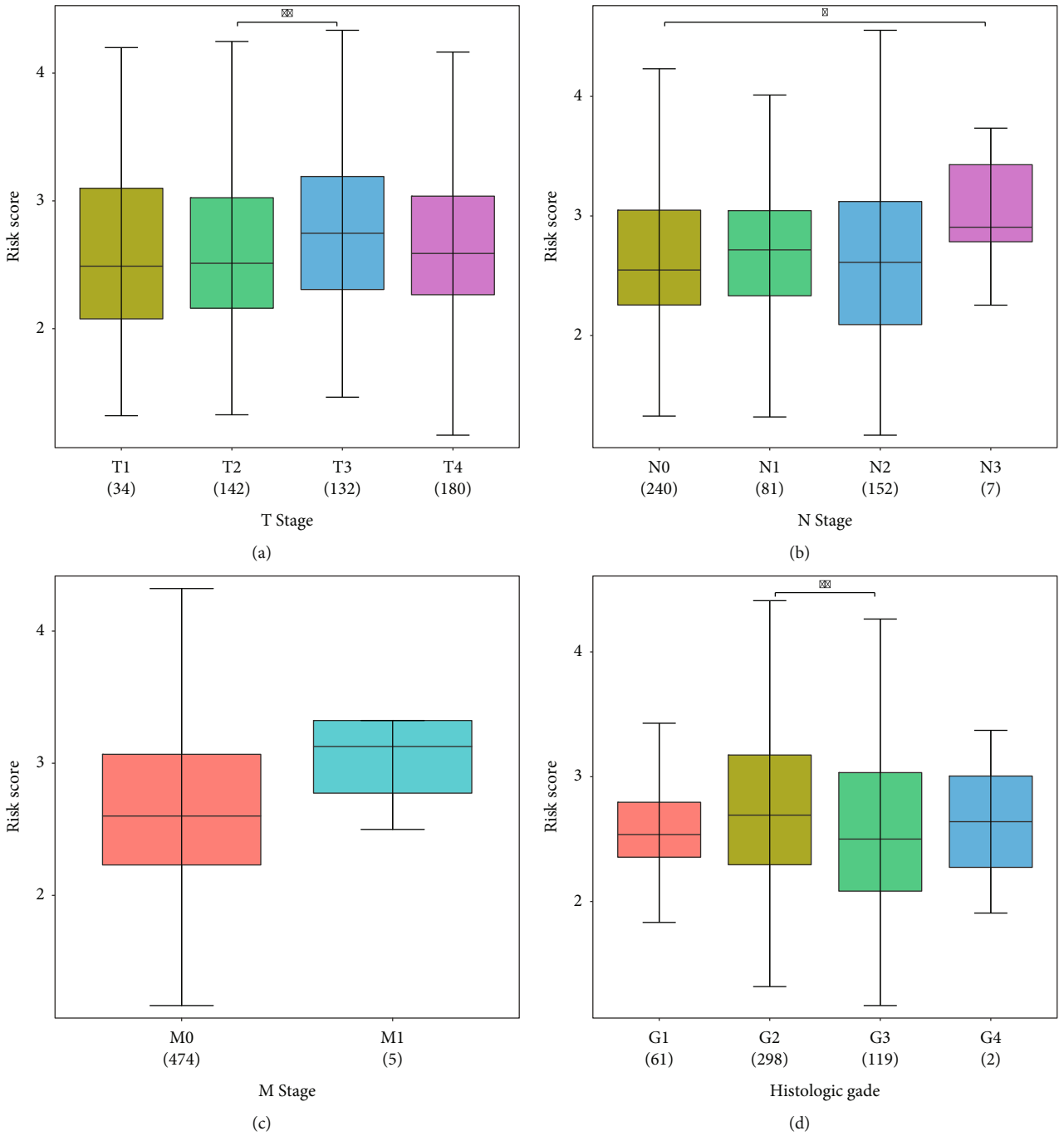

Figure 5: Continued.

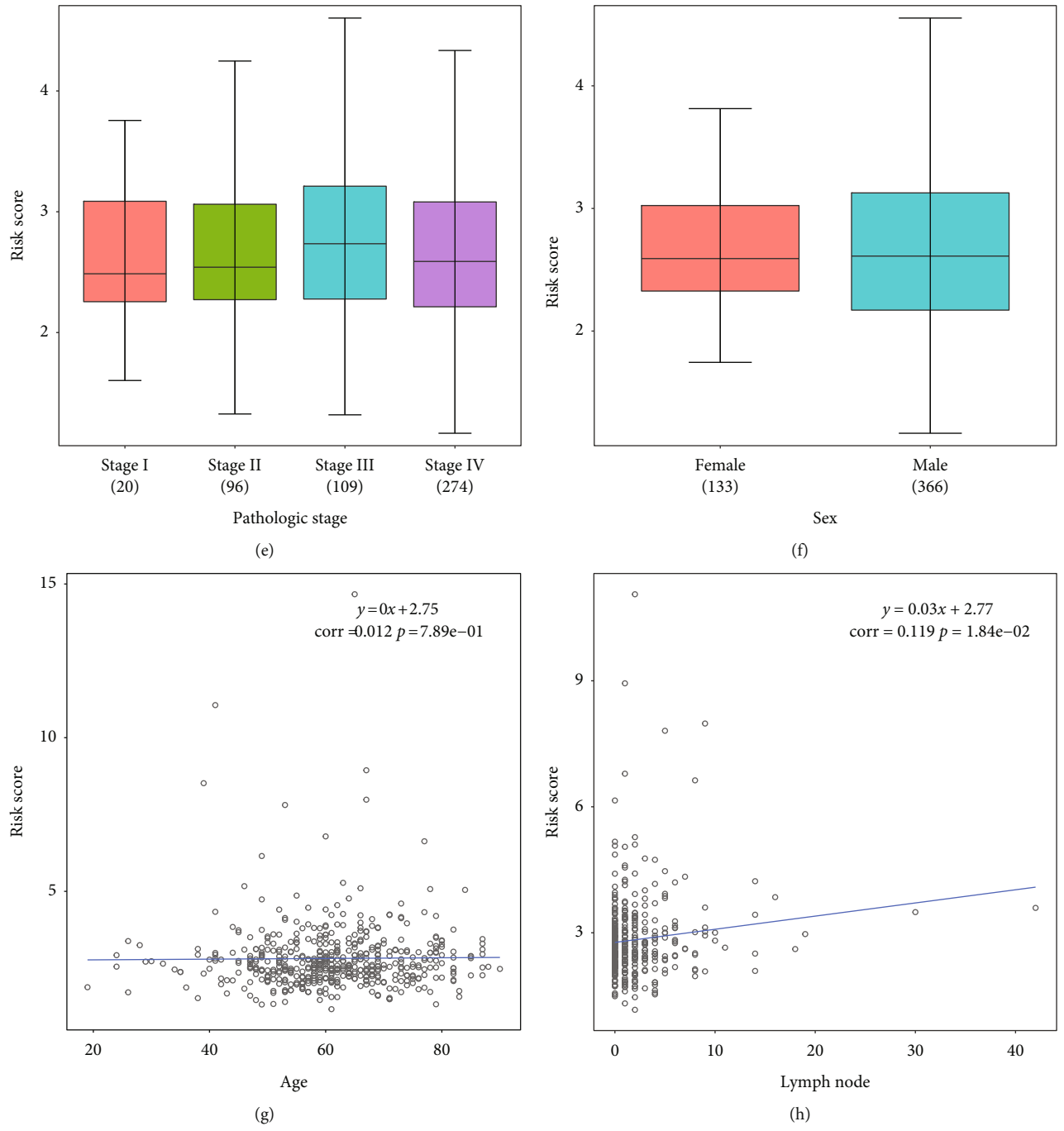

Figure 5: Continued.

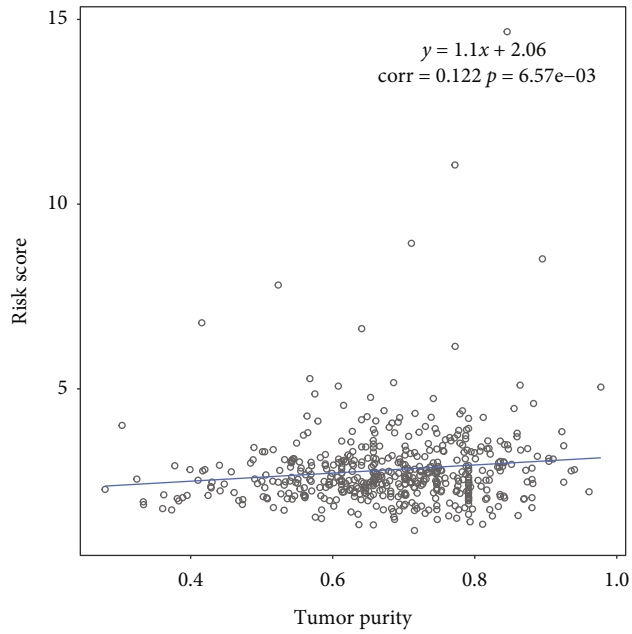

(i)

Figure 5: Clinical characteristics. Relationship between the risk score and clinical data in the (a) T stage, (b) N stage, (c) M stage, (d) histological grade, (e) pathological stage, and (f) sex groups. Correlation between the risk score and (g) age, (h) lymph node, and (i) tumor purity groups.

results from the internal and external verification cohorts confirmed that UPR-associated genes affected HNSCC patient survival.

3.3. Identification of Biological Characteristics Associated with the UPR-Associated Gene Prognostic Signature. Further exploration of the relationship between UPR-associated genes and clinical features was performed by studying the differences in risk scores by histopathological grade, sex, age, T stage, N stage, and M stage. The difference in the risk score in each group is shown in Figures 5(a)–5(f). According to these results, sex, M stage, and pathological stage did not affect the risk score. In Figures 5(g)–5(i), tumor purity, lymph node status, and age were all factors that were related to the risk score.

3.4. Construction and Validation of the Nomogram. Although multiple prognostic factors were selected, the complex interrelationships among variables and the contribution of each factor to tumor formation and development remain unclear. Therefore, a more comprehensive prognostic prediction model is needed. In this study, we created a nomogram model consisting of age, N stage, M stage, and the risk score based on the point scale to predict survival in HNSCC patients (Figure 6(a)). The nomogram model predictive accuracy was evaluated using calibration curves and ROC curves (Figures 6(b) and 6(c)). Based on our results, the nomogram model is able to accurately predict OS for HNSCC patients.

3.5. Anticancer Drug Responses. To predict the response of a cancer patient to a therapeutic agent, we performed research on the difference in the IC50 score between the HR and LR UPR-associated gene groups. The outcomes (Figure 7) showed that anticancer drugs such as AKT inhibitor III, CCT007093, vinblastine, EHT 1864, elesclomol, and AS601245 were the most sensitive drugs in HR patients. Sorafenib, mitomycin C, obatoclax mesylate, PHA665752, and VX702 were the most sensitive anticancer drugs in the LR patients. Based on these findings, guidance for clinical treatment, which may vary depending on the type of UPR-associated gene, is provided.

3.6. Immune Infiltration Analysis. To explore the immune cells that may remarkably differ between different risk groups, we performed an immune infiltration analysis. The differences in M0 macrophages, follicular helper T cells, naive CD4 T cells, CD8 T cells, and resting NK cells were significant between the two test groups (Figure 8), which indicates that these immune cells may be associated with UPR-associated gene.

3.7. Gene Set Enrichment Analysis (GSEA). We performed GSEA to understand the potential biological processes of UPR-associated gene, cellular components, molecular functions, and pathways that may vary considerably between different risk groups. As shown in Figure 9(a), the positive regulation of phosphatase activity, cellular extravasation, and positive regulation of phosphatidylinositol 3-kinase activity were significantly enriched in the HR group. The establishment of protein localization to the ER, protein targeting to the membrane, and protein localization to the ER was highly enriched in the LR group. Cellular component analysis showed that UPR-associated genes were related to the phosphatidylinositol 3-kinase complex, phagocytic cup, and plasma membrane raft in the HR group, and the

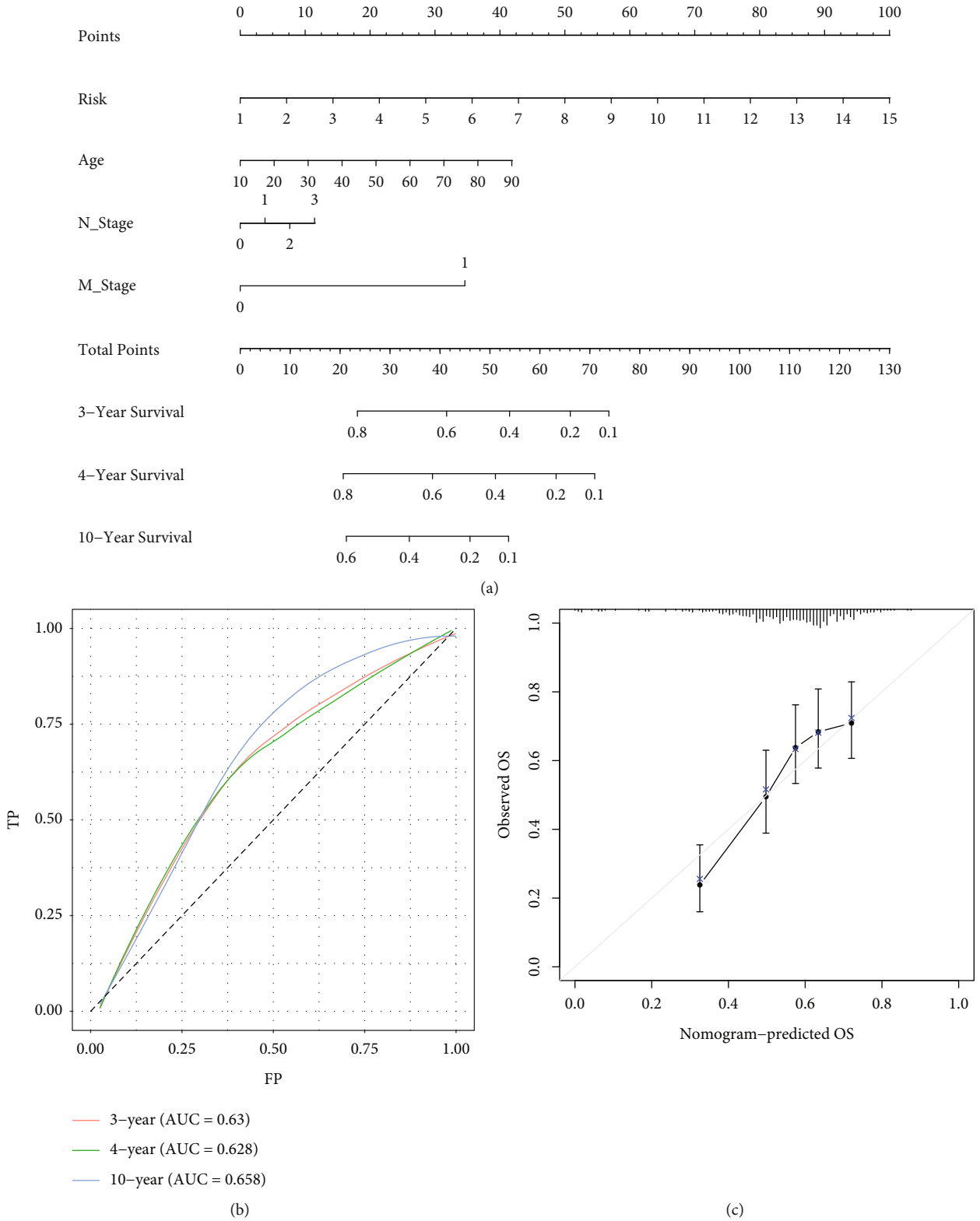

Figure 6: An algorithm based on the UPR-associated gene signature was constructed and validated. (a) Nomogram for predicting the OS probability of HNSCC patients. (b) Nomogram ROC curve analysis with time dependence. (c) The calibration of the nomogram for predicting OS.

preribosome large subunit precursor, U1 snRNP, and large ribosomal subunit were enriched in the LR group (Figure 9(b)). Figure 9(c) shows that SH2 domain binding, cytokine binding, and RNA polymerase II transcription factor binding were highly enriched in the HR group, and disulfide oxidoreductase activity, which acts on NAPDH/quinone

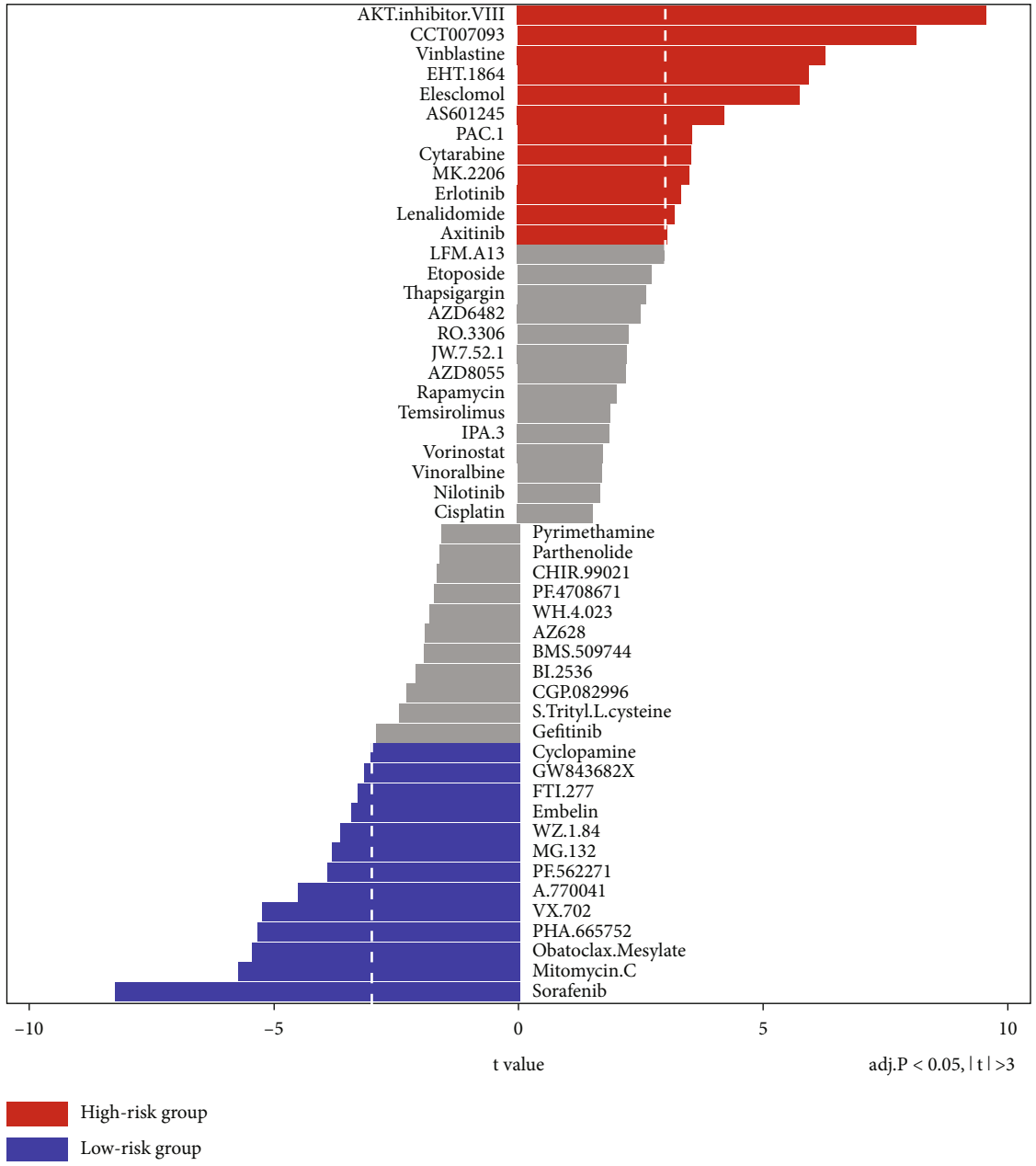

Figure 7: A half-maximal inhibitory concentration (IC50) analysis in the HR and LR groups.

or similar compounds as acceptors, and structural constituents of ribosomes were enriched in the LR group. Platelet activation, gap junctions, and the thyroid hormone signaling pathway were related to UPR-associated genes in the high-risk group. Oxidative phosphorylation, olfactory transduction, and ribosomes were enriched in the LR group in the KEGG pathway analysis (Figure 9(d)). By analyzing enrichment analysis results, we were able to understand the molecular mechanisms underlying the UPR-associated genes affecting HNSCC, clarifying their role in affecting prognosis.

4. Discussion

The UPR is an adaptive signaling network that is evoked by physiological and pathological conditions. Researchers have examined the relationship between UPR activation markers and the prognosis of cancer [26, 27]. The results demonstrated that activation of the UPR was related to shorter OS, increased tumor aggressiveness, and increased metastasis in breast cancer, colorectal carcinoma, glioblastoma, and hepatocellular carcinoma [28–30]. Accumulated evidence also suggests that the UPR signaling pathway and ER stress play a functional role by regulating crucial tumor biological processes in HNSCC, including progression and therapy resistance [16]. However, few studies have revealed whether UPR status predicts prognosis in HNSCC patients. Additionally, HR patients with different UPR statuses should also be assessed for their immune status to increase the effectiveness of their immunotherapy. Therefore, our study is aimed at constructing a model based on UPR-

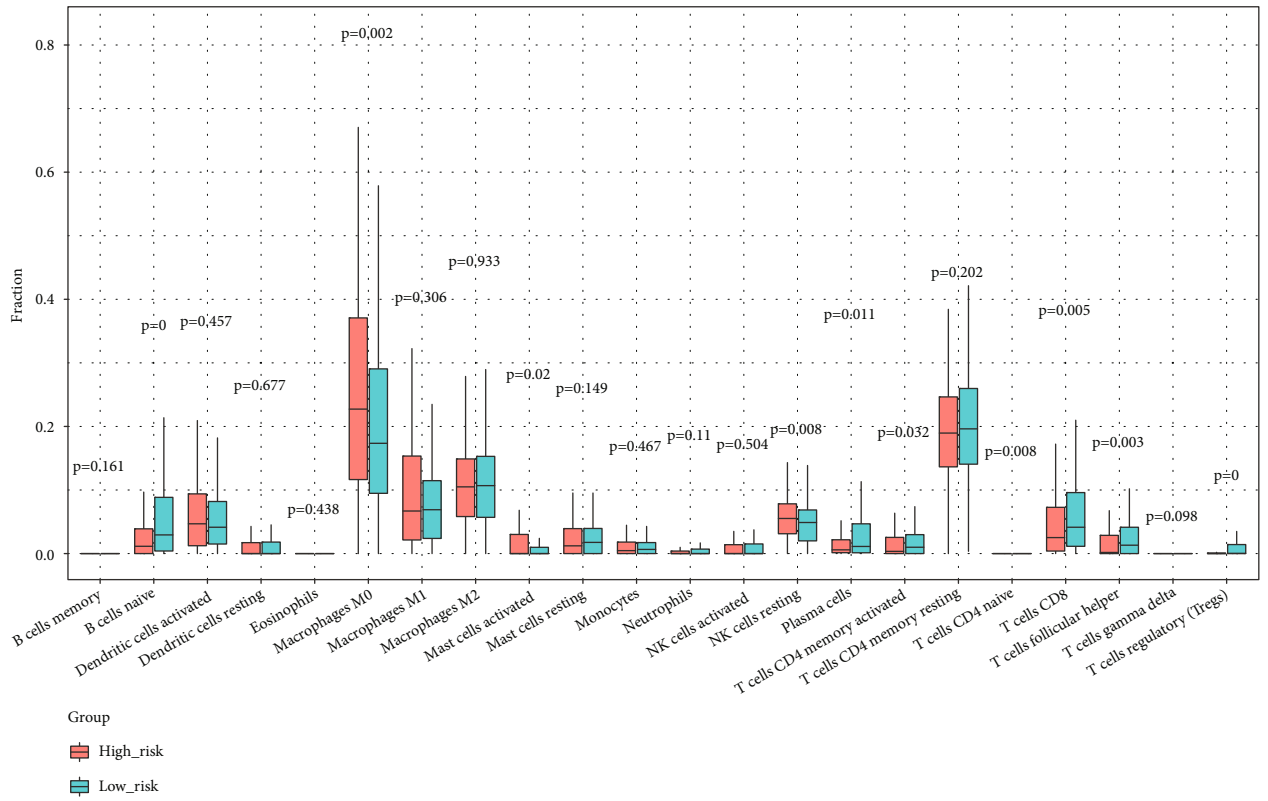

Figure 8: Immune cell infiltration analysis between the two test groups.

associated genes for predicting HNSCC prognosis and further characterizing the IC50 scores and immune infiltration levels between the two UPR risk groups. The most significant conclusion from this study is that UPR status is an important determinant of prognosis in HNSCC patients, and the UPR-associated gene risk score combined with age, N stage, and M stage may be used to develop a robust prediction model for survival analysis. The IC50 analysis and immune infiltration analysis may improve decision-making at the individual patient level.

The univariate Cox analysis identified 14 key UPR-associated genes that affected HNSCC prognosis (ADGRG1, ALDOA, ERP44, GAK, GARS1, GHITM, MYH11, PFKM, PKD1, RDH11, TJP3, TPM3, TPT1, and VDAC1). ER-resident protein 44 (ERP44) is a redox sensor and regulates the location of critical enzymes that operate in the ER. ERP44 promotes progression in nasopharyngeal carcinoma via its interaction with ATP citrate lyase and regulation of epithelial-mesenchymal transition (EMT) [31]. Nasopharyngeal cancer cells release exosomes expressing ERP44, which may be delivered to adjacent cells to enhance chemoresistance under ER stress [32]. The above information suggests that ERP44 is an important gene influencing tumor progression and chemoresistance in HNSCC. Protein kinase D1 (PKD1) is a member of the serine/threonine kinase family and activates protective signals against ER stress. Several investigations have shown that PKD1 plays a role in the regulation of various tumor-related pathways [33]. PKD1 is closely related to the redifferentiation of keratinocytes and the increase in cell proliferation, and it may enhance the activity of the ERK/MAPK pathway [34]. Higher expression of PKD1 correlated with poor differentiation in oral squamous cell carcinoma [35]. PKD1 is frequently downregulated at both the transcriptional and protein levels in HNSCC cell lines [36]. However, there are no related reports about the effects of PKD1 on the prognosis of HNSCC. MYH11 is a novel gene for predicting OS in HNSCC and may be a drug target based on bioinformatic analysis [37, 38], but experiments supporting these findings have not been conducted. The effects of PFKM, ADGRG1, ALDOA, GAK, RDH11, TJP3, TPM3, TPT1, and VDAC1 on the prognosis of HNSCC and the immunological changes in the HNSCC microenvironment have rarely been reported and need further investigation. We also demonstrated that the UPR-associated genes were differentially expressed in different T stage, N stage, and histological grade groups. We revealed that the UPR risk score was related to cancer purity, lymph node status, and age. These results indicated that UPR-associated genes affected the biological behavior of HNSCC.

Several differences emerged between the prediction results of the model and the external validation results of the GSE41613 dataset. We speculate that this result may be related to the classification of HNSCC. HNSCC is divided into oral squamous cell carcinoma (OSCC), oropharyngeal carcinoma, nasopharyngeal carcinoma, laryngeal carcinoma, etc. The pathogenic factors of these cancers are diverse, and survival outcomes differ in the different subsites of HNSCC [39]. Therefore, HNSCC information in TCGA database is relatively mixed. Deviations in the grouping of the training

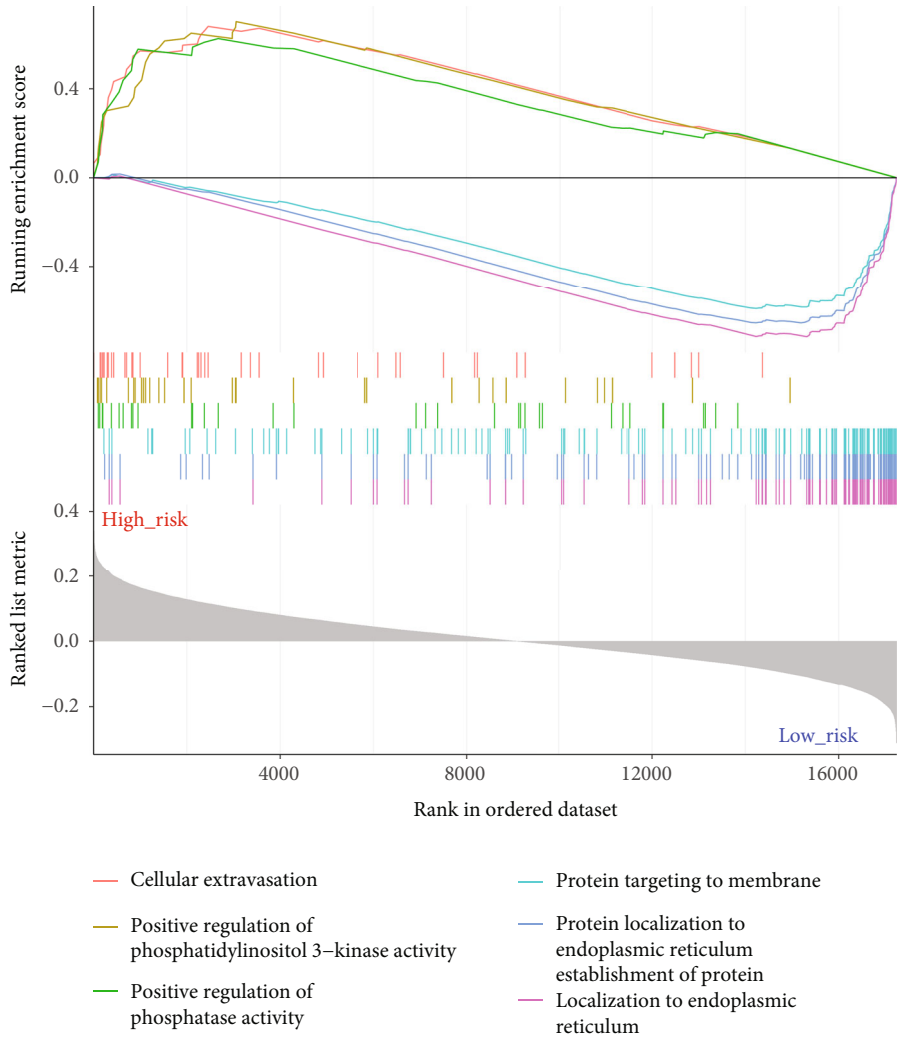

(a)

Figure 9: Continued.

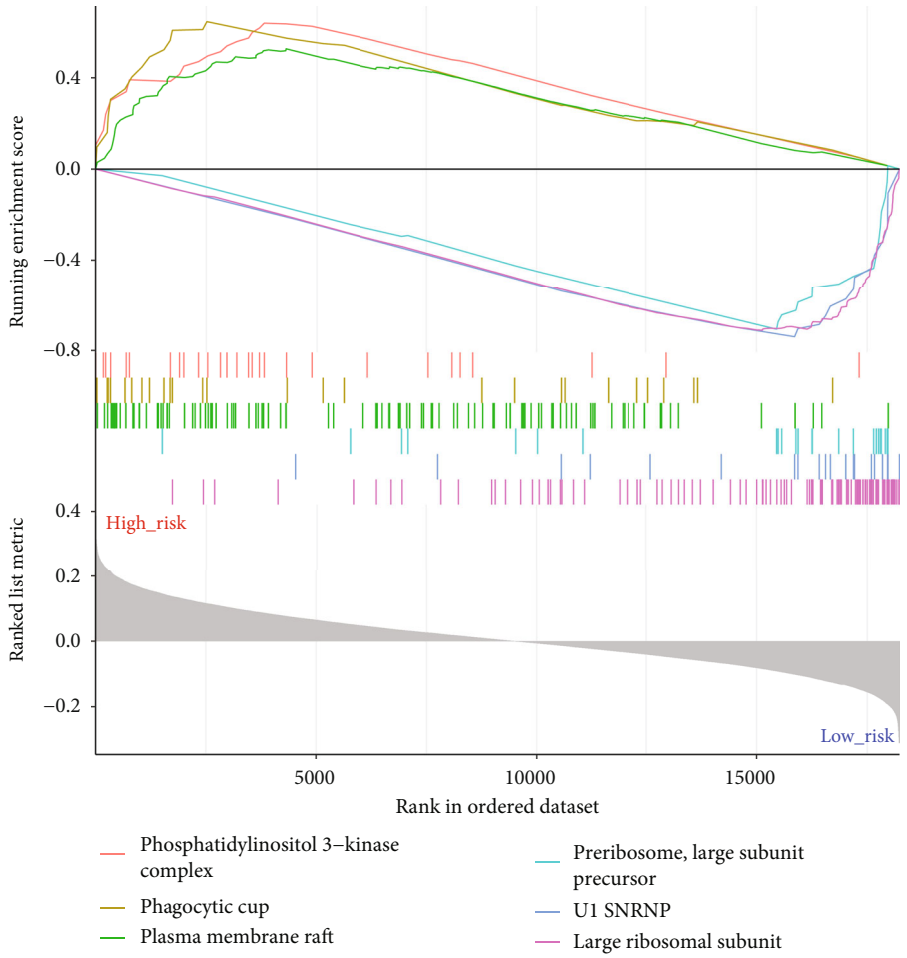

(b)

Figure 9: Continued.

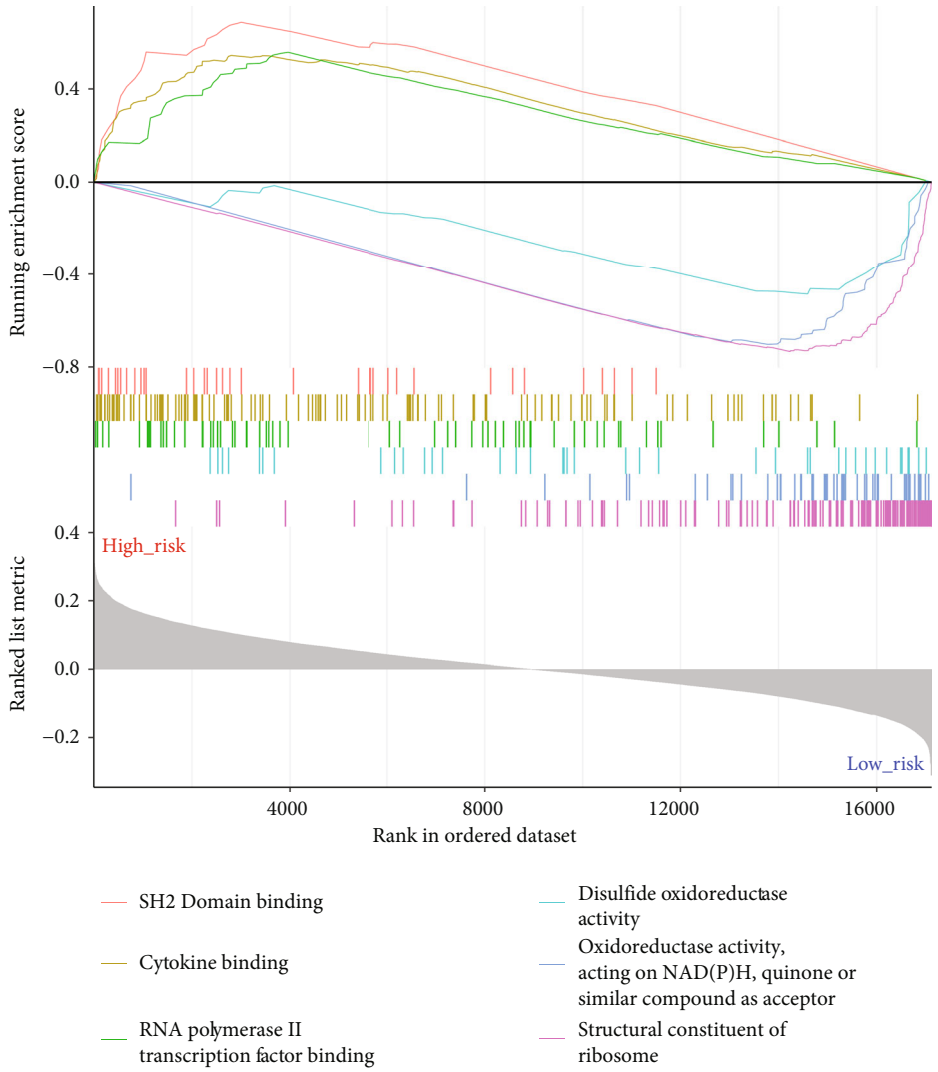

(c)

Figure 9: Continued.

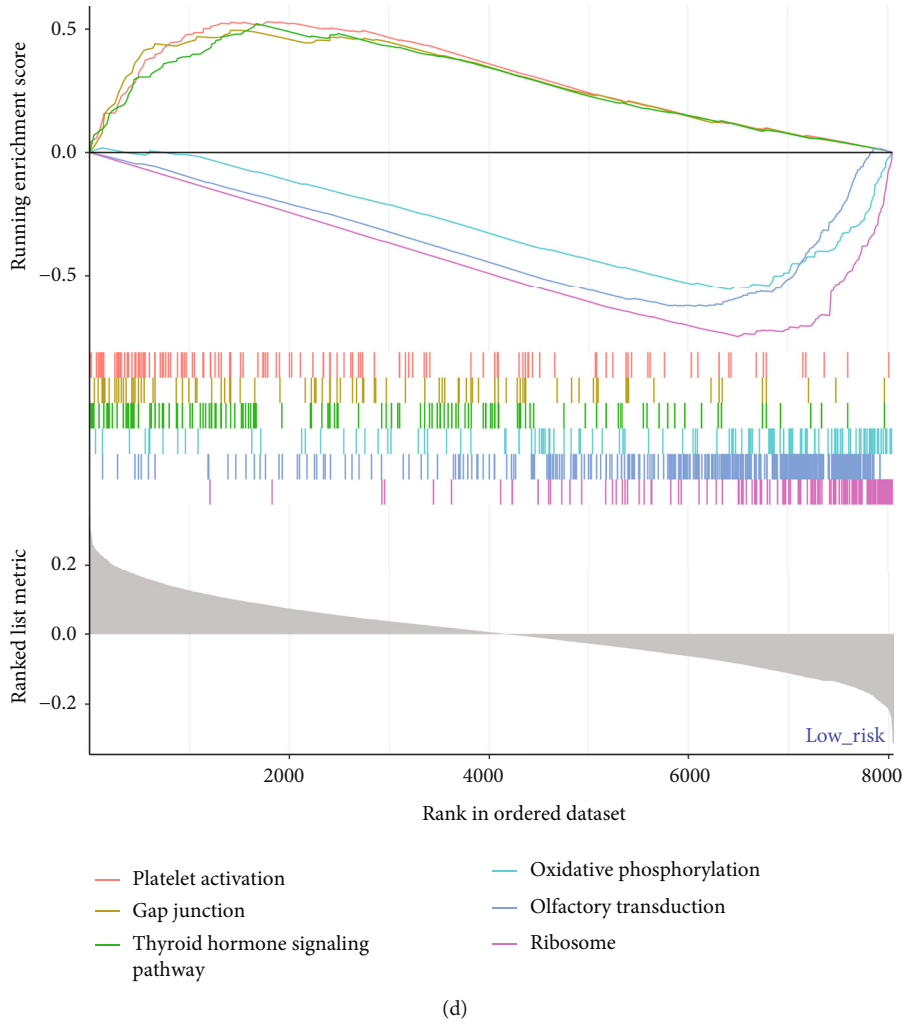

Figure 9: Gene set enrichment analysis (GSEA) in the HR and LR groups. The graph shows six items in (a) biological processes, (b) cellular components, (c) molecular functions, and (d) KEGG pathways.

cohort and test cohort may lead to the above unsatisfactory results. Therefore, we suggest that future analysis of the prognosis at one subsite of HNSCC, such as OSCC, should be based on the data of this subsite rather than on HNSCC with mixed multiple sites. However, this model has the principal benefit of bringing a complementary perspective to individual tumors and establishing a scoring framework for patients. Therefore, our nomogram may be a favorable tool for clinicians in the future. However, whether the UPR-associated gene model predicts the recurrence of HNSCC is not known. This relationship is our future focus, and we will investigate the role of UPR-associated genes in the recurrence of HNSCC.

It is becoming increasingly recognized that heterogeneity is significant in tumor progression and clinical decisions. The present evidence supports that chemotherapy resistance in cancers is linked to the UPR and ER stress [32]. One problem with the existing anticancer drugs is that a particular drug shows different sensitivities in different individuals. Targeting UPR branches is a promising way to enhance the efficacy of chemotherapy for cancers [40]. Considering the above problem, we performed a UPR-related IC50 analysis to explore sensitivities and help HNSCC patients obtain personalized medication regimens. AKT inhibitor III, CCT007093, vinblastine, EHT 1864, elesclomol, AS601245, etc. may be the most sensitive anticancer drugs in HR patients whose outcome survival is much poorer than that of LR patients. However, more research is needed to verify whether these drugs can achieve the predicted sensitivity. A recent study [41] explored the best metric for predicting drug sensitivity, and they found that the area above the dose-response curve was better than the IC50. To further verify the anticancer sensitivity of these drugs in different UPR risk groups, in vivo and in vitro experiments should be conducted.

Previous studies have shown that the UPR evades the immune response by regulating the tumor microenvironment. The ER stress state of tumor cells is transmitted to macrophages and dendritic cells (DC) in the microenvironment. This communication leads to the upregulation of the expression of some proinflammatory cytokines and chemokines, which inhibits the maturation of DCs. It also inhibits

the activation of CD8+ T cells and secretes arginine by reducing the process of antigen presentation, which inhibits T cell activation and leads to tumor immune escape [18]. Therefore, we further investigated the role of the UPR in the tumor microenvironment by evaluating immune cell infiltration. The results revealed significant differences in M0 macrophages, follicular helper T cells, naive CD4 T cells, CD8 T cells, and resting NK cells between the HR and LR groups. This finding provides important insights into the tumor immune microenvironment affecting the UPR.

Different risk groups showed enrichment in different pathways in the GSEA. The UPR genes included in the signature were primarily involved in platelet activation, gap junctions, and the thyroid hormone signaling pathway in the HR group. The platelets seem to play a critical role in malignant tumor metastasis. Cancer metastasis is promoted by the interaction between platelets and circulating tumor cells (CTCs). CTCs activate platelets, and activated platelets accumulate and protect CTCs from NK cells and shear stress. Finally, CTC hypoxia tolerance is promoted by platelets, along with angiogenesis, EMT, extravasation, and ultimately metastasis [42]. Our results suggested an explanation for why HR group patients have a poorer outcome than LR patients, and the status of platelet activation may be a vital factor.

In summary, we identified 14 genes associated with the UPR in HNSCC patients that affected their prognosis. Based on these genes, we investigated the prognostic significance of the UPR risk score for HNSCC patients and established a nomogram prediction model combining this risk score with age, N stage, and M stage. The infiltration of immune cells in the microenvironment was further analyzed, which provided some information for immunotherapy in different risk groups. This study also described therapeutic regimens in different risk groups of HNSCC, and it may be used as a reference for further studies on clinical medication. Notably, the prognosis of HNSCC was analyzed from the perspective of the UPR, and the changes in the immune microenvironment and possible effective drug regimens were described, which provided certain help for the treatment of HNSCC. However, because our study was based on bioinformatic analysis, there are some limitations, and our results must be confirmed in further clinical studies. This limitation means that the study findings must be interpreted cautiously. The function and mechanism of these UPR-associated genes, either individually or in combination, should be investigated to support their clinical application.

5. Conclusions

We developed a potent model based on the UPR-associated gene signature, i.e., the UPR risk score combined with age, N stage, and M stage, and this model may be used to predict HNSCC survival prognosis. Our study enhances the understanding of genes associated with UPR pathways in HNSCC and can improve decision-making at the individual patient level.

Data Availability

The data presented in this study are openly available in TCGA and GEO databases.

Conflicts of Interest

The authors have declared that the publication of this article does not involve any conflict of interest.

Authors' Contributions

Tao Wang and Lingling Chen contributed equally to this work.

Acknowledgments

This research was funded by the Young Teacher Education Scientific Program of the Fujian Province, China (grant number JAT190230), and the Qihang Program of Fujian Medical University, China (grant number 2019QH1129). The authors would like to thank Hong Wang for excellent support and Dr. Yang Chen for critically reviewing the manuscript.

References

[1] H. Sung, J. Ferlay, R. L. Siegel, M. Laversanne, and F. Bray, "Global Cancer Statistics 2020: GLOBOCAN estimates of incidence and mortality worldwide for 36 cancers in 185 countries," *CA A Cancer Journal for Clinicians*, vol. 71, no. 3, pp. 209–249, 2021.

[2] A. von Witzleben, C. Wang, S. Laban, N. Savelyeva, and C. H. Ottensmeier, "HNSCC: tumour antigens and their targeting by immunotherapy," *Cell*, vol. 9, no. 9, article 2103, 2020.

[3] N. Vigneswaran and M. Williams, "Epidemiologic trends in head and neck cancer and aids in diagnosis," *Oral & Maxillofacial Surgery Clinics of North America*, vol. 26, no. 2, pp. 123–141, 2014.

[4] E. E. Cohen, R. B. Bell, C. B. Bifulco et al., "The Society for Immunotherapy of Cancer consensus statement on immunotherapy for the treatment of squamous cell carcinoma of the head and neck (HNSCC)," *Journal for Immunotherapy of Cancer*, vol. 7, no. 1, pp. 1–31, 2019.

[5] M. Jakob, K. Sharaf, M. Schirmer et al., "Role of cancer stem cell markers ALDH1, BCL11B, BMI-1, and CD44 in the prognosis of advanced HNSCC," *Strahlentherapie und Onkologie*, vol. 197, no. 3, pp. 231–245, 2021.

[6] C. Hou, H. Cai, Y. Zhu, S. Huang, F. Song, and J. Hou, "Development and validation of autophagy-related gene signature and nomogram for predicting survival in oral squamous cell carcinoma," *Frontiers in Oncology*, vol. 10, article 558596, 2020.

[7] D. E. Johnson, B. Burtness, C. R. Leemans, V. W. Y. Lui, J. E. Bauman, and J. R. Grandis, "Head and neck squamous cell carcinoma," *Nature reviews Disease primers*, vol. 6, no. 1, pp. 1–22, 2020.

[8] G. R. Bhat, R. G. Hyole, and J. Li, "Head and neck cancer: Current challenges and future perspectives," *In Advances in Cancer Research*, vol. 152, pp. 67–102, 2021, Academic Press.

[9] C. R. Leemans, P. J. F. Snijders, and R. H. Brakenhoff, "The molecular landscape of head and neck cancer," *Nature Reviews. Cancer*, vol. 18, no. 5, pp. 269–282, 2018.

[10] C. Hetz, K. Zhang, and R. J. Kaufman, "Mechanisms, regulation and functions of the unfolded protein response," *Nature Reviews. Molecular Cell Biology*, vol. 21, no. 8, pp. 421–438, 2020.

[11] T. Zhang, N. Li, C. Sun, Y. Jin, and X. Sheng, "MYC and the unfolded protein response in cancer: synthetic lethal partners in crime?," *EMBO Molecular Medicine*, vol. 12, no. 5, article e11845, 2020.

[12] L. Sisinni, M. Pietrafesa, S. Lepore et al., "Endoplasmic reticulum stress and unfolded protein response in breast cancer: the balance between apoptosis and autophagy and its role in drug resistance," *International Journal of Molecular Sciences*, vol. 20, no. 4, p. 857, 2019.

[13] C. Hetz and E. Chevet, "Theme series–UPR in cancer," *Seminars in Cancer Biology*, vol. 33, pp. 1-2, 2015.

[14] N. Andruska, X. Zheng, X. Yang, W. G. Helferich, and D. J. Shapiro, "Anticipatory estrogen activation of the unfolded protein response is linked to cell proliferation and poor survival in estrogen receptor α-positive breast cancer," *Oncogene*, vol. 34, no. 29, pp. 3760–3769, 2015.

[15] M. Wang, M. E. Law, R. K. Castellano, and B. K. Law, "The unfolded protein response as a target for anticancer therapeutics," *Critical Reviews in Oncology/Hematology*, vol. 127, pp. 66–79, 2018.

[16] O. Pluquet and A. Galmiche, "Impact and relevance of the unfolded protein response in HNSCC," *International Journal of Molecular Sciences*, vol. 20, no. 11, p. 2654, 2019.

[17] T. Avril, E. Vauleon, and E. Chevet, "Endoplasmic reticulum stress signaling and chemotherapy resistance in solid cancers," *Oncogene*, vol. 6, no. 8, article e373, 2017.

[18] A. Papaioannou and E. Chevet, "Driving cancer tumorigenesis and metastasis through UPR signaling," *Current Topics in Microbiology and Immunology*, vol. 414, pp. 159–192, 2018.

[19] S. Hnzelmann, R. Castelo, and J. Guinney, "GSVA: gene set variation analysis for microarray and RNA-Seq data," *BMC Bioinformatics*, vol. 14, no. 1, pp. 1–15, 2013.

[20] P. Langfelder and S. Horvath, "WGCNA: an R package for weighted correlation network analysis," *BMC Bioinformatics*, vol. 9, no. 1, article 559, 2008.

[21] M. TherneauTerry, "A package for survival analysis in S," *R package version*, vol. 2, no. 7, 2020.

[22] J. Friedman, T. Hastie, and R. Tibshirani, "Regularization paths for generalized linear models via coordinate descent," *Journal of Statistical Software*, vol. 33, no. 1, pp. 1–22, 2010.

[23] P. Geeleher, N. Cox, and R. S. Huang, "pRRophetic: an R package for prediction of clinical chemotherapeutic response from tumor gene expression levels," *PLoS One*, vol. 9, no. 9, article e107468, 2014.

[24] M. E. Ritchie, B. Phipson, D. Wu et al., "limma powers differential expression analyses for RNA-sequencing and microarray studies," *Nucleic Acids Research*, vol. 43, no. 7, pp. e47–e47, 2015.

[25] B. Chen, M. S. Khodadoust, C. L. Liu, A. M. Newman, and A. A. Alizadeh, "Profiling tumor infiltrating immune cells with CIBERSORT," *Methods in Molecular Biology*, vol. 1711, pp. 243–259, 2018.

[26] A. Patel, M. Oshi, L. Yan, R. Matsuyama, I. Endo, and K. Takabe, "The unfolded protein response is associated with cancer proliferation and worse survival in hepatocellular carcinoma," *Cancers*, vol. 13, no. 17, p. 4443, 2021.

[27] X. Yan, M. Chen, C. Xiao et al., "Effect of unfolded protein response on the immune infiltration and prognosis of transitional cell bladder cancer," *Annals of Medicine*, vol. 53, no. 1, pp. 1048–1058, 2021.

[28] S. Lhomond, T. Avril, N. Dejeans et al., "Dual IRE1 RNase functions dictate glioblastoma development," *EMBO Molecular Medicine*, vol. 10, no. 3, 2018.

[29] S. Wu, R. Du, C. Gao, J. Kang, J. Wen, and T. Sun, "The role of XBP1s in the metastasis and prognosis of hepatocellular carcinoma," *Biochemical and Biophysical Research Communications*, vol. 500, no. 3, pp. 530–537, 2018.

[30] Y. X. Feng, D. X. Jin, E. S. Sokol, F. Reinhardt, D. H. Miller, and P. B. Gupta, "Cancer-specific PERK signaling drives invasion and metastasis through CREB3L1," *Nature Communications*, vol. 8, no. 1, p. 1079, 2017.

[31] H. Tian, S. Shi, B. You, Q. Zhang, M. Gu, and Y. You, "ER resident protein 44 promotes malignant phenotype in nasopharyngeal carcinoma through the interaction with ATP citrate lyase," *Journal of Translational Medicine*, vol. 19, no. 1, p. 77, 2021.

[32] T. Xia, H. Tian, K. Zhang et al., "Exosomal ERp44 derived from ER-stressed cells strengthens cisplatin resistance of nasopharyngeal carcinoma," *BMC Cancer*, vol. 21, no. 1, p. 1003, 2021.

[33] C. R. LaValle, K. M. George, E. R. Sharlow, J. S. Lazo, P. Wipf, and Q. J. Wang, "Protein kinase D as a potential new target for cancer therapy," *Biochimica et Biophysica Acta*, vol. 1806, no. 2, pp. 183–192, 2010.

[34] A. Jadali and S. Ghazizadeh, "Protein kinase D is implicated in the reversible commitment to differentiation in primary cultures of mouse keratinocytes," *J Biol Chem*, vol. 285, no. 30, pp. 23387–23397, 2010.

[35] H. L. Chen, B. M. Cui, Y. Z. Kang et al., "Expression level of protein kinase D in oral squamous cell carcinoma with diverse differentiation," *Sichuan Da Xue Xue Bao. Yi Xue Ban*, vol. 51, no. 6, pp. 755–759, 2020.

[36] L. Zhang, Z. Li, Y. Liu et al., "Analysis of oncogenic activities of protein kinase D1 in head and neck squamous cell carcinoma," *BMC Cancer*, vol. 18, no. 1, p. 1107, 2018.

[37] H. Zheng, H. Liu, Y. Lu, and H. Li, "Identification of a novel signature predicting overall survival in head and neck squamous cell carcinoma," *Frontiers in Surgery*, vol. 8, article 717084, 2021.

[38] T. Islam, R. Rahman, E. Gov et al., "Drug targeting and biomarkers in head and neck cancers: insights from systems biology analyses," *OMICS*, vol. 22, no. 6, pp. 422–436, 2018.

[39] P. García-Cabo, F. López, M. Sánchez-Canteli et al., "Matched-pair analysis of survival in the patients with advanced laryngeal and hypopharyngeal squamous cell carcinoma treated with induction chemotherapy plus chemo-radiation or total laryngectomy," *Cancers*, vol. 13, no. 7, article 1735, 2021.

[40] M. Yu, J. Lun, H. Zhang et al., "Targeting UPR branches, a potential strategy for enhancing efficacy of cancer chemotherapy," *Acta Biochim Biophys Sin (Shanghai)*, vol. 53, no. 11, pp. 1417–1427, 2021.

[41] H. Sharifi-Noghabi, S. Jahangiri-Tazehkand, P. Smirnov et al., "Drug sensitivity prediction from cell line-based pharmacogenomics data: guidelines for developing machine learning models," *Briefings in Bioinformatics*, vol. 22, no. 6, 2021.

[42] Y. Liu, Y. Zhang, Y. Ding, and R. Zhuang, "Platelet-mediated tumor metastasis mechanism and the role of cell adhesion molecules," *Critical Reviews in Oncology/Hematology*, vol. 167, article 103502, 2021.